Australian Government
Department of Defence
Defence Science and
Technology Organisation

An Evaluation of the Effective Block Approach Using P-3C and F-111 Crack Growth Data (U)

C. Wallbrink, R. Amaratunga, W. Hu, P. Jackson and D. Mongru

Air Vehicles Division
Defence Science and Technology Organisation

DSTO-TR-2195

ABSTRACT

Recently an effective block approach has been proposed to address the experimentally observed growth rates of fatigue cracks at critical locations on F/A-18 airframes. In this approach, each program of spectrum load is treated as an equivalent constant amplitude cycle, and the baseline crack growth rate data are obtained using a similar spectrum load of interest. A procedure was devised to allow the use of the model parameters obtained under one load spectrum to predict the crack growth under a different load spectrum. In this study, we critically evaluate the capability of the effective block approach, using data obtained for the F-111 and P-3C coupon test programs, to gauge its general applicability to other aircraft operated by the Royal Australian Air Force. The data used in the evaluation encompasses different load spectra, different materials and different crack configurations. This investigation has found that the effective block approach was able to model fatigue crack growth in 2024-T851 aluminium under the F-111 flight spectra examined, but it could not produce an acceptable estimation of the total crack growth life for the P-3C spectra studied. It was, however, able to produce reasonable predictions of fatigue crack growth in a chosen interval of crack length. This report provides an independent evaluation and guidance for the application of the effective block approach.

Published by

Air Vehicles Division
DSTO Defence Science and Technology Organisation
506 Lorimer St
Fishermans Bend, Victoria 3207 Australia

Telephone: (03) 9626 7000
Fax: (03) 9626 7999

AR-013-294
September 2008

APPROVED FOR PUBLIC RELEASE

An Evaluation of the Effective Block Approach Using P-3C and F-111 Crack Growth Data

Executive Summary

One of the objectives of the Defence Science and Technology Organisation (DSTO) is to evaluate and report on a number of non-traditional crack growth estimation methods, including the method known as the "effective block approach (EBA)". The EBA treats each program of spectrum load as an equivalent constant amplitude cycle and the baseline crack growth rate data are obtained using a similar spectrum load of interest. Predictions of crack growth under an untested spectrum are achieved by estimating the relative severity of the untested spectrum to a tested spectrum and then using the relative severity to modify the EBA crack growth parameters. This approach has been shown to effectively predict crack growth in materials and spectra used on the F/A-18. It has been suggested that the EBA may be applicable to other aircraft, including the P-3C and the F-111.

In this study, we critically evaluate the capability of the EBA, using data obtained from different load spectra, different material and different crack configurations, to gauge its general applicability to other aircraft operated by the Royal Australian Air Force. Crack growth data obtained from P-3C coupon tests conducted by the National Aerospace Laboratory of the Netherlands, and F-111 coupon tests conducted by the Defence Science and Technology Organisation were used for the evaluation. The report addresses the determination of the model parameters and whether they are dependent on the stress level of the spectrum. It also investigated the soundness of the procedure used for transferring the model parameters from one spectrum to another; the performance of the model under the same spectrum and under different spectra.

The present investigation has shown that the effective block approach was able to model fatigue crack growth in 2024-T851 aluminium under F-111 flight spectra. The application of the large loads in the cold proof load test does not appear to affect the technique's ability to predict fatigue crack growth curves. The EBA was not able to produce accurate predictions of total crack growth life for the P-3C spectrum, however, predictions of fatigue crack growth in a chosen interval were reasonable.

Importantly, the application of the EBA as a predictive tool hinges on the capability of a third-party tool, such as FASTRAN, to correctly predict the relative severity between the tested and an untested spectrum. Any inaccuracy or uncertainty in the predicted relative severity will directly affect the performance of the EBA. Transferability of the EBA-based predictions between different notch features has not been evaluated.

Authors

C. Wallbrink
Air Vehicles Division

Chris Wallbrink graduated in 2005 with a PhD from Monash University in the department of Mechanical Engineering. He then held the position of research fellow at Monash University till the end of 2006 where his research interests included, modelling of fatigue crack growth, infrared NDT technologies and fibre optic corrosion detection devices.

He has since joined the DSTO in 2007 in the Air Vehicles Division and in currently conducting research into methods for fatigue crack growth modelling and also airworthiness standards.

R. Amaratunga
Air Vehicles Division

Mr Amaratunga graduated in 1997 with a Bachelor of Engineering (Aeronautical) from the University of Sydney. Since commencing employment at the then Aeronautical and Maritime Research Laboratory in 1998, Mr Amaratunga has worked in the fields of aircraft structural integrity, risk and reliability assessment of fixed wing aircraft, and Air6000 cost and capability. Mr Amaratunga's experience ranges from repair design, probabilistic assessment of aircraft, to configuration comparison between high performance fighter aircraft.

W. Hu
Air Vehicles Division

Weiping Hu joined DSTO in 1998 as a research scientist. He is currently a senior research scientist leading the development of modelling capabilities for the analysis of structural integrity of aircraft structures.

After obtaining his PhD degree in 1993 at Dublin City University Ireland, he held various academic positions at Dublin City University, Monash University and Deakin University. His current research interests include fatigue crack growth in aircraft structures, constitutive models and plasticity, and numerical methods in engineering.

P. Jackson
Air Vehicles Division

Philip Jackson graduated form the Royal Melbourne Institute of Technology in 1981 with a Bachelor of Aeronautical Engineering (with Distinction). He spent the next 15 years as an engineering officer with the Royal Australian Air Force in both squadron and staff engineering posts specialising in aircraft structural integrity and fatigue management. In 1988 he completed a Masters of Science in Aerospace Vehicle Design at Cranfield Institute of Technology, UK and from 1991-94 was attached to the Canadian National Research Council, Ottawa, Canada as part of the F/A-18 International Follow-on Structural Test Project. He joined DSTO in 1997 and has been the technical and program lead for the DSTO contributions to international P-3 Service Life Assessment Program (SLAP). He is currently Head, Helicopter and Transport Aircraft Structral Integrity in the Aircraft Structures Branch of Air Vehicles Division as well as leading a divisional research effort on airworthiness and aircraft design standards.

David Mongru
Air Vehicles Division

Mr Mongru graduated from RMIT in 1990 with a Bachelor of Aerospace Engineering (Honours). He commenced work at DSTO in 1994 working on loads development and fatigue interpretation for the PC9 fatigue test. He joined IFOSTP in 1996 performing fatigue analysis of critical components on the aft fuselage of the F/A-18. In 2001 he commenced work on the P-3 SLAP. His primary functions included fatigue test interpretation and provison of technical support to the P-3 empennage test. He is currently working on the standards and lifing methodologies task.

Contents

1. Introduction

Recently an effective block approach (EBA) has been proposed to address the experimentally observed growth rates of fatigue cracks at critical locations on F/A-18 airframes (McDonald and Molent 2004; McDonald, Molent et al. 2006). It was claimed that the growth of these cracks in structures made of 7050 aluminium alloy could not be adequately predicted using classical models such as Paris law (Paris and Erdogan 1963) or the plasticity-induced crack closure models (Budiansky and Hutchinson 1978; Newman 1981), based on constant amplitude (CA) crack growth rates (CGR). Consequently, a new approach was proposed that treats each program (block) of spectrum load as an equivalent CA cycle. In essence, this approach treats all the spectrum loads as a crack-growth equivalent CA cycle, hence formally eliminating the complication of sequence effects in the linear elastic fracture mechanics (LEFM) approach. The CGR is expressed in a similar equation to that of the Paris law, with two model parameters to be determined: the crack growth coefficient and the Paris exponent, and they are determined by fitting the experimental data obtained from spectrum loading tests. However, since each spectrum is equivalent to a unique CA cycle, these model parameters are expected to be dependent on the spectrum, the peak stress, as well as the geometry and the material. A procedure was then devised to allow the use of the model parameters obtained under one load spectrum (the tested spectrum) to predict the crack growth under a different load spectrum (the untested spectrum). This procedure relies on the relative severity of these two spectra being determined using an independent third-party model or tool, which generally uses CA growth rates to predict the crack growth under spectrum loading. The EBA has been shown to produce crack growth curves that correlate well with the experimental results for the F/A-18 cases studied (McDonald, Molent et al. 2006). During the preparation of this document, concurrent investigations took place with relation to the EBA and its use with the F-111. The results of which have recently been published in DSTO-TR-2124 (Zhuang, Boykett et al. 2008).

In this study, we critically evaluate the capability of the EBA, using data obtained from different load spectra, different material and different crack configurations, to gauge its general applicability to other aircraft operated by the Royal Australian Air Force (RAAF). Questions about the effectiveness of the EBA approach that we wish to address include the determination of the model parameters and whether they are dependent on stress level of the spectrum; the soundness of the procedure used to transfer the model parameters from one spectrum to another; the performance of the model under the same spectrum with different stress levels and under different spectra; and the length of the spectrum, relative to the total life of the structure. The evaluation was conducted using the experimental data obtained from fatigue-critical locations on P3-C transport aircraft and F-111 fighter aircraft.

2. Effective Block Approach Overview

In this section we detail the concept of the EBA and its numerical procedure of application. In doing so, we also hope to clarify the particular model to be evaluated in this report; correctly interpret the procedure devised to transfer the model parameter from one spectrum to another; and to set the scope of the evaluation to be carried out.

It is worth pointing out that the concept of treating a spectrum as a CA cycle for crack growth modelling is not new. In particular, Gallager and Stalnaker (Gallagher 1976; Gallagher and Stalnaker 1978) developed a very similar model in 1970s, in which the CGR equation was defined as crack growth per flight and related to the maximum stress intensity factor in a Paris-type equation. The main difference between the EBA evaluated here and that of Gallager and Stalnaker is that the former proposed a procedure to apply the model parameters developed from a tested spectrum to other untested spectra. Apart from noting this difference, the terms effective block approach and its abbreviation both refer to the approach developed in McDonald, Molent et al. (2006).

2.1 The Concept of the Effective Block Approach

In traditional crack growth modelling based on LEFM, the CGR is defined for each cycle. For example, the well-known Paris law is expressed as (Paris and Erdogan 1963):

$$\frac{da}{dN} = C\Delta K^m, \tag{1}$$

where a is the crack length, N is the load cycle, ΔK is the stress intensity range. C and m are two material constants known as the coefficient and the exponent of Paris law, and they are determined by fitting the above equation to experimental data obtained under CA loading. Both the success and the limitation of the Paris law are well-known, and various attempts have been made to improve its performance under spectrum loading, by modelling the sequence effects using concepts such as plasticity-induced closure (Budiansky and Hutchinson 1978; Newman 1981). McDonald, Molent et al. (2006) show that neither the plain Paris law nor the crack closure model, as implemented in AFGROW (Harter 2004) and FASTRAN (Newman 1992), was able to adequately predict the crack growth behaviour of 7050 aluminium alloy subjected to the service load of the F/A-18 fighter planes. To make the matter worse, the predictions by these methods are generally non-conservative (McDonald, Molent et al. 2006). Consequently, EBA was proposed. In essence, the EBA treats all the spectrum loads as a crack-growth equivalent CA cycle; hence it formally eliminates the complication of sequence effects in the Paris law. Using a similar equation to that of Paris, the CGR for the EBA is expressed as:

$$\dot{a} = \frac{da}{dB} = CK_{\text{ref}}^m \ . \tag{2}$$

Here K_{ref} is a reference stress intensity factor specified later, and C and m are the model parameters. In this report B is a measurement of time and is used in the CGR $da/d\mathrm{B}$ to signify that the CGR has been calculated based on spectrum blocks. The shorthand notation of CGR, $\dot{a}$, is introduced here for brevity; it does not signify a derivative with respect to real time. This notation will be used later for the discussion of the transfer of model parameters. All crack growth data are presented in terms of simulated flight hours for direct comparison.

It should be noted that, in general, the model parameters in Eqn. (2) are numerically different from those defined in Eqn. (1). In equation 2, C and m depend not only on the material properties but also on the load spectrum applied and even the stress level of the same spectrum, and they are determined by fitting the equation to the experimental CGR data obtained under the load spectrum of interest. A question arises, then, as to how the EBA could be used as a predictive tool, if the model parameters have to be determined using the experimental CGR data obtained under the very same load spectrum for which the crack growth is to be predicted. The predictive capability of the approach, therefore, hinges on (1) whether the dependence of C and m on the load spectrum is so weak that they can be effectually treated as material constants; or if that is not the case, (2) whether the model parameters for an untested spectrum could be deduced from those obtained from a tested spectrum. (McDonald, Molent et al. 2006) proposed a procedure, based on the relative severity estimation obtained from a third-party tool, for transferring the model parameters determined using one spectrum to another, and it is detailed in Section 2.2. The focus of this report is to examine the soundness of this procedure, using experimental data obtained under F-111 and P3-C load spectra.

The EBA requires the following information prior to an analysis:

- Crack length as a function of time, or the number of cycles, or flight hours, or blocks of spectrum loading;
- Full load history at the location of interest;
- The reference stress to be used in the region of interest;
- Relevant boundary correction factors in the region of interest (β factors).

Provided that all the necessary data exist, the EBA can then be used to evaluate the model parameters C and m. The following three steps are used in the process:

1. Calculating the stress intensity factors at the reference stress;
2. Calculating the crack growth rate;
3. Determining the constants C and m.

2.1.1 Calculation of the Stress Intensity Factors at the Reference Stress

The reference stress intensity factors are calculated using the following equation:

$$K_{ref} = \sigma_{ref} \beta \sqrt{\pi a}\,, \tag{3}$$

where K_{ref} is the stress intensity factor at the reference stress σ_{ref}, a is the crack length, and β is the boundary correction factor. The maximum stress of a spectrum is usually selected as the reference stress.

2.1.2 Calculation of the Crack Growth Rate

The CGR is evaluated at each crack length in the experimental data, using a "three-point" technique. Thus, the CGR is evaluated at each crack length by performing a linear regression of the logarithms of three consecutive crack lengths a_{i-1}, a_i, a_{i+1}. Here the crack growth measurements a_{i-1}, a_i, a_{i+1} are taken at the end or each spectrum block. The time interval between the beginning and end of the block is B_T (the total spectrum block). The slope of this line is then used for the calculation of the CGR at a_i. Figure 1 schematically shows how the method works. The slope of the line, $\frac{d(\ln(a))}{dB_T}$, is related to the CGR through the following equation:

$$\frac{da}{dB_T} = a\frac{d(\ln(a))}{dB_T} \tag{4}$$

This calculation is performed at every experimental data point. The subscript T indicates the use of the total spectrum block and the subscript S indicates the use of sub-blocks in the analysis.

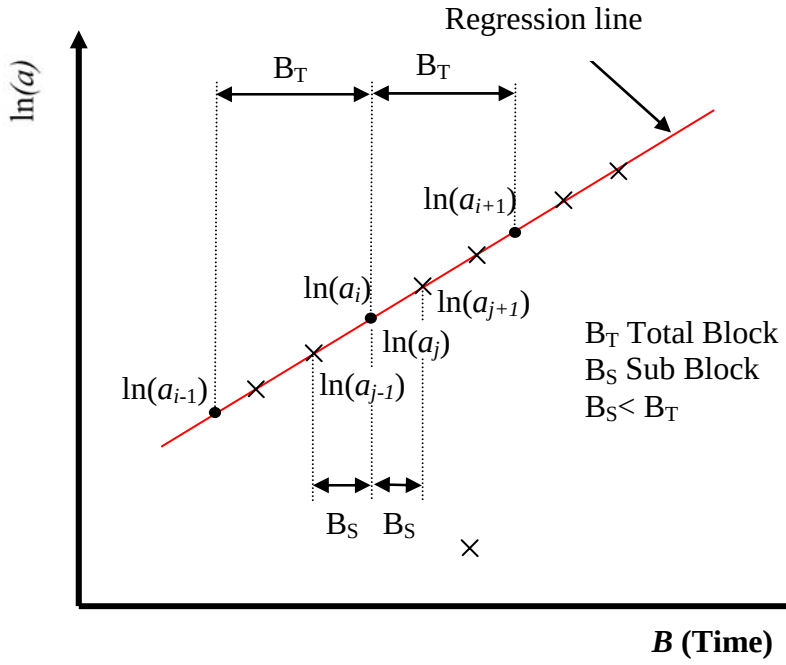

Figure 1: Evaluation of the crack growth rate per block

The CGR $\frac{da}{dB_T}$ defined using B_T indicates the CGR has been evaluated using total blocks. This CGR should be equivalent to $\frac{da}{dB_S}$ which is the CGR evaluated in terms of sub-blocks B_S

using the points a_{j-1}, a_j, a_{j+1}. The equivalence of these CGRs is only true if the crack growth remains steady state (Gallagher 1976).

2.1.3 Determination of the Crack Growth Constants *C* and *m*

The derived CGRs and the associated stress intensity factors are then plotted on a log-log scale. The slope of the straight line that best fits the data is determined from a linear regression using the following equation; $\ln\left(\frac{da}{dB}\right) = \ln(C) + m\ln(K_{\text{ref}})$. The slope represents the CGR exponent m, and the y-intercept, $\ln C$, gives the CGR coefficient.

2.2 The EBA as a predictive tool

There are two issues central to the capacity of the EBA to be used as a predictive tool, the initial crack size and a means to transfer the model parameters from a tested spectrum to an untested spectrum. In the following two sub-sections we describe the original procedure developed by McDonald (2005), and a modified procedure developed by Wallbrink and Hu (2008). The issue of initial crack size will be dealt with later.

2.2.1 The original method (fixed m approach)

Once the model parameters are determined, the EBA can be used to "predict" the crack growth for the same geometry, same material subjected to the same spectrum loading. To apply the model to the same geometry, same material subjected to a different spectrum loading, the model parameters C and m for the new spectrum need to be determined. Obviously they should not be determined from experimental data as that will defeat the purpose of "prediction". In order to make the EBA into a predictive tool, a numerical procedure was developed by McDonald (2005) by assuming that, for two similar but different spectra, the crack growth parameters determined from experiments and those obtained from a predictive tool such as AFGROW (Harter 2004) are proportional, although the raw crack growth results from the predictive tools may be inaccurate. It further assumes that m remains the same for both the tested and the untested spectrum. Based on these assumptions the following relationship is obtained. Thus,

$$\frac{C_{2,E}}{C_{1,E}} = \frac{C_{2,P}}{C_{1,P}} \tag{5}$$

Here the subscripts 1 (tested) and 2 (untested) represent spectra 1 and 2 and the subscripts P and E indicate terms obtained from a predictive tool and experiment respectively. Hence, $C_{1,\text{E}}$ has been determined from experimental data for spectrum 1, and $C_{1,\text{P}}$ and $C_{2,\text{P}}$ are calculated from a crack growth tool for spectrum 1 and 2. Then Eqn. (5) can be used to evaluate the CGR parameter $C_{2,\text{E}}$ for spectrum 2. The exponent m evaluated from the experimental data under spectrum 1 was directly transferred to the new spectrum, spectrum 2.

2.2.2 The variable-m approach

The initial implementation of the EBA assumed that the exponent m remained constant between spectra. In other words, experimental CGR obtained under spectrum 1 should have the same exponent m as CGR obtained under spectrum 2. Investigations with quantitative fractography (QF) data have shown that this assumption holds true for various spectra used with the F/A-18 (McDonald, Molent et al. 2006), but this may not be the case for all spectra. For instance, CA loading is a limiting case for variable amplitude loading, yet the CGR data obtained under CA loading typically give Paris exponent of between 2~4. Indeed, such an assumption is not necessary, as shown below.

Implicit in the original assumption of equivalence of relative severity between the tested and the untested spectra is the following relationship:

$$\frac{\dot{a}_{2,\mathrm{E}}}{\dot{a}_{1,\mathrm{E}}} = \frac{\dot{a}_{2,\mathrm{P}}}{\dot{a}_{1,\mathrm{P}}}, \tag{6}$$

which reduces to Eqn. (5) if m is assumed constant (*cf* Eqn. (2)). Thus, Eqn. (6) is a more fundamental assumption, which asserts that the ratio of CGRs for two different spectra are correctly predicted by tools such as AFGROW, although the rates themselves may not be correct. Here, $\dot{a} = \mathrm{d}a/\mathrm{d}B$ as noted earlier. If this assumption is accepted, then Eqn. (6) may be used to determine the model parameters for a new untested spectrum, when experimental data exist for the same material under a tested spectrum.
To do this, we substitute Eqn. (2) into Eqn. (6) to obtain:

$$\frac{C_{2,\mathrm{E}} K_{\mathrm{ref}}^{m_{2,\mathrm{E}}}}{C_{1,\mathrm{E}} K_{\mathrm{ref}}^{m_{1,\mathrm{E}}}} = \frac{C_{2,P} K_{\mathrm{ref}}^{m_{2,\mathrm{P}}}}{C_{1,P} K_{\mathrm{ref}}^{m_{1,\mathrm{P}}}}. \tag{7}$$

Rearranging Eqn. (7) and collecting terms, we get:

$$C_{2,\mathrm{E}} K_{\mathrm{ref}}^{m_{2,\mathrm{E}}} = \frac{C_{2,\mathrm{P}}}{C_{1,\mathrm{P}}} C_{1,E} K_{\mathrm{ref}}^{m_{2,\mathrm{P}} - m_{1,\mathrm{P}} + m_{1,\mathrm{E}}} \tag{8}$$

Since the above relationship holds true for any $K_{\mathrm{ref}} \neq 0$, it should also be true for $K_{\mathrm{ref}} = 1$. Therefore,

$$C_{2,\mathrm{E}} = \frac{C_{2,\mathrm{P}}}{C_{1,\mathrm{P}}} C_{1,\mathrm{E}} \tag{9}$$

In Eqn. (9) the constants $C_{1,\mathrm{E}}$ $C_{2,\mathrm{E}}$ $C_{1,\mathrm{P}}$ and $C_{2,\mathrm{P}}$ are independent of K_{ref} and thus we can substitute Eqn. (9) into Eqn. (8) to obtain:

$$\frac{C_{2,\mathrm{P}}}{C_{1,\mathrm{P}}} C_{1,\mathrm{E}} K_{\mathrm{ref}}^{m_{2,\mathrm{E}}} = \frac{C_{2,\mathrm{P}}}{C_{1,\mathrm{P}}} C_{1,\mathrm{E}} K_{\mathrm{ref}}^{m_{2,\mathrm{P}} - m_{1,\mathrm{P}} + m_{1,\mathrm{E}}}. \tag{10}$$

or, upon cancelling common factors,

$$K_{\text{ref}}^{m_{2,\text{E}}} = K_{\text{ref}}^{m_{2,\text{P}} - m_{1,\text{P}} + m_{1,\text{E}}}, \tag{11}$$

which gives:

$$m_{2,\text{E}} = m_{2,\text{P}} - m_{1,\text{P}} + m_{1,\text{E}}. \tag{12}$$

Thus, Eqn. (9) and Eqn. (12) provide a more general means for determining the CGR constants for an untested spectrum from the constants determined from a tested spectrum. This approach will be used, together with the initial implementation of the EBA, to assess the EBA's applicability to P-3C and F-111 crack growth data sets.

In summary, three variants of the methods for transferring the model parameters from a tested spectrum to an untested spectrum will be evaluated. They are:

- Method 1: $m_{2,E}$ = Constant = 2
  This method sets the crack growth exponent equal to 2 for both spectra and uses Eqn. (5) to calculate the CGR coefficient $C_{2,E}$. It essentially assumes a log-linear relationship between the crack growth and the simulated flight history.
- Method 2: $m_{2,E} = m_{1,E}$
  This method is similar to method 1, but instead of setting $m_{2,E} = 2$, $m_{2,E}$ is set equal to $m_{1,E}$. The CGR coefficient $C_{2,E}$ is again calculated with Eqn. (5).
- Method 3: Variable-*m*
  This method uses Eqn. (12) to evaluate $m_{2,E}$ and uses Eqn. (5) to evaluate the constant CGR parameter $C_{2,E}$.

In the following sections, the EBA is evaluated using the experimental data available for F-111 and P3-C load spectra and geometries. Specifically, the following issues will be examined:

1. whether the EBA can adequately represent the experimental data, *i.e.*,
   a. whether the CGRs under a spectrum can be adequately represented by Eqn. (2);
   b. whether C and m are independent of the reference stress of the spectrum;
   c. whether there is a limit on the level of stress for this independence;
2. the transferability of C and m between different spectra, *i.e.*,
   a. whether the assumptions in Eqn. (9) and (12) are valid;
   b. what role is played by third-party crack growth tools such as AFGROW and CGAP (FASTRAN), an in-house crack growth analysis tool (Hu and Walker 2006);
   c. how to reconcile the view that these third-party tools do not give accurate predictions in terms of absolute values but their predictions of relative severity are acceptable.

3. Evaluation of the EBA Using P-3C Coupon Data

3.1 National Aerospace Laboratory (NLR) coupon test data

The data used for this part of the evaluation were obtained from a coupon test program conducted by the National Aerospace Laboratory (NLR) (Veul and Ubels 2003). The NLR coupon test program tested 72 coupons under 5 different spectra manufactured from 2.02 mm (0.08") thick 7075-T6 rolled sheet material. For the current work only two spectra were considered, the full scale fatigue test (FSFT) spectrum and the RAAF spectrum. The aim was to use the FSFT notched coupon crack growth data to predict the crack growth under the RAAF spectra using the EBA, and compare it to the actual RAAF notched coupon crack growth data. This approach mimicked the P-3 service life assessment program (SLAP) test interpretation logic whereby FSFT results were used to calculate lives under a RAAF P-3C spectrum (Teunisse, Phillips et al. 2006).

The detailed material properties, coupon geometry and the loading spectra are given in Veul and Ubels (2003). The crack growth data were measured using the direct current potential drop (DCPD) method.

Three coupons were tested under the FSFT spectrum, and four coupons were tested under the RAAF spectrum. Both spectra are a flight-by-flight non-repeating blocks of 15,000 hours.

The crack growth data for the three coupons tested under the FSFT spectrum are presented in Figure 2, in which the crack length a was measured from the edge of the notch. The crack growth data has been plotted against simulated flight hours (SFH). The crack growth data represents less than two spectrum blocks.

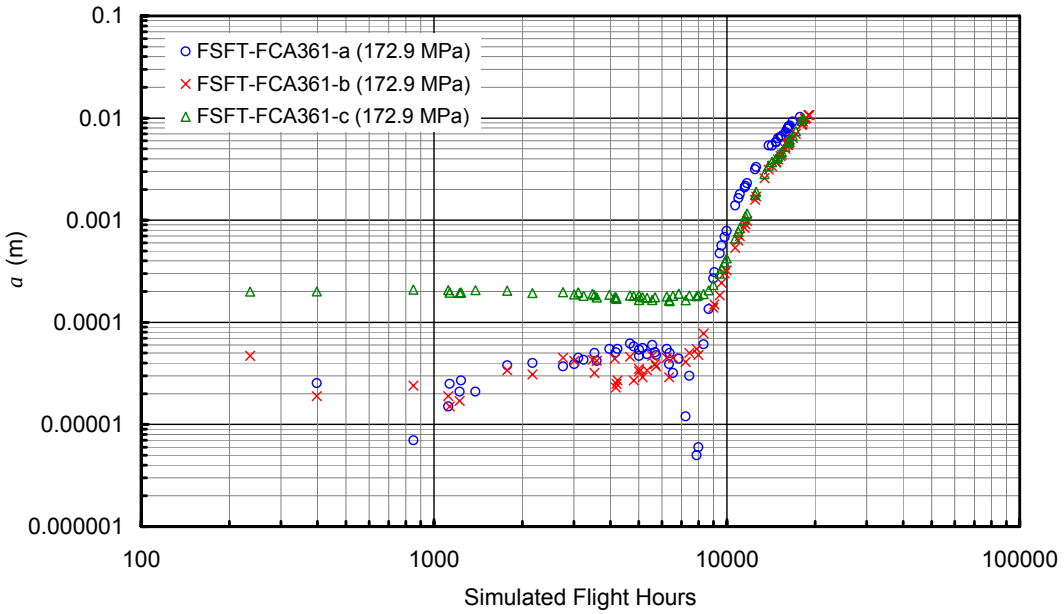

Figure 2: FSFT Raw Coupon Data

The DCPD measurements in Figure 2 indicate that the limits of the DCPD are potentially affecting the accuracy of measurements in the early stages of crack growth. The crack must grow to a size above the minimum operation limit of the system where the DCPD signal could detect the presence of a crack. The present data indicates that the crack must be greater than 0.254 mm to produce reliable measurements.

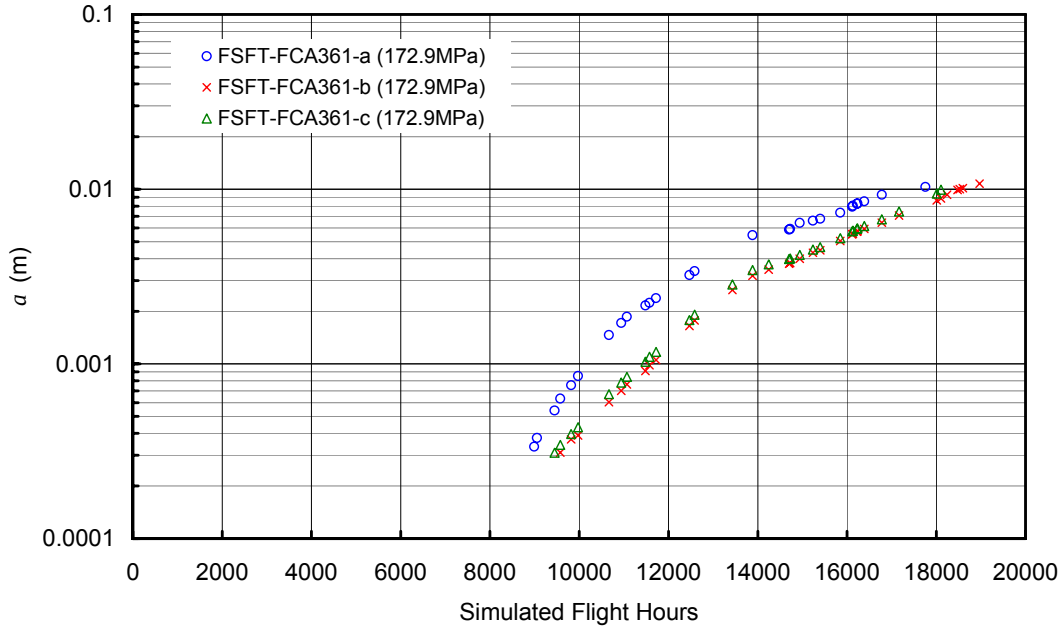

Figure 3: FSFT Data with "Noise" Removed

An attempt was made to remove the initial "anomalous" data in order to isolate the actual crack growth measurements. The clean up consisted of first removing the measurements regarded as noise, below the limits of detection of the DCPD system then removing all the points that result in a negative crack increment. The resulting data are shown in Figure 3.

It is possible that in the process of removing anomalistic data, a number of legitimate points may have been removed. It is also possible that a number of anomalous data points have escaped the clean-up process. However, the majority of the data removed were from the period when crack length was below the limits of detection of the DCPD system. The remaining data were considered representative of the actual crack growth in the test coupons.

3.2 Representation of P-3C FSFT Coupon Data Using the EBA

Figure 4 shows a plot of CGR versus the reference stress intensity factor for the FSFT spectrum, using Eqn. (2). In the calculation of the reference stress intensity factor, the boundary correction factor β was obtained from a 3D finite element analysis using energy methods (Gravina 2006), as shown in Figure 5. The σ_{ref} used was the maximum stress in the FSFT spectrum which was 167.78 MPa (24.335 ksi). The crack size, a, was based on the measured coupon data. A linear regression of the experimental data gave $m_{1,E} = 1.36$ and $C_{1,E} = 9.71\times10^{-9}$.

It is important to note that in order to apply the EBA to the P-3C spectrum, it was necessary to subdivide the total spectrum into smaller blocks (sub-blocks). This assumes the spectrum is "steady - state" (Gallagher 1976). The sub-blocks were based on the intervals of data acquisition used by the DCPD system. While this has been used to derive the EBA parameters, no attempt was made to compare the crack growth sub-block by sub-block.

From Figure 4, it can be seen that Eqn. (2) gives a reasonable representation, with a coefficient of determination[1] of 0.8. Also in Figure 4 we see that the $m_{1,E} = 1.36$ which is markedly different from the value of $m = 2$ obtained in the F/A-18 studies.

[1] The coefficient of determination (R^2) is the percentage of the variation that is explained by the model. It can be used to assess the degree of variability about a model of interest.

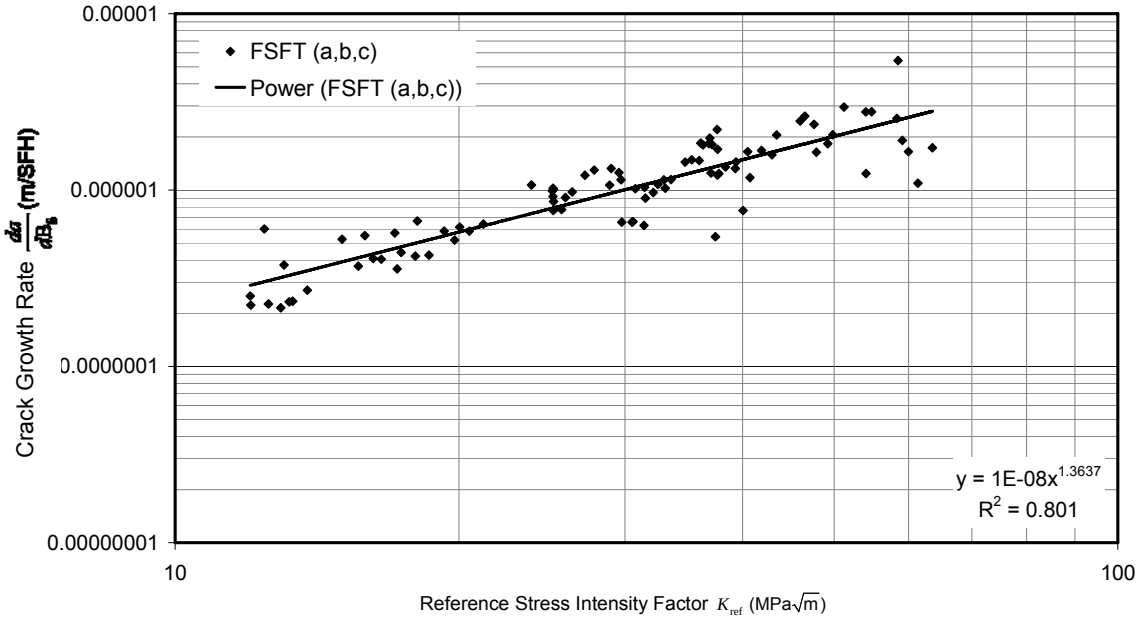

Figure 4: Crack growth rate vs K_{ref} for FSFT coupon data

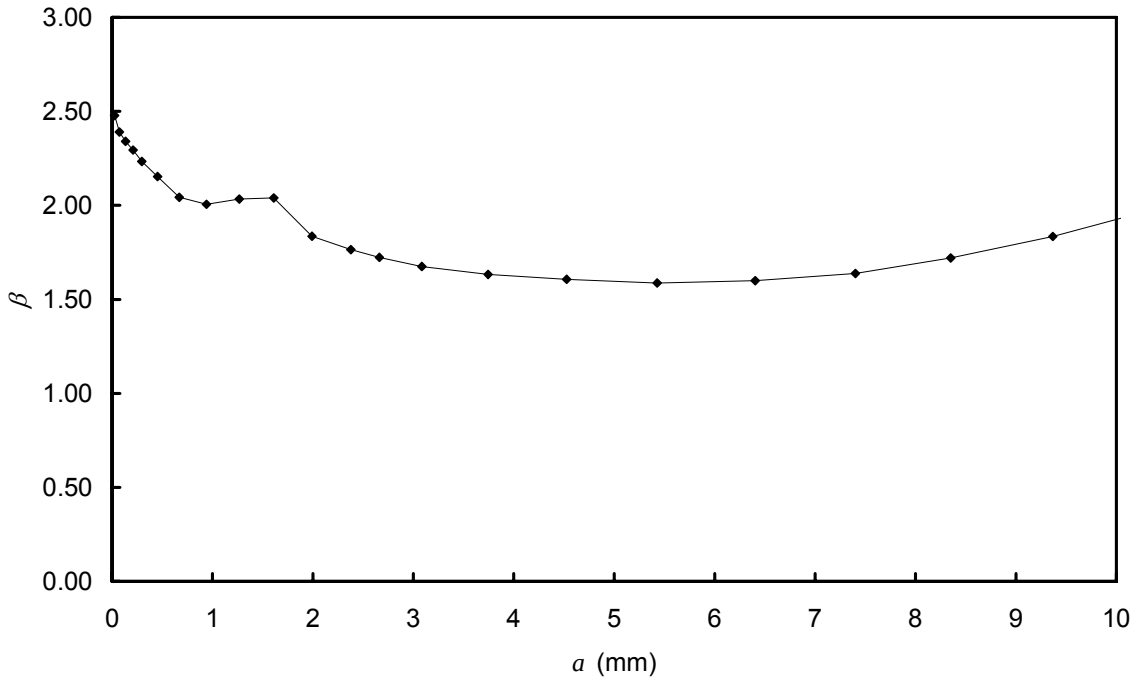

Figure 5: Coupon Beta Solution

3.3 Crack Growth Prediction Using the EBA

With the model parameters determined in the previous section, next we proceed to use them to predict crack growth. This includes "predicting" the crack growth under the same (FSFT) spectrum and under a different spectrum (RAAF), but before doing either, we need to determine what initial flaw size to use. We also need to determine the model parameters corresponding to the untested RAAF spectrum. These are discussed in the following three sub-sections.

3.3.1 Determining the initial flaw size

If the initial flaw size is a_0 and the final crack size is a_f, which could be the critical crack size a_{crit}, then the crack growth life in terms of the number blocks is obtained by integrating (Eqn. 2),

$$B = \int_{a_O}^{a_f} \frac{1}{CK_{\text{ref}}^m} da \tag{13}$$

However, as noted in McDonald, Molent et al. (2006), the final life is "markedly influenced by the choice of a_0". A fundamental tenet of the EBA is that, for a particular material, the value of a_0 is independent of the spectrum and the stress level. Moreover, the value of a_0 will be consistent with the crack initiating microstructure or surface features observed by fractography. There will be, of course, some scatter associated with the estimated value of a_0, and from the aluminium 7050 coupons used for the F/A-18 in McDonald, Molent et al. (2006) a_0 was typically between 0.1 and 0.01 mm (0.004 and 0.0004 inches).

A significant proportion of the F/A-18 crack growth data displays a straight line trend on a log-linear scale, from which it is relatively easy to extrapolate back to time zero to estimate an initial flaw size (McDonald 2005). In the case of the P-3C coupon data, the determination of the initial flaw size was not as straightforward. As no quantitative fractography measurements were carried out, no direct measurements of the initial flaw size could be made. Further more, because valid crack growth data began at approximately 10000 hours, there is a long period in which the crack growth data were considered "anomalous" as the crack size was obviously below the DCPC detectable threshold. Nevertheless to estimate the initial flaw size we must extrapolate the crack growth curve back to time zero, disregarding these "anomalous" data.

In McDonald (2005) the initial flaw size was estimated by back predicting the Paris equation using the EBA constants, but when this method was applied to the P-3C coupon data it failed to produce a meaningful estimate of the initial flaw size. Through subsequent internal DSTO discussions a recommendation was made, based on past experience with the F/A-18 and the apparent trend observed in the P-3C data, to exponentially back-extrapolate (a straight line on a log-linear plot) the raw crack growth data to time zero to estimate the initial flaw size. Another method that has been tried involved back-predicting the crack growth curve using FASTRAN.

A backward-exponential extrapolation of coupon data under the FSFT spectrum shown in Figure 6 gave an approximate initial flaw size of 1.52×10^{-5} m. As a comparison, a back-exponential extrapolation of the RAAF coupon data is also shown in Figure 6. Clearly, very different estimates of the initial flaw size are obtained for the RAAF data and the FSFT data. This result highlights a fundamental issue that will ultimately affect the EBA's ability to consistently estimate the total life of a structure or at least for the P-3C spectra considered in this analysis. The present treatment of the problem produces an effective initial flaw size which appears to be dependent on the spectrum. If we are to accurately estimate the total life of a structure we will also need the ability to estimate the effective initial flaw size or modify the present methodology so that predictions can be made from an intrinsic flaw size independent of the spectrum applied.

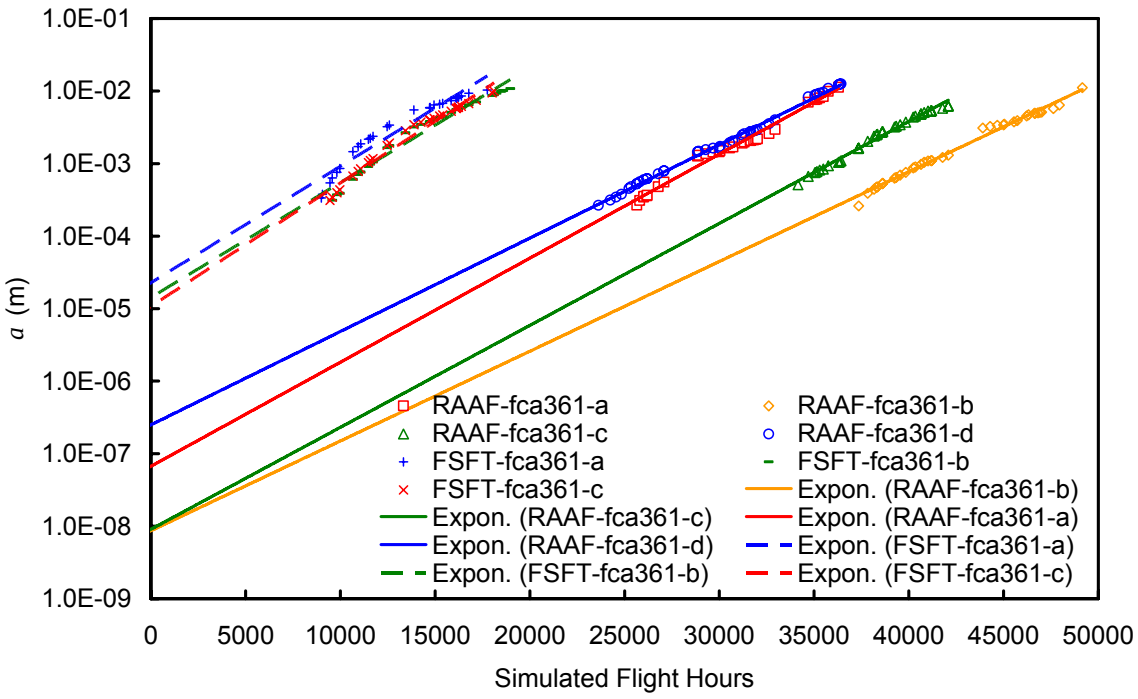

Figure 6: Exponential extrapolation to evaluate a_0

FASTRAN was also used to estimate the initial flaw size by altering a_0 to match the final life. Figure 7 shows the FASTRAN predicted curve and the coupon crack growth data for the FSFT coupons which gives an initial flaw size of 5.08×10^{-5} m.

If we use FASTRAN to back-predict the RAAF crack growth data, a new initial flaw size of 2.54×10^{-5} m can be obtained as shown by point B in Figure 7. While the crack growth under each spectrum appears to be satisfactorily modelled above 0.5 mm, below this value the predictions would not be reliable. This difference in the estimated initial flaw size again

highlights a problem associated with predicting the total life under another spectrum using existing crack growth software tools e.g. FASTRAN in this study.

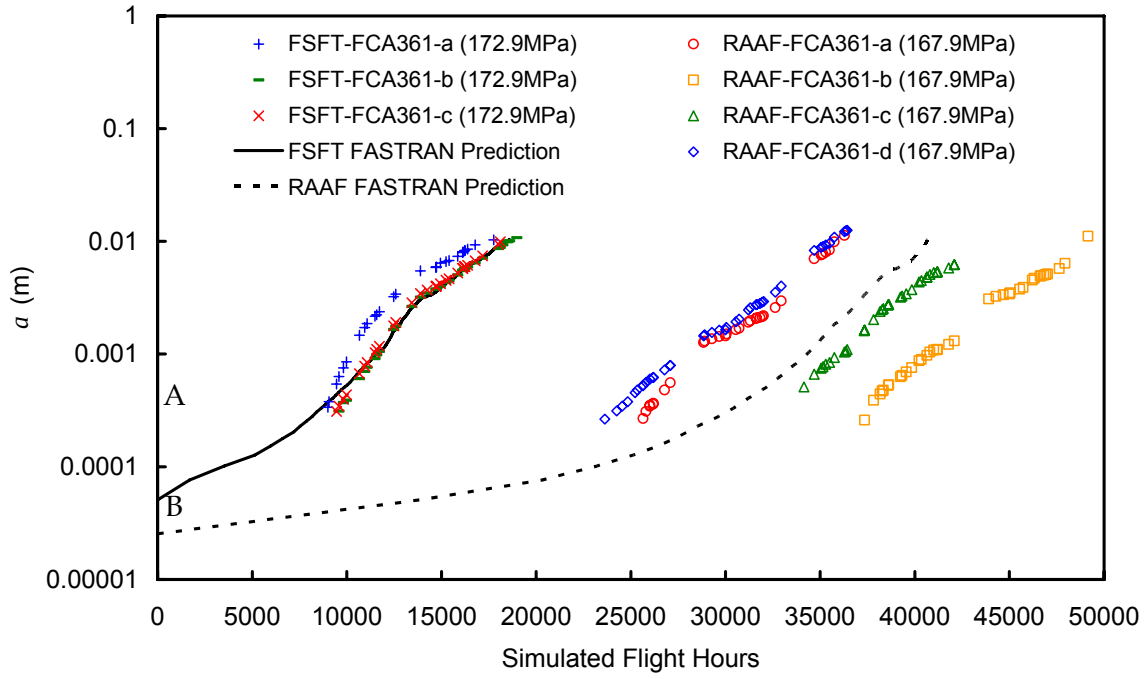

Figure 7: Comparison of the RAAF FASTRAN using an initial flaw size of 0.025 mm to the FSFT FASTRAN prediction using an initial flaw size of 0.05 mm

3.3.2 Evaluating the relative severity of RAAF and FSFT spectra

In order to determine the model parameters $m_{2,E}$ and $C_{2,E}$ for an untested spectrum from those of a tested spectrum, the EBA requires the relative severity of the two spectra. The EBA does not provide its own means of assessing relative severity; rather, it relies on third-party tools such as AFGROW or FASTRAN. For this analysis, the version of FASTRAN originally calibrated and used in the DSTO P-3 SLAP work (Teunisse, Phillips et al. 2006) was selected.

Using FASTRAN, the crack growth curves were generated for the FSFT and the RAAF spectra, with an initial flaw size of 0.05 mm and using the beta function from Figure 5. Note that FASTRAN has significantly under predicted the final fatigue life for the RAAF spectrum, as seen in Figure 8.

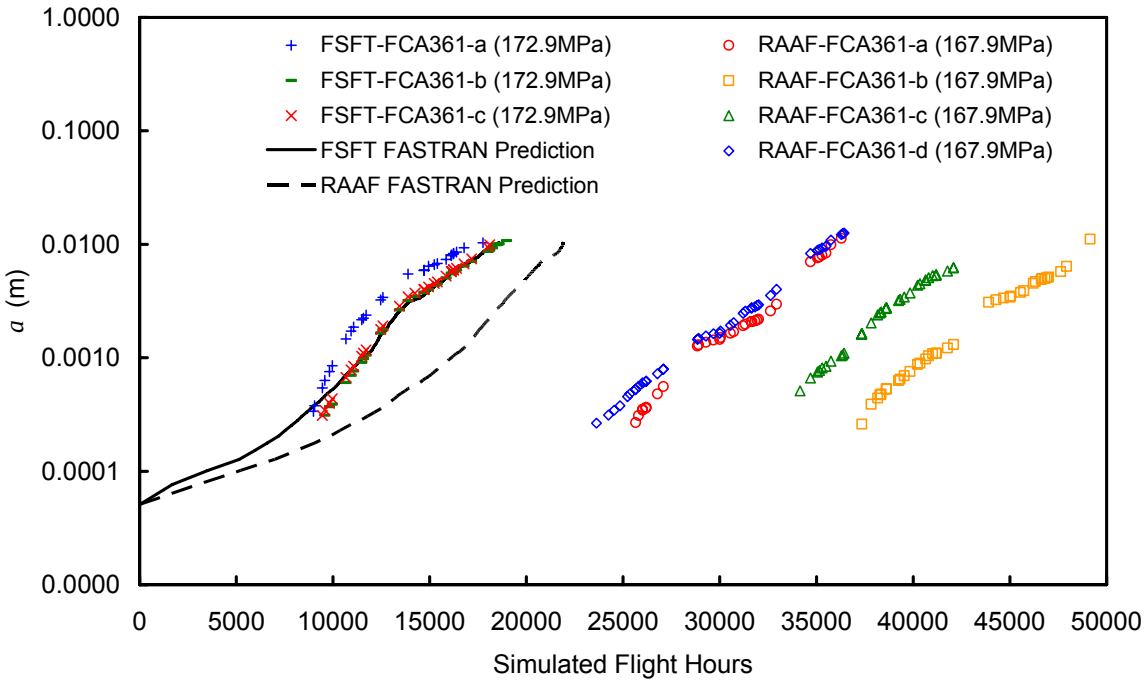

Figure 8: FASTRAN Predictions for FSFT and RAAF spectra, a_0=0.05 mm

The FASTRAN crack growth curves were then converted to rate data and thus allowed the Paris constants to be calculated using the method described in Section 2.2. Figure 9 shows the CGRs evaluated from the two FASTRAN predictions and the linear regressions. Clearly there is large scatter in the rate data, which was a result of the large number of points generated by FASTRAN, and more importantly the inherent variability in the cycle- by-cycle crack growth calculation due to the periodic calculation of the crack opening stress. In order to extract both a C and an m value with any confidence, the rate data was refined to maintain a regular sample spacing. This was accomplished via the use of Origin® 6.0. An interpolation curve was created using five-point averaging from which 150 equally spaced points were output and used to generate the curve in Figure 10

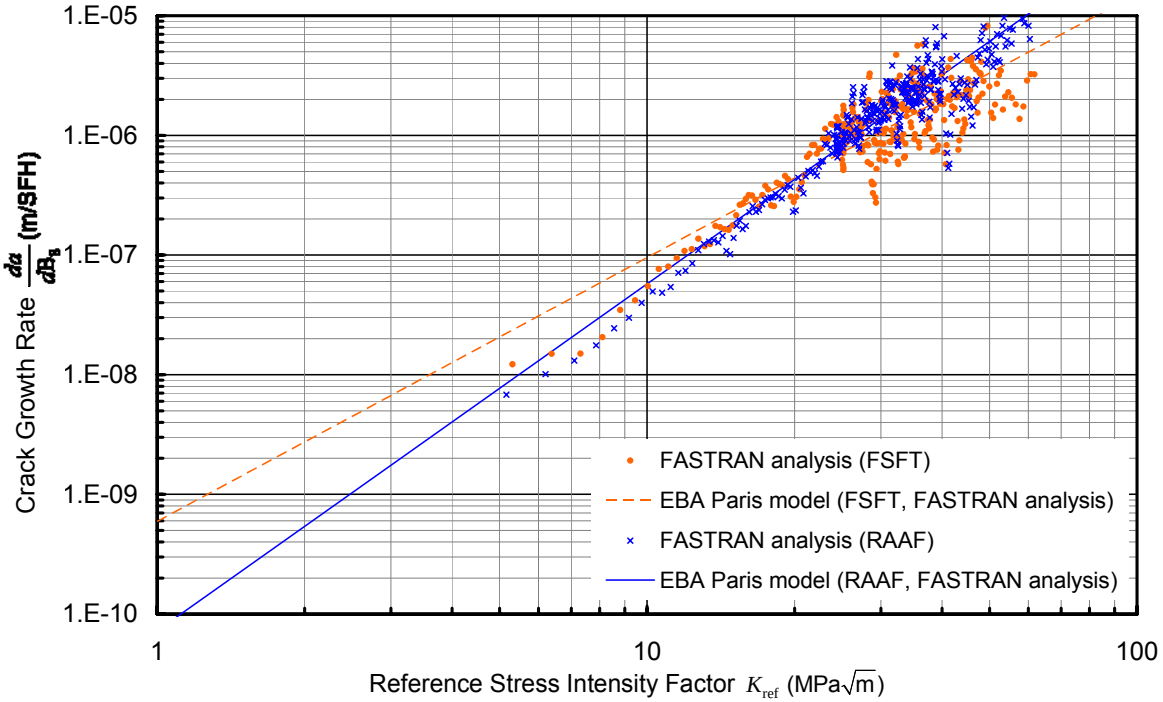

Figure 9: Crack Growth Rate data for FASTRAN Runs without smoothing

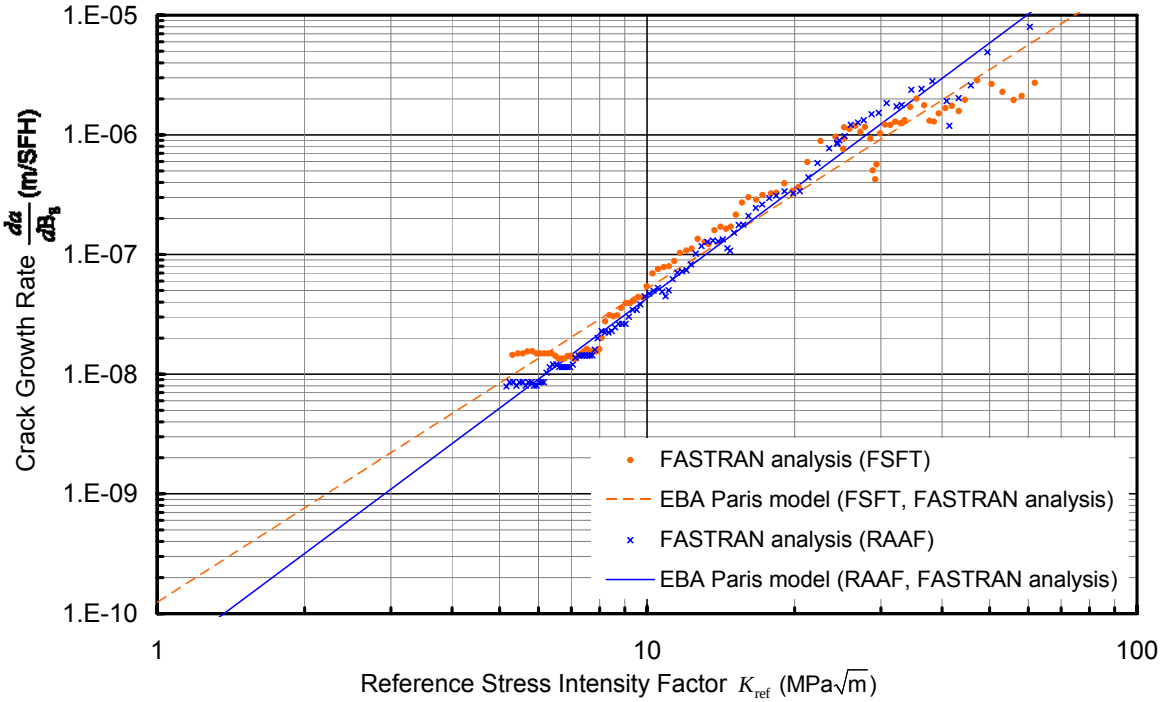

Figure 10: Crack Growth Rate data for FASTRAN Runs with smoothing

3.3.3 Determining $m_{2,E}$ and $C_{2,E}$ for the RAAF spectrum

The CGR for the RAAF spectrum was predicted using the EBA parameters evaluated from FASTRAN and the FSFT coupon data (See section 3.2). The three methods described in Section 2.2 were each used to generate a prediction. The experimental and the predicted CGRs are plotted in Figure 11.

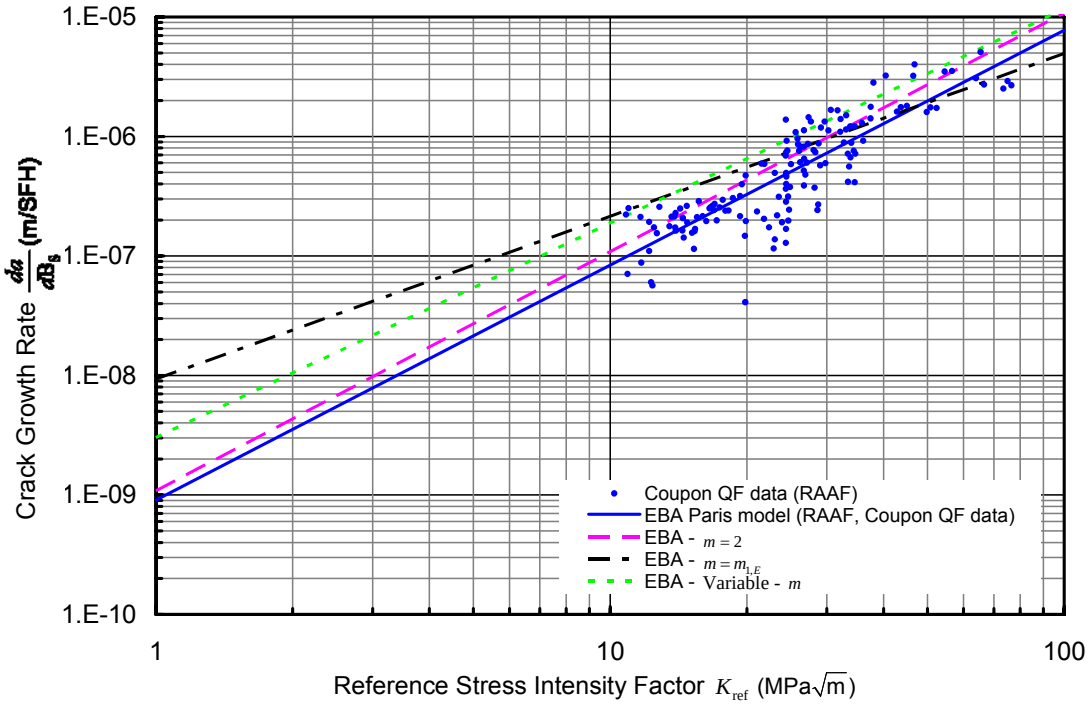

Figure 11: EBA prediction of the crack growth rate under the RAAF spectrum evaluated from the FSFT coupon crack growth data

Coefficients of determination were evaluated for each of the predictions and are presented in Table 1. The results indicate that method 1, which involved setting $m_{2,E}$ = 2, provided the highest correlation. The least-square fit of the RAAF coupon data is presented as a comparison for the predictions.

Table 1: EBA prediction of the crack growth rate parameters under the RAAF spectrum evaluated from the FSFT coupon crack growth data

Method	***m***	***C***	**R^2**
Least Squares fit	*1.966*	*9.052×10^{-10}*	*0.7362*
EBA - Method 1: $m = 2$	2.000	1.083×10^{-9}	0.7093
EBA - Method 3: Variable - m	1.793	3.021×10^{-9}	0.5993
EBA - Method 2: $m = m_{1,E}$	1.362	9.317×10^{-7}	0.5100

3.3.4 Prediction of crack growth under RAAF spectrum

The EBA constants for the RAAF spectrum were then used to predict the crack growth. Crack growth curves corresponding to the variable-m, $m_{2,E} = m_{1,E}$ and $m_{2,E} = 2$ approaches are plotted in Figure 12 along with experimental data and the least squares fit. The initial crack size used in this plot is that obtained using exponential extrapolation of the FSFT crack growth curve, i.e. 1.52×10^{-5} m. Figure 13 shows the same results on a linear scale. Figure 14 and Figure 15 show a similar comparison between the experimental data and the FASTRAN prediction.

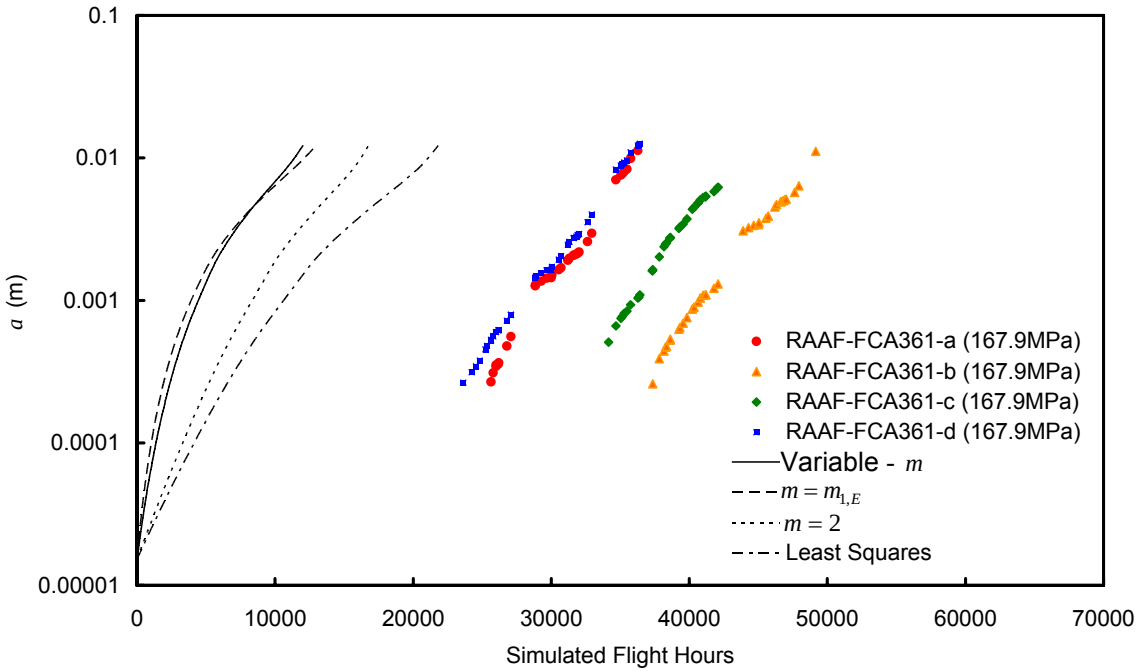

Figure 12: EBA prediction for the RAAF spectrum using an initial crack size of 1.52×10^{-5} m compared to the RAAF coupon data

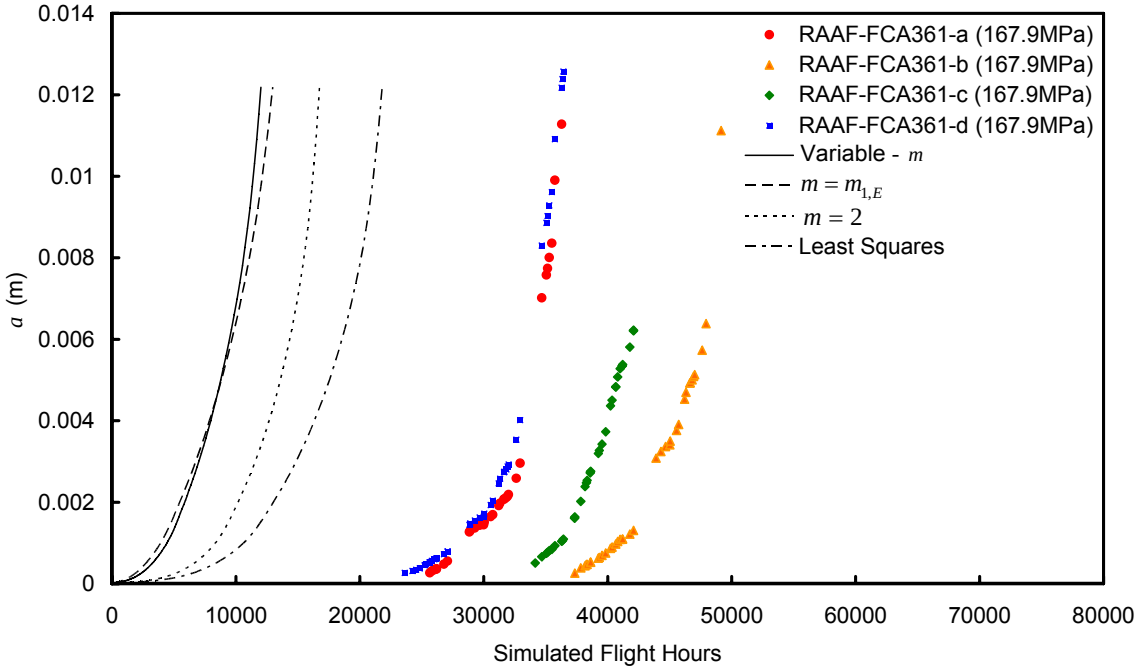

Figure 13: EBA prediction for the RAAF spectrum using an initial crack size of 1.52×10^{-5} m compared to the RAAF coupon data

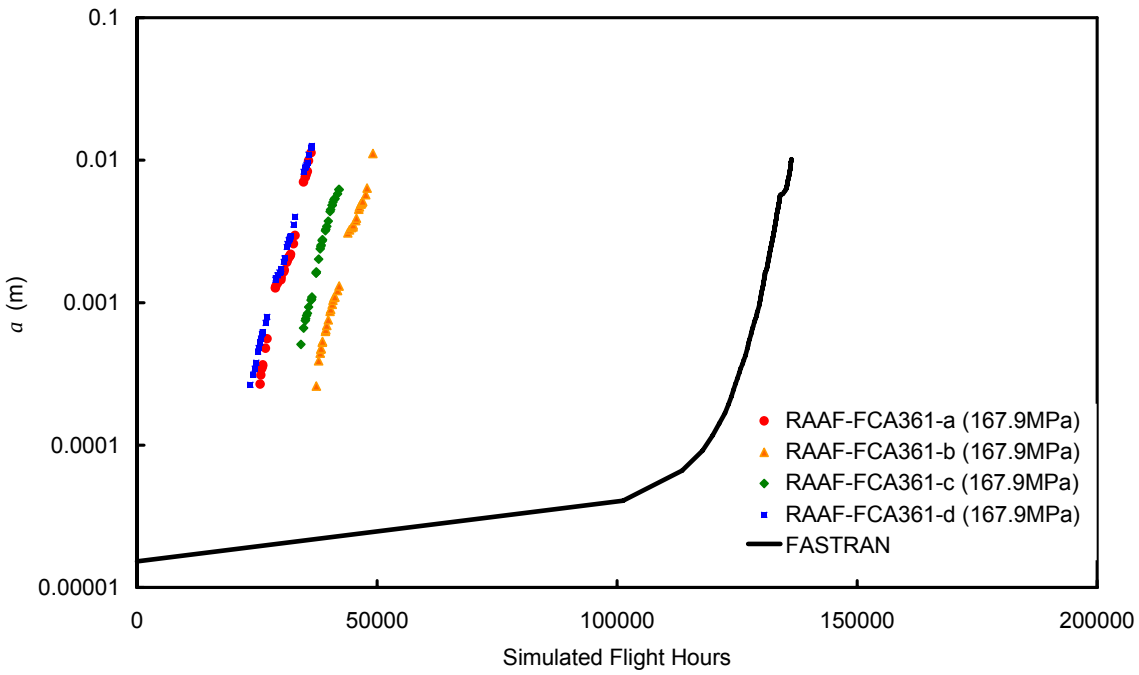

Figure 14: FASTRAN prediction for the RAAF spectrum using an initial crack size of 1.52×10^{-5} m compared to the RAAF coupon data

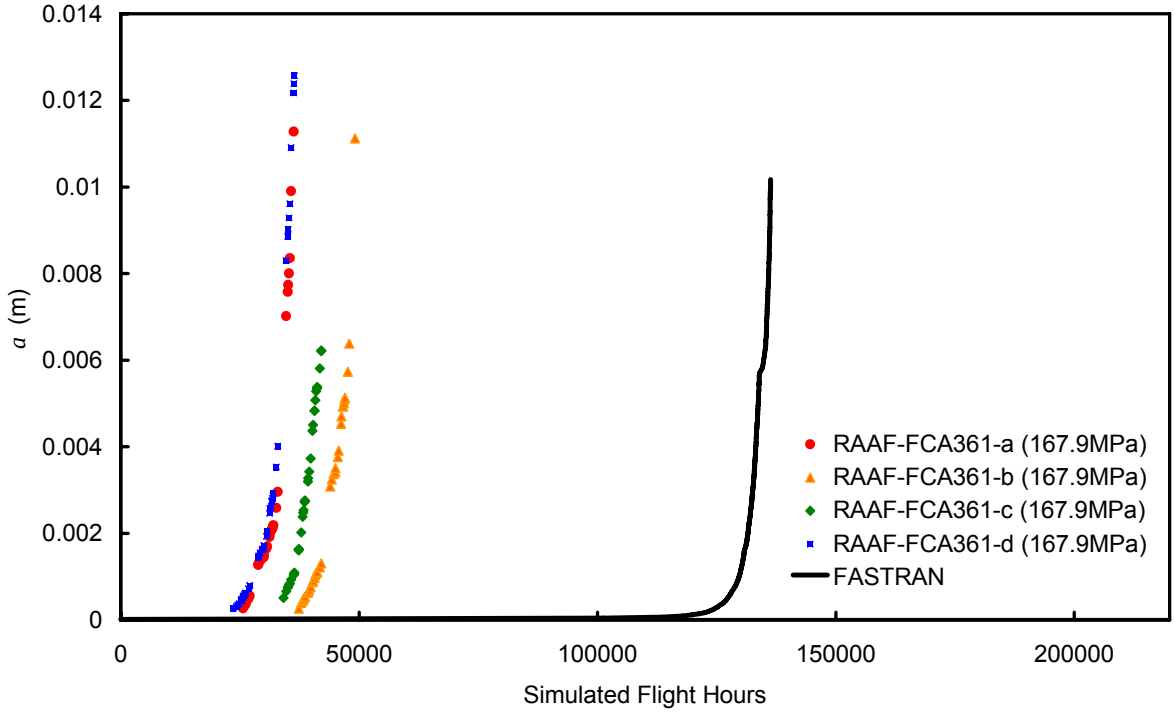

Figure 15: FASTRAN prediction for the RAAF spectrum using an initial crack size of 1.52×10^{-5} m compared to the RAAF coupon data

Table 2: Comparison of total life

	Total life (a_f = 10 mm) (SFH)	***Difference between the prediction and the RAAF coupon average (%)***
RAAF Coupon average	40986	
EBA - Method 1: $m = 2$	16312	60.2%
EBA - Method 2: $m = m_{1,E}$	12261.5	70.1%
EBA - Method 3: Variable - m	11502.7	71.9%
FASTRAN (RAAF spectrum)	136288	-232.5%

The predictions presented in Figure 12 to 15 demonstrate that in the case of the P-3C coupon data that both the EBA and FASTRAN solutions displayed poor correlation in terms of the crack growth curves below 0.5 mm and also in terms of the final life at a_f = 10 mm.

3.3.5 A comparison of inspection intervals

While the above analysis has compared the total crack growth life to a final crack length of a_f = 10 mm, this section seeks to compare the inspection intervals calculated using both FASTRAN and the EBA. The previous analysis has shown that modelling the initial stages of crack growth has resulted in poor estimates of the total life. A comparison of the inspection interval will provide an indication to the quality of the prediction in the final stages of crack growth when the crack is of sufficient size to be detectable.

The simulated flight hours between a crack first detected (a_{NDI}) with a length of 1.27 mm (a typical bolt hole eddy current size (Teunisse, Phillips et al. 2006)) and a final crack length of 10 mm has been recorded in Table 3. The final crack length was chosen based on the typical final crack length observed for the coupons. The percentage difference between each of the predictive methods is compared to the RAAF coupon data. As can be seen in this table, predictions of the inspection interval appear to be far more reliable than predictions of total life. In this particular case the EBA produced better results than FASTRAN. Method 1 produced the best estimate of the inspection interval.

Table 3: Comparison of total crack growth interval between 1.27 mm and 10 mm

	Life (1.27 mm – 10 mm) (SFH)	***Difference between the prediction and the RAAF coupon average (%)***
RAAF Coupon average	7444	
EBA - Method 1: $m = 2$	7401	0.6%
EBA - Method 2: $m = m_{1,E}$	7890	-6.0%
EBA - Method 3: Variable - m	6647	10.7%
FASTRAN (RAAF spectrum)	6009	19.3%

3.4 Outer Wing Lower Panel/Cap Splice

Finally, we attempt to apply the EBA to predict the crack growth in a real aircraft structure subjected to the FSFT spectrum. Quantitative fractography has been conducted on a crack located in the outer wing lower panel/cap splice at a location designated WS 220. During the testing of the wing fuselage FSFT article, a crack was found after 16,785 hours of FSFT cycling in panel 1 at WS 220. This crack, designated FCA361-CDN-4, was in the fastener that is common to the front spar cap and panel 1 splice.

The quantitative fractography conducted at the DSTO (Grummett and Goldsmith 2003), Figure 16, has been used here to examine the use of the EBA applied to a real problem. A log-linear extrapolation of the data was used to estimate an initial flaw size of 0.018 mm.

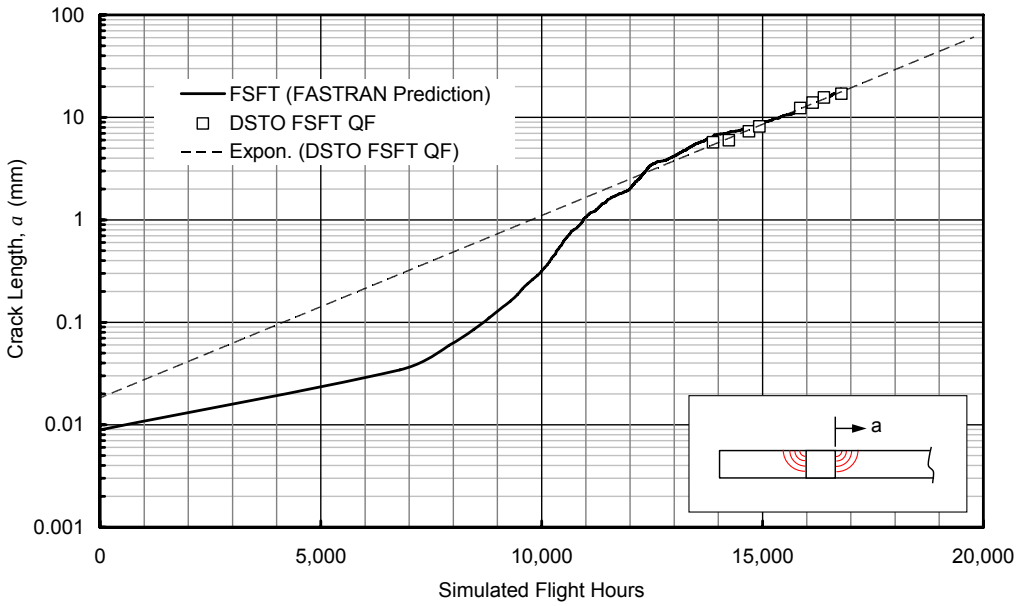

Figure 16: Log-linear extrapolation and a FASTRAN back prediction of the quantitative fractography obtained from crack FCA361-PSS-4

The beta factors solution shown in Figure 17 was originally developed by Lockheed-Martin evolving a corner crack through to a through crack for the relevant location of interest. This solution has been used in the P-3 test interpretation report DSTO-TR-1929 (Teunisse, Phillips et al. 2006).

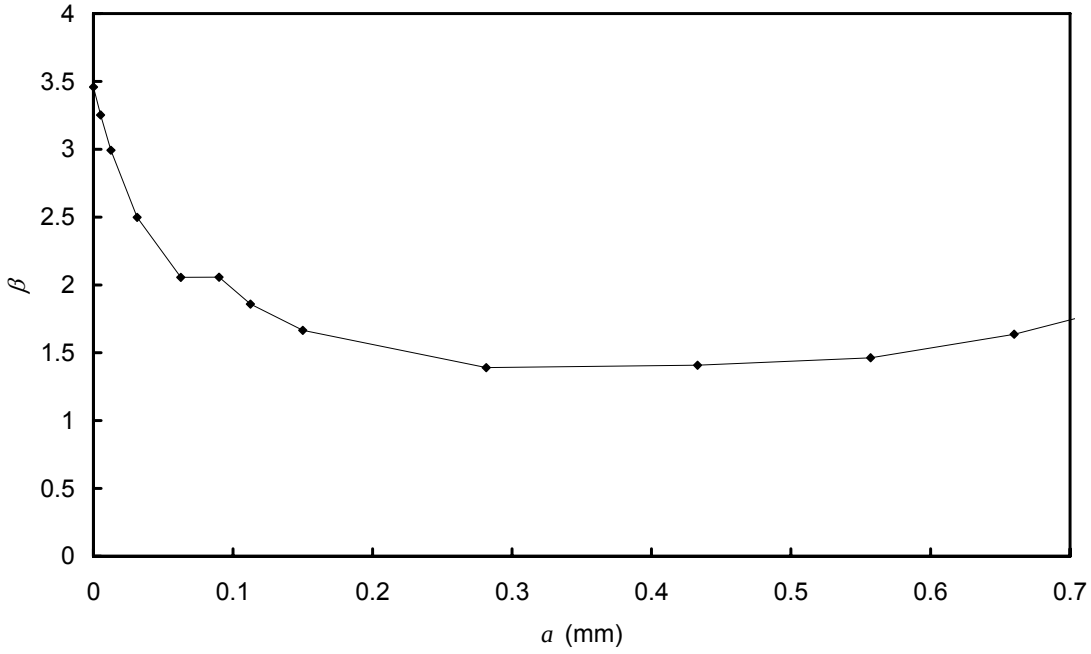

Figure 17: Outer wing lower panel/cap splice beta solution

The EBA crack growth parameters were evaluated using the quantitative factography data from FCA361-PSS-4 as shown in Figure 18.

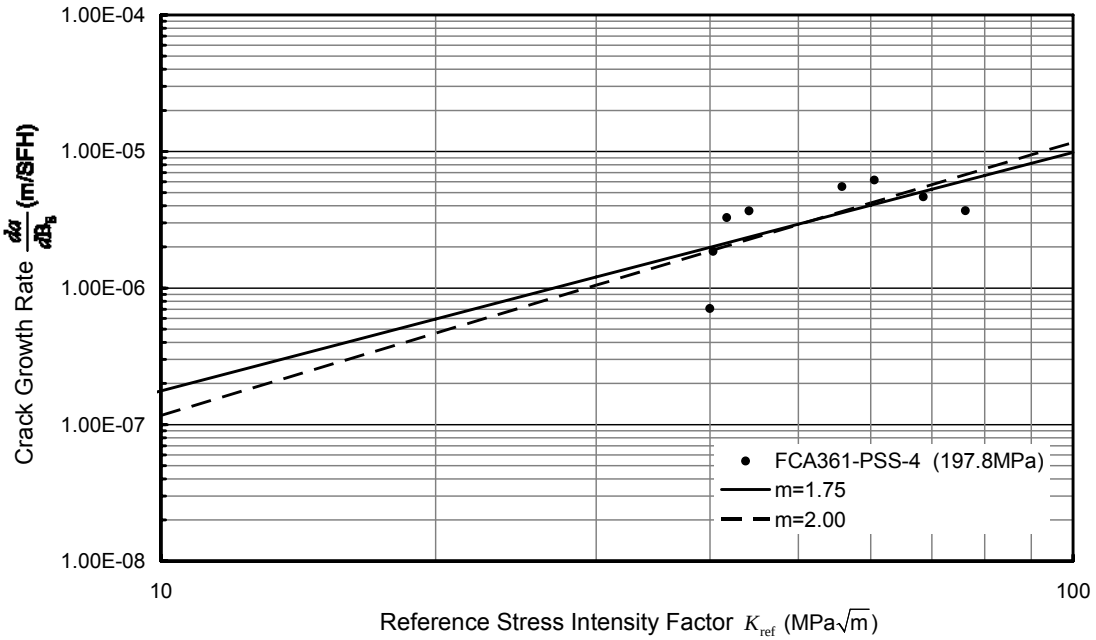

Figure 18: Crack growth rate evaluated from the FCA361-PSS-4 quantitative fractography data

Earlier work conducted by (Jackson and Amaratunga 2007) identified that a back prediction using the EBA in some cases produced unrealistic estimates of the initial flaw size. Following discussions (Zhuang and Molent 2007) advice was given to use log-linear back extrapolation to estimate the initial flaw size. In response to these discussions it was agreed that a log-linear back extrapolation produced reasonable estimates of the initial flaw size and should be used in conjunction with the EBA. If the exponent m is set to 2 and beta is kept constant we would expect to see a straight line on a log-linear scale in Figure 19. The EBA predictions presented in Figure 19 display significant curvature as the beta solution in Figure 18 is not constant and larger when the crack is small.

The EBA constants evaluated from the FCA361-PSS-4 quantitative fractography data and the coupon data were used to predict the crack growth from an initial flaw of 0.018 mm. These predictions were then compared to the original FCA361-PSS-4 quantitative factography data in Figure 19.

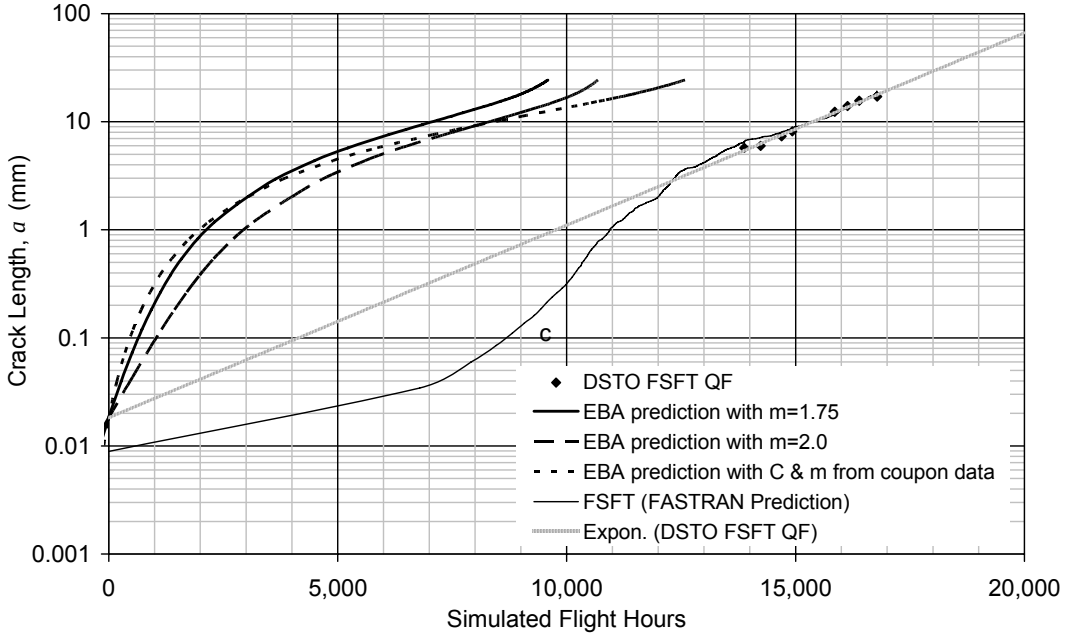

Figure 19: EBA predictions of a crack with an initial flaw size of 0.018 mm located at WS 220

A comparison of the total predicted life and the total life of FCA361-PSS-4 is presented in Table 4. Here a substantial difference is noted between the experimental data and the EBA prediction. The differences noted in Table 4 increase if we use an estimate of the initial flaw size based on exponential back extrapolation.

Table 4: Comparison of total life

	Total life (SFH a_f = 17 mm)	***Difference between the FSFT article and EBA predictions (%)***
FSFT article	16785	
EBA prediction with m = 1.75	8826	47.4%
EBA prediction with m = 2.00	10026	40.3%
EBA prediction with C and m evaluated from the coupon test data	11144	33.6%

If now we consider a crack growth interval instead of the total life we can peg the EBA predictions to the final crack length experimentally observed in Figure 19. Table 5 compares the crack growth interval between the first quantitative fractographic measurement at 13880 hours and the final quantitative factographic measurement at 16785 hours. As can be seen the results are slightly better for the EBA parameters predicted from the FCA361-PSS-4 data. However, there is significant uncertainty associated with these parameters due to the limited data set. A 95% confidence interval on the exponent $m_{2,E}$ indicates an uncertainty of ±2.13, which is significant in comparison with the estimated exponents. In terms of the crack growth

interval between 5.7 mm and 17 mm the original P-3 SLAP FASTRAN prediction provides the best result.

Table 5: Comparison of crack growth intervals between 5.7 mm and 17 mm

	Life (5.7 mm - 17 mm) (SFH)	***Difference between the FSFT article and EBA predictions (%)***
FSFT article	2905	
EBA prediction with $m = 1.75$	3606	-24.2%
EBA prediction with $m = 2.00$	3642	-25.4%
EBA prediction with C and m evaluated from the coupon test data	5279	-81.7%
FASTRAN	3030	-4.3%

4. The EBA Evaluation using F-111 LITV Coupon Data

This section further evaluates the EBA using F-111 coupon data for coupons manufactured from 2024-T851 aluminium alloy. A similar procedure to the one used in the previous section is used here to examine whether the CGR could be represented by the EBA and whether the model parameters could be transferred to an untested spectrum. The effect of small scale yielding is also investigated.

4.1 F-111 loads interpretation and truncation validation coupon test data

The recent loads interpretation and truncation validation (LITV) test program yielded quantitative fractographic data for several load spectra. A draft report (Diab and Goldsmith 2007) of the program was made available to aid the assessment of the EBA. On a critical assessment of the fractography data it became clear that the LITV program experienced technical difficulties during the test. These difficulties resulted in the rejection of the results from a significant number of coupons. While sufficient data were obtained for the primary objective of the LITV program, only a small amount of data is useful for the assessment of the EBA.

Table 6 lists the data sets that were considered valid for the evaluation of the EBA, although these data have been rejected by the LITV program, on the basis that the old test controller used on these tests was not able to reach the nominal load. But assuming that the problem with the old controller was systematic, hence the error in the peak load achieved was systematic, these data would still be valid for the evaluation of the EBA. In the present analysis the reference stress is defined as the peak stress in the spectrum, as listed in Table 6, although it should be understood as nominal, given the technical difficulties experienced by the test controller.

Table 6 Summary of experimental data rejected by LITV program, but included in EBA evaluation[2]

Data set designation	Reference stress
R4(FL3), R5(FL3)	218.9MPa
R6(FL4), R7(FL4), R8(FL4), W7(FL4)	240.7MPa
T1(FL5), T2(FL5), T3(FL5)	196.7MPa
T4(FL6), T4(FL6)	218.9MPa
U1(FL7), U2(FL7), U4(FL7)	240.7MPa
U5(FL8), U6(FL8), U7(FL8)	196.7MPa

The coupons used in the LITV coupon test program were double edge notch tension specimens with a stress concentration factor of K_{tn} = 2.5, to simulate a generic location on the

[2] The F-111 data sets are designated as a combination of specimen ID plus load spectrum ID, *e.g.*, R4(FL3) indicates that specimen "R4" subjected to spectrum FL3. Detailed description of the specimens and the spectra are given in (Diab and Goldsmith, 2007).

lower skin surface of an F-111 wing. The coupons are identical to those used for the F-111 relative severity coupon test program, and further details are available in Ord (2004).

For the calculation of the reference stress intensity factor, the boundary correction factors developed by (McDonald 2006) have been used here. This solution was obtained for a corner crack that transitions to a through-thickness crack. No attempt has been made to assess the validity or quality of this solution.

4.2 The EBA's Ability to Model the F-111 LITV Coupon Test Data

In order to evaluate the ability of the EBA to model the LITV data, it was desirable to have data at several load levels. This permitted the assessment of the EBA to model the data at a particular stress level and the examination of the effect of the peak stress of the spectrum on the model parameters. The selected LITV data were obtained from two spectra with three stress levels. The spectra considered are based on the F-WELD test spectrum at FASS 226 (Diab and Goldsmith 2007).

4.2.1 The EBA applied to the F-111 LITV coupon test data

To examine the ability of the EBA to model the test data and establish the possible independence of the CGR parameters C and m on the applied reference stress, a comparison of CGR versus the reference stress intensity factor at several scaling stress levels was performed. A statistical analysis of the data has been conducted to examine the log-linearity of the crack growth data and can be found in Appendix A. The statistical analysis of the experimental data in Appendix A indicates that all the regression curves are essentially the same within experimental scatter. The results indicate that a linear regression of the data is a satisfactory approximation, supporting the Paris-type model used in the EBA. The analysis also demonstrates that within experimental uncertainty, increasing or decreasing the reference stress by 10% does not significantly alter the observed CGRs.

The fatigue CGR data for FL3, FL4 and FL5 spectra have been plotted in Figure 20 along with prediction intervals (see Appendix A for an explanation of the "prediction interval") associated with the regression analysis of these load spectra. This figure provides further confidence that one regression analysis is sufficient to predict CGRs for future measurements with 95% confidence.

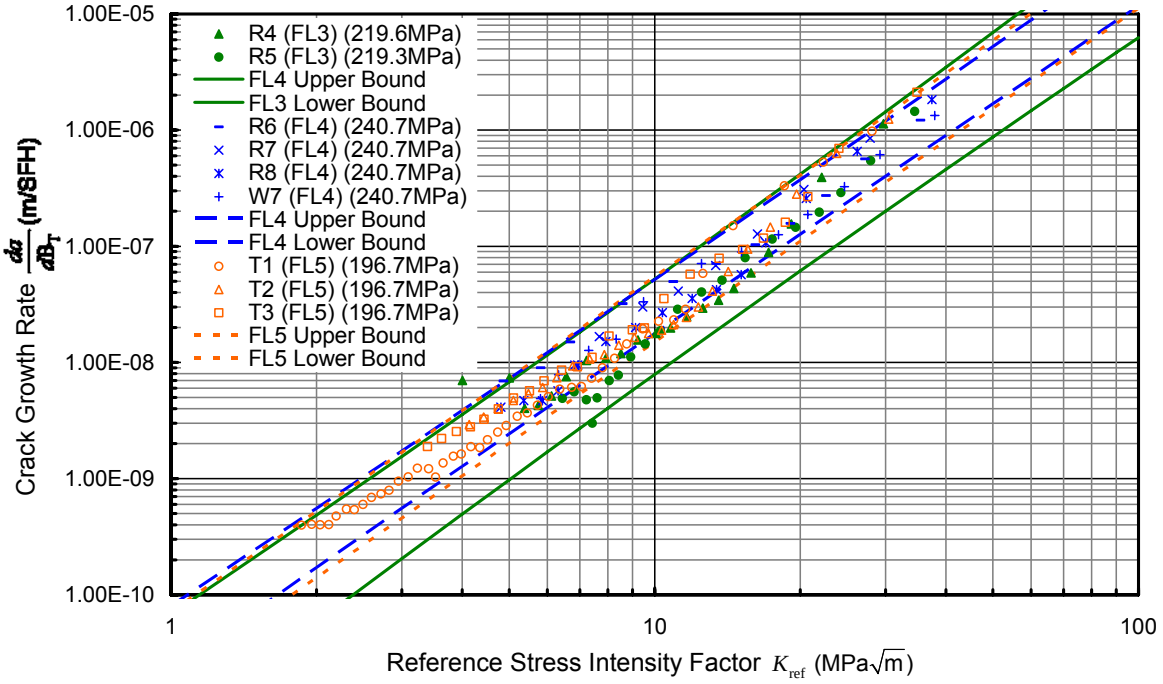

Figure 20: Prediction intervals (upper and lower limits) for FL3, FL4 and FL5 crack growth rate data sets

Accepting that increasing or decreasing the applied reference stress by 10% does not affect the CGR parameters C and m then pooling all the data allows us to reduce the error in C and m to yield more representative estimates for C and m. The results are presented in Table 7.

Table 7. Pooled Crack Growth Constants for the F-WELD test spectra

Spectra	*m*	*Uncertainty in m*	*ln(C)*	*Uncertainty in ln(C)*	*R^2*	*No. of Coupons*
FL3,FL4,FL5	2.87	0.08	-24.05	0.18	0.9659	9

Analysis was also conducted for the FL6, FL7 and FL8 spectra. The fatigue CGR data for FL6, FL7 and FL8 spectra have been plotted in Figure 21 along with prediction intervals associated with the regression analysis of these load spectra. Despite the different slope of the regression through the FL6 data, reasonable agreement between all three data sets can be observed in the region of $1< K_{ref} <100$.

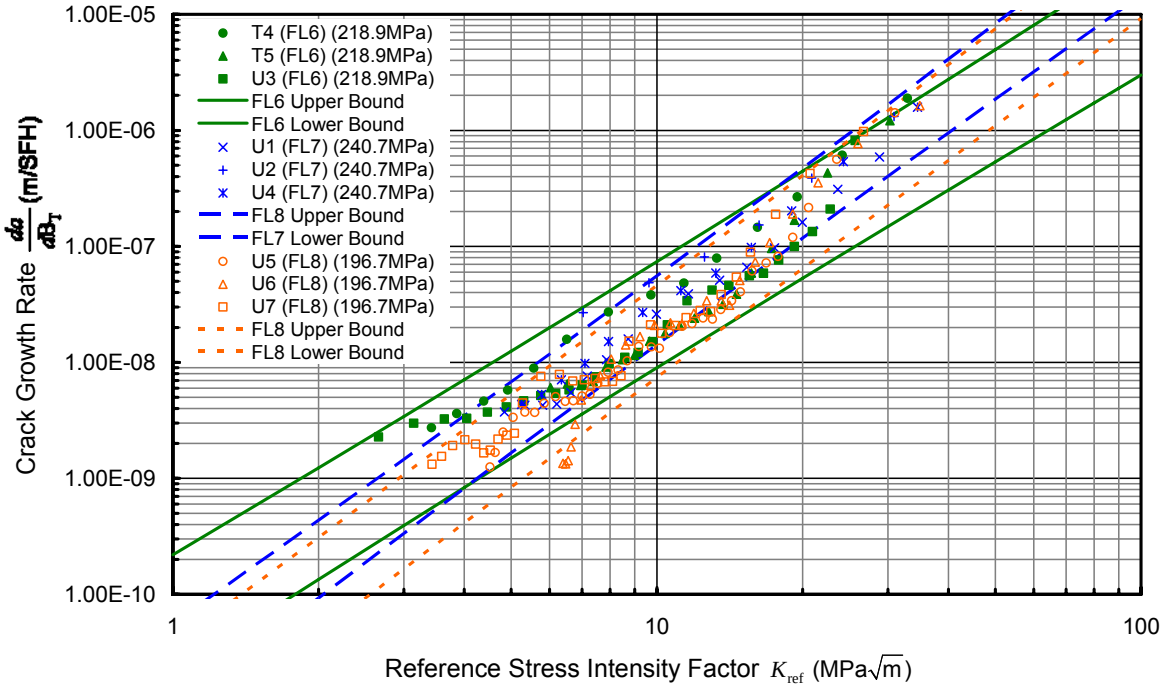

Figure 21: Prediction intervals for FL6, FL7 and FL8 crack growth rate data sets

Similarly accepting that increasing or decreasing the applied reference stress by 10% does not affect the CGR parameters C and m then pooling all the data together yields new improved estimates for C and m. The results are presented in Table 8.

Table 8. Pooled Crack Growth Constants for the discriminated F-WELD test spectra

Spectra	*m*	*Uncertainty in m*	*ln(C)*	*Uncertainty in ln(C)*	R^2	*No. of Coupons*
FL6,FL7,FL8	2.94	0.13	-24.05	0.31	0.9116	9

4.2.2 The small scale yield (SSY) criterion applied to the LITV coupon test data

An overview of the SSY criterion is presented in Appendix B. The load spectra most likely to violate SSY conditions due to the Cold Proof Load Test† (CPLT) were FL4 and FL7, both scaled up by 10% from the baseline value. See (Diab and Goldsmith 2007) for an description of the test procedure. Table 9 shows an example of the criterion applied to coupon R6 in the form of Eqn. (B3) in Appendix B, where if $\rho/a \le 0.5$ then SSY conditions are satisfied.

† The CPLT is a periodic proof loading program performed on the F-111 (nominally conducted every 2,000 aircraft flight hours) to confirm the absence of any flaws in the D6ac steel structure above a very small critical size. The aircraft is cooled in a special environmental chamber to -40°C (-40°F), which reduces the fracture toughness of the D6ac steel structure.

Table 9. The SSY plane stress criterion applied to the R6 coupon test data

SFH	a (mm)	K (@ CPLT) MPa√m	K (@ max nom) MPa√m	ρ (@ CPLT) mm	ρ (@ max nom) mm	ρ/a (@ CPLT)	ρ/a (@ max nom)
2000	0.038	4.71	3.04	0.044	0.018	1.17	0.49
4000	0.054	5.62	3.63	0.063	0.026	1.16	0.48
6000	0.073	6.48	4.18	0.083	0.035	1.14	0.48
8000	0.124	8.31	5.36	0.137	0.057	1.11	0.46
10000	0.206	10.57	6.82	0.222	0.092	1.08	0.45
12000	0.324	12.97	8.37	0.335	0.139	1.03	0.43
14000	0.494	15.62	10.08	0.486	0.202	0.98	0.41
16000	0.745	18.46	11.91	0.678	0.282	0.91	0.38
18000	1.149	21.87	14.11	0.952	0.396	0.83	0.34
20000	1.928	26.34	16.99	1.380	0.574	0.72	0.30
22000	3.717	34.31	22.13	2.342	0.974	0.63	0.26

As can be seen in Table 9, the application of the CPLT load violates the SSY for much of the fatigue life of the coupon. This is true for all the coupons tested. The maximum nominal load in the test spectra was also examined to evaluate compliance with SSY conditions. Flight spectra applied at a nominal level and with a scaling of -10% conformed to SSY conditions. In the cases where the nominal stress level of the test spectra was raised by 10% a significant proportion of the test cases came close to violating the SSY conditions.

Despite some of the loads violating SSY conditions the application of the EBA to the data appears to be satisfactory. Log-linearity of the CGR curves does not appear to be significantly effected. Therefore, it would be reasonable to assume that the effects of SSY are sufficiently accounted for in the CGR parameters evaluated with the EBA.

4.3 Crack Growth Rate Predictions Using the EBA

The LITV coupon test program provided quantitative fractography data for coupons tested under several load spectra. Unlike in the previous sub-section, all the coupon crack growth data in the following sections were obtained with the new digital test controllers and deemed valid for the LITV coupon test program (Diab and Goldsmith 2007). Data obtained on the old analogue test controllers were not considered in the following analysis. As such four separate spectra comparisons have been conducted in the following section.

Shown in Table 10 is a list of the data sets used to evaluate the predictive ability of the EBA. Here, spectrum 1 represents the spectrum for which C and m were determined from experimental quantitative fractography data and spectrum 2 is the spectrum for which we want to predict the new C and m and compare them to the experimental data.

Table 10: The cases considered to examine the EBA's predictive capability

Case	*Spectrum 1 (Measured)*	*Spectrum 2 (Predicted)*
1	FL10	FL1B
2	FL1B	FL10
3	FL11	FL2B
4	FL2B	FL11
5	FL10	FL3
6	FL3	FL10
7	FL15	FL14
8	FL14	FL15

Table 11 relates the spectrum ID used in this report to the actual spectrum and its location on the aircraft (Diab and Goldsmith 2007). Table 11 also provides an indication to the amount of data collected for each of the spectra and used in the subsequent predictions.

Table 11: The experimental data available for the comparisons

Spectrum ID	*Spectra*	*Location*	*No. Coupons*	*No. Data Points*
FL1B	A15-5	FASS 226	4	67
FL10	D20	FASS 226	6	156
FL11	A15-5	FASS 281	4	22
FL2B	D20	FASS 281	6	102
FL3	F-WELD	FASS 226	3	101
FL14	F-WELD	CSS 135	4	66
FL15	D20	CSS 135	4	194

Appendix C contains results for an EBA analysis of the comparisons in Table 10. Included in Appendix C are figures that compare the quantitative fractography data and FASTRAN predictions for the crack growth rate. The eight cases considered here predominantly show that the variable-m approach provided the best correlation, followed very closely by the $m_{2,E} = m_{1,E}$ approach, as detailed in Table 23 to 30 in Appendix C. This result is not unexpected. If we examine Eqn. (12), which defines the variable-m approach, we see that the $m_{1,P}$ exponent evaluated from spectrum 1 using FASTRAN is subtracted from the $m_{2,P}$ exponent evaluated from spectrum 2 using FASTRAN. In all the cases considered here FASTRAN produced similar slopes, as seen in the figures in Appendix C. Hence, we have $m_{2,P} = m_{1,P}$, which leads to $m_{2,E} = m_{1,E}$ according to Eqn. (12). Thus, for the cases considered here the two methods, variable-m and $m_{2,E} = m_{1,E}$ approaches are very similar.

4.4 F-111 Fatigue Crack Growth Predictions Using the EBA

In the previous section, the EBA CGR constants were derived for a new spectrum for which we have no experimental crack growth data. In this section we will use those constants to predict fatigue crack growth and compare the result with quantitative fractography coupon data. As in the case of P-3C in Section 3.3, the prediction of a crack growth curve involves the further complication of estimating the effective initial flaw size (EIFS). In this report the EIFS refers to an estimate of the initial flaw based on a model back projection. The model used here

is the Paris law implementation of the EBA. The determination of the EIFS is consistent with that of (Potter and Yee 1982) except in the P-3C case studied earlier where this method did not generate reasonable values. In this case other methods were explored. A description of the methodologies used to estimate the EIFS is presented in the next section.

4.4.1 Estimating the effective initial flaw size

In practice, experimental data exists for crack growth under a tested spectrum, spectrum 1. As such an estimate of the EIFS can be evaluated from these data. To make a fatigue crack growth prediction under an untested spectrum, spectrum 2, an inference must be made with relation to the EIFS. In the advocated EBA methodology (McDonald, Molent et al. 2006), EIFS is theorized as being dependent upon the material condition and independent of the applied spectrum, stress and K_t. This conjecture has some support from the F/A-18 coupon test programs. In the absence of experimental data from which to estimate the EIFS under spectrum 2 an EIFS must be evaluated from spectrum 1 and assumed to be the same for spectrum 2. This approach presents several problems. Evaluating the EIFS via the EBA may produce estimates of the EIFS that are dependant on the spectrum. Further complications arise if the flaw distribution in the area of interest differs significantly from the flaw distribution from which the experimental data was derived.

Without knowledge of the associated flaw distributions in the 2024-T851 etched aluminium specimens, estimates of the EIFS were made from the available experimental data under spectrum 1 and used to predict fatigue crack growth under spectrum 2.

EBA constants were evaluated for each individual crack growth curve obtained under spectrum 1. These constants were used to back predict the initial flaw size from the final crack length using the IntegrateParis macro in Excel (McDonald, Molent et al. 2006). The Paris based model in the macro does not include the influences of fracture toughness on the final crack growth. As a result, using IntegrateParis to back predict the crack growth from the final crack length back to the initial flaw size will over predict the true initial flaw size, as is illustrated in Figure 22.

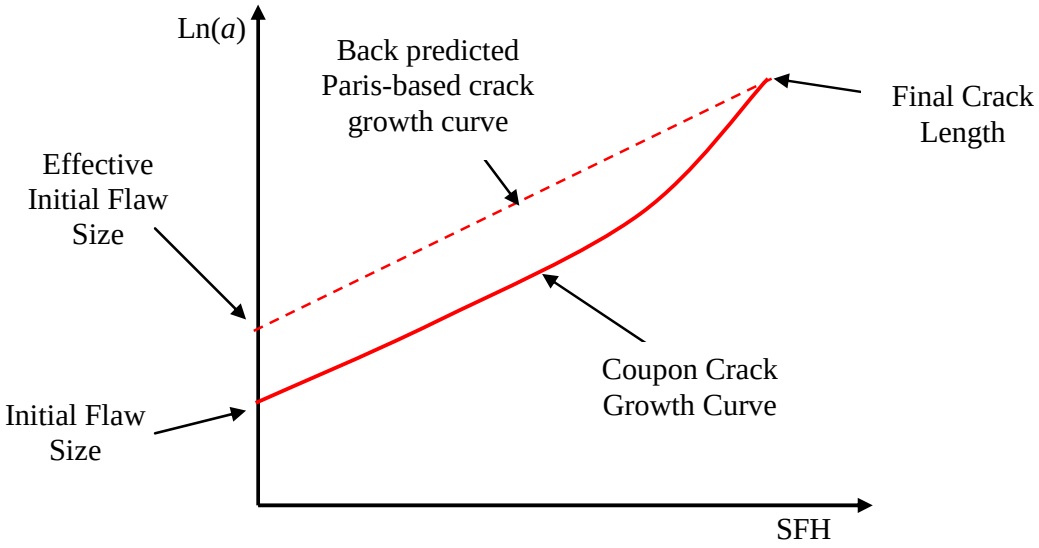

Figure 22: Crack growth back prediction using a Paris-based model without a correction for the influences of fracture toughness on the final crack growth

McDonald (McDonald, Molent et al. 2006) used the following technique to improve the prediction by applying a correction to the back predicted crack growth curve. This correction was in the form of an additional block offset evaluated through a least squares fit. If the prediction matches the experimentally observed crack growth life then the offset will be zero. If it does not the addition of an offset will allow the evaluation of an EIFS that will best predict the experimentally observed fatigue crack growth life.

$$Life_{\text{Exp}} = Life_{\text{Predicted}} + Life_{\text{offset}} \tag{14}$$

Let

$$Q = \sum \left(Life_{\text{Exp}} - Life_{\text{Predicted}} - Life_{\text{offset}} \right)^2 \tag{15}$$

To minimise Q we set the partial derivative of Q with respect to $Life_{\text{offset}}$ to zero.

$$\frac{\partial Q}{\partial Life_{\text{offset}}} = 2\sum \left(Life_{\text{Exp}} - Life_{\text{Predicted}} - Life_{\text{offset}} \right) = 0 \tag{16}$$

$$nLife_{\text{offset}} = \sum \left(Life_{\text{Exp}} - Life_{\text{Predicted}} \right) \tag{17}$$

$$Life_{\text{offset}} = \frac{\sum Life_{\text{Exp}} - \sum Life_{\text{Predicted}}}{n} \tag{18}$$

Using Eqn. (18) we can find the crack growth curve that best fits the experimental observations using the previously evaluated EBA constants. Thus Eqn. (18) can be used to improve the estimate of the EIFS.

Several spectrums have been considered here. For each spectrum, data for several crack growth curves exists. Using these curves an estimate of the initial flaw size can be established using the above technique. Thus we can obtain a mean EIFS for each individual spectrum.

As the same coupons were used for all the tests conducted it is reasonable to consider the possibility that the EIFS is spectrum independent. If the EIFS is spectrum independent then it would be reasonable to establish one estimate of the EIFS based on the mean of all the EIFS evaluated for each crack growth curve. But to do this we must first establish that the mean EIFS for each individual spectrum is independent of the spectrum. To assess the independence of the EIFS to the applied spectrum, a one-way analysis of means was performed to assess the possibility that means are the same. The R programming environment was used to implement the one-way analysis. The following output was obtained:

```
        One-way analysis of means (not assuming equal variances)

data:  aini and fspec
F = 4.984, num df = 6.000, denom df = 9.182, p-value = 0.01556
```

The one-way analysis is similar to analysis of variance, but does not assume that variances are equal between groups of data. The p-value indicates that we are only 1.6% confident that the mean EIFS for each individual spectrum is the same. Thus, the present data indicates a possible dependence on the spectrum. Further analysis involving the EBA in this report will use individual EIFSs for each of the spectra. Presented in Figure 23 are all the individually evaluated EIFS plotted against the spectra. The mean is presented with error bars that represent one standard error.

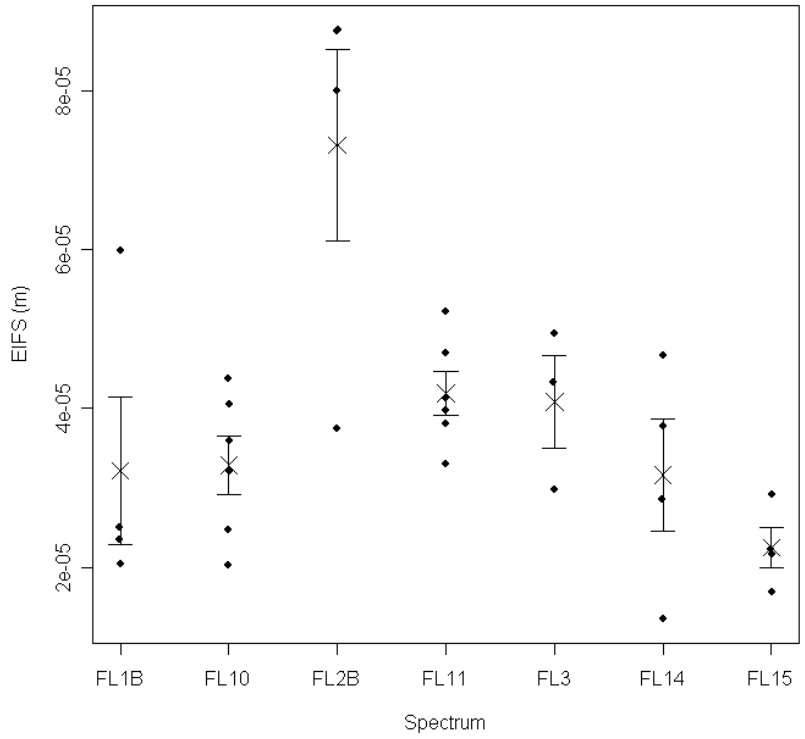

Figure 23:Estimates of the EIFS against the spectrum

Presented in Table 12 are the mean EIFSs evaluated for each tested spectrum considered in the analysis. The number of specimens used in the evaluation of the EIFS is also given.

Table 12: The average EIFS for each spectrum evaluated from the QF coupon test data

Spectrum ID	***No. Coupons***	***EIFS (meters)***	***Standard Deviation***
FL1B	4	2.96×10^{-5}	1.15×10^{-5}
FL10	6	3.15×10^{-5}	1.12×10^{-5}
FL11	6	3.58×10^{-5}	1.66×10^{-5}
FL2B	4	7.91×10^{-5}	7.66×10^{-5}
FL3	3	3.51×10^{-5}	1.07×10^{-5}
FL14	4	2.64×10^{-5}	3.54×10^{-6}
FL15	4	2.12×10^{-5}	5.60×10^{-6}

The mean EIFSs in Table 12 have been used in conjunction with the EBA to make predictions of fatigue crack growth and are presented in Appendix D.

4.4.2 Crack growth predictions

The initial flaw sizes evaluated in the previous section and the CGR constants evaluated in section 4.3 were used to predict the crack growth under spectrum 2. The actual calculation was carried out using the IntegrateParis macro in Excel spreadsheet. Crack growth curves have been obtained for each of the three approaches detailed in Section 2.2 used to evaluate the CGR constants. The predictions have been plotted in Figure 46 ~ Figure 60 in Appendix D, together with the experimental crack growth data for comparison. Also plotted in Appendix D is a crack growth curve using the CGR constants evaluated with a least squares fit of the crack growth data we are trying to predict. This curve provides the best possible prediction we can expect from this approach. The coefficients of determination for each of the predicted curves in Appendix D have been evaluated and presented in Table 13.

Table 13: Coefficients of determination evaluated between the predicted crack growth and experimentally observed crack growth

Prediction	***EBA***			***FASTRAN***	***Least Squares***
	Variable-m	***m* = $m_{1,E}$**	***m* = 2**		
FL1B predicted from FL10	0.8707	0.8458	0.8077	0.5402	0.8318
FL10 predicted from FL1B	0.6796	0.6468	0.5991	0.5190	0.8623
FL11 predicted from FL2B	0.6258	0.6209	0.5882	0.5101	0.6267
FL2B predicted from FL11	0.5911	0.5752	0.7876	0.5190	0.8454
FL10 predicted from FL3	0.7272	0.7659	0.7154	0.5322	0.8161
FL3 predicted from FL10	0.8771	0.9217	0.8218	0.5190	0.9161
FL14 predicted from FL15	0.6685	0.6356	0.6504	0.5205	0.8219
FL15 predicted from FL14	0.6071	0.5766	0.5800	0.5449	0.9110

In five of the eight cases the variable-m approach used to evaluate the CGR constants C and m produced the highest correlation, as can be seen in Table 13. It must be noted that the least-square result is not a prediction; it is a representation of the spectrum we are trying to predict. It uses C and m values determined from the data set we are trying to predict and the EIFS from the original data set we are using for our prediction. Thus, we expect in the majority of cases the least squares approach will yield the highest correlation for all the cases considered. This provides us with an estimate of the best prediction we can expect from the EBA.

For the case in which crack growth under the FL11 load spectrum was predicted from the FL2B load spectrum, Figure 53 we see that the least-square coefficient of determination is significantly smaller. This has resulted from the estimate of the initial flaw size evaluated from the FL2B crack growth data set. If the effective initial flaw size evaluated through the method described in Section 4.4.1 is spectrum-dependant then this result may indicate potential problems in predicting crack growth. However, only a small amount of data was obtained for crack growth under the FL2B load spectrum. Further testing is required to ascertain the validity of the initial flaw size under these spectra.

The EIFSs were evaluated by determining the mean value based on a normal distribution of predicted initial flaw sizes from the spectrum crack growth data. Evidence exists to support the view that initial flaw sizes are distributed log normally (Molent and Sun 2006). If that is

the case, then the initial flaw sizes used in the present analysis should conservatively estimate the actual mean initial flaw size. Therefore crack growth predictions should also be on the conservative side.

5. Discussion

The aim of this investigation was to evaluate the EBA described in McDonald (2006) and McDonald, Molent et al. (2006) using P-3C and F-111 crack growth data. The following issues have been investigated: (1) whether the EBA was able to represent the experimental data adequately for a given spectrum at a given stress level; (2) whether this representation is independent of the stress level for a given spectrum; (3) whether this representation can be transferred reliably to an untested spectrum. This investigation has shown that the EBA has clear potential in lifing the F-111, but it demonstrated difficulty in lifing the P-3C. In the following, we discuss these difficulties in detail.

5.1 Representation of the Experimental Data by the EBA

While the EBA was able to represent the F-111 crack growth data with good correlation, the application of the EBA to the P-3C data was not so successful. For F-111 spectra, the CGR, da/dB, was approximately linear on a log-linear scale when plotted against the reference stress intensity factor. More importantly, it appears that the model parameters were independent of the stress level.

With the application of CPLT loads in the F-111 sequences many of the loads came close to or exceeded SSY conditions if plane stress is assumed. If plane strain is assumed then the CPLT loads are not large enough to violate the SSY condition. In reality the stress state is between plane stress and plane strain. If SSY conditions were indeed violated then this could have significant implications when applying an LEFM model to the F-111. However, the present results seem to support the application of the EBA. In the present analysis the CGR has been evaluated in terms of blocks. It was shown in Sections 1 and 2 that crack growth data plotted in terms of crack growth per block versus the reference stress intensity factor approximated a linear relationship. From this we might draw the conclusion that any large plastic zone formation or small scale tearing that might occur, behaves in a self similar[‡] mode. Or any deviations from self similarity are small with relation to the total crack growth per spectra block. In either case the CGR constants C and m evaluated in terms of crack growth per spectra block must include these effects. Hence, the application of the EBA still appears to be suitable.

Difficulties were encountered in the application of the EBA to the large spectrum block sizes of P-3C spectra (less than two blocks over the crack growth history for the examples used here). This investigation highlighted several issues in this regard:

- To obtain adequate CGR data the block must be subdivided.
- Subdivision of the block assumes that the damage potential of each sub-block is approximately equivalent.

[‡] Self similarity is a mathematical term to describe something that looks “roughly” the same at any scale.

- The CGR data based on sub blocks displayed a higher level of scatter than did the F-111 CGR data based on blocks. As indicated by the higher coefficient of determination evaluated for the cases involving the F-111

In comparison to the F-111 and F/A-18 CGR curves, the P-3C spectra showed significantly increased scatter in CGR measurements per sub-block as opposed to the CGR per block for the F-111 and F/A-18. This indicates a possible violation of the assumption that each sub-block has the same damage potential. The effect of increased scatter due to subdividing spectra is discussed in Gallagher (1976). Increasing the sub-block size could help to minimise scatter, however the number of points available to construct a CGR curve would also be reduced. The consequence of increased scatter in the CGRs leads to increased uncertainty in the EBA constants. Differences in the subdivided blocks could also lead to non-linearity of the CGR curve.

Another source of scatter in the CGR data comes from DCPD measurements. Some doubt could be placed on the accuracy of the results at very small crack sizes. A coupon test program that measures both DCPD and fractography data is needed to resolve this issue. The fractography data may also be able to measure smaller crack sizes, thus aiding analysis at small crack sizes. A coupon test program is being planned to explore both these issues.

While estimates of total life using the P-3C coupon data did not yield solutions with high accuracy, the period between a_{NDI} and the final crack length appeared to produce much better results. Further coupon testing with other spectra may be needed to confirm this observation.

5.2 Stress Level Sensitivity

One point of interest in the application of the EBA is the effect of a change in the scaling stress (maximum stress) on the CGR parameters. The data in the LITV coupon test program offered the opportunity to investigate this aspect. Fatigue crack growth data for the F-WELD spectra at FASS 226 was recorded at a nominal scaling stress, a scaling stress increased by 10% and a scaling stress decreased by 10%. Comparison of regression lines through the CGR versus K_{ref} data appears to support the notion that increasing or decreasing the scaling stress does not appreciably affect the value of the EBA CGR parameters C and m, within this range of variation in stress level. Non-uniformity in the observed fatigue crack growth behaviour between coupons suggests that further coupon tests may be required to achieve a higher level of confidence.

In order to compare the F-111 stress invariance observation against other data a similar analysis was conducted on F/A-18 coupon test data obtained under the APOL spectrum. This analysis is presented in Appendix E. In this analysis, four stress levels were examined, where the maximum increase was 32%. This analysis of the F/A-18 data displayed a similar finding to that of the analysis of the F-111 spectra. The analysis showed that an increase of 32% in scaling stress did not significantly affect the EBA CGR parameters.

To aid the analysis of the quantitative fractography data, the variability between coupons was not taken into account. The small number of coupons did not provide adequate information to make reliable estimates of the variability between the coupons. As such the quantitative

fractography data under each spectrum was pooled to obtain a pooled sample variance. Hence it is likely that the variance has been under-predicted as a result of the limited number of coupons tested. But it should be noted that from a statistical point of view a larger variance would relax conditions on which the regression curves are accepted as identical. Nevertheless, agreement in the slopes was still achieved, indicating that increasing or decreasing the peak stress by 10% has an insignificant effect on the CGRs as parameters.

It should be noted that a significant portion of the data used to assess the effect of scaling stress of the EBA CGR constants were rejected in the LITV coupon test program. Analysis has been conducted under the assumption that the spectra applied by the analogue test controllers were repeatable. No load histories were recorded during these tests to validate this assumption. Further testing maybe required to support the assumption that the spectra applied by the analogue test controllers are equivalent.

5.3 Predictive Capability of the EBA

5.3.1 Initial Flaw Size

The EBA approach as developed from the F/A-18 experience assumes there is no period of crack initiation or incubation. Instead, cracks are said to initiate on 'day one'. Where observations cannot confirm this, cracks are regarded as having grown in a log-linear manner from an initial size that is compatible with the microstructure of the material, *i.e.*, from an inclusion or surface irregularity or pit. Whilst this certainly has a basis in the F/A-18 coupon data (See Figure 6 in McDonald, Molent et al. (2006)), particularly at the higher stress levels and for etched coupons, this has not been observed in the case of the P-3C data used in this report.

In application where a prediction of the total life is required, then an appropriate estimate of the initial flaw size is required. The present investigation has shown that determining an appropriate initial flaw size for use with the EBA from the P-3C coupon data proved problematic. Using the EBA crack growth constants to back-predict the crack growth curve to estimate the initial flaw size did not result in a realistic value. Predicting the initial flaw size through exponential back-extrapolation and FASTRAN both resulted in crack growth predictions that significantly differed between spectra. The observed difference may be attributed to a period of crack initiation in the P-3C coupon data that is not observed in the F/A-18 and F-111 data. The crack growth threshold of the material maybe limiting the number of spectrum cycles that are contributing toward crack growth. The large block size of the P-3C spectrum may also be contributing to problems in estimating an initial flaw size. A Paris-type EBA may be inadequate if significant changes in spectrum severity are observed between sub blocks. Inadequate material definitions for small crack analysis may also explain FASTRAN's inability to estimate an initial flaw size. Further, differences in the experimental data may also be attributed to differences in the type of initiating flaw i.e. surface versus subsurface flaws. As can be seen in the analysis none of the predictions using either the EBA or FASTRAN produced predictions that provided confidence in this approach for P-3C

coupon data. A lack of data in the early stages of crack growth has not helped to identify the underlying problems that could be influencing the predictions.

Analysis of a crack in the outer wing lower panel/cap splice of the P-3C under the FSFT spectrum was conducted. Limited quantitative fractography data increased the uncertainty of the derived EBA parameters. Using EBA parameters evaluated with coupon data did not help the prediction of total life or the inspection interval. Differing β factors between the location of interest and the coupons may also have contributed to uncertainty in the prediction. The effect of differing β factor solutions between coupons and the location of interest on the EBA has not yet been investigated. The ability to accurately estimate the appropriate effective initial flaw size and the increased scatter associated with subdivision of large block spectra have also contributed to the observed error in the total life predictions. These difficulties contributed to poor fatigue crack growth predictions using the EBA for the crack investigated in the wing lower panel/cap splice.

With regard to the F-111 several crack growth curves were recorded for each spectrum. Considering one spectrum, each of the crack growth curves was used to back predict the initial flaw size at time zero. This resulted in several measurements of the EIFS for that particular spectrum. By pooling these EIFSs an average EIFS was obtained. The average EIFSs for each spectrum considered in this report are presented in Table 12. A statistical analysis of the EIFSs obtained has shown a dependence on the applied spectrum based on the experimental data in this report. This does not preclude the possibility that further experimental data may alter this conclusion. Averaging the EIFS approach assumes that the initial flaw sizes are distributed normally, although a log-normal approximation maybe more appropriate (Molent and Sun 2006). However, using a normal approximation is likely to produce more conservative estimates of fatigue crack growth.

5.3.2 Model Parameter Transferability

A method that uses the EBA to predict CGRs under a new spectrum (spectrum 2) was proposed in McDonald (2005). The method requires coupon data for the tested spectrum and crack growth predictions for both the tested and untested spectra using a predictive tool such as FASTRAN or AFGROW. This technique assumes there is a systematic error in predictions obtained using current predictive tools, but the relative severity is predicted accurately. The method used in McDonald (2005) attempts to eliminate this error by taking the ratio of the crack growth constants C and assuming m is the same between spectra. Essentially asserting that the predicted CGR is solely determined by the parameter C. (McDonald 2005) evaluated two approaches where m was equal to 2 and one where m was fixed and not equal to 2. A modification to the above methodology is presented in this report that allows the exponent m to also be variable. All three methods were considered in this investigation.

CGR curves were evaluated for the F-111 using the methods described in Section 2.2 for the untested spectrum. These curves were plotted along with quantitative fractography data for the untested spectrum. A least-square fit of the CGR quantitative fractography data was calculated and used as a benchmark with which to compare the three predictions. In five of the eight cases examined, the variable-m approach yielded the highest correlation, but the results were very similar to the $m_{2,E} = m_{1,E}$ approach. This result was not unexpected as the

FASTRAN prediction for each spectrum produced very similar m exponents which cancelled each other in both the variable-m and $m_{2,E} = m_{1,E}$ approaches, as shown in Eqn. (12). Thus for the cases considered here $m_{1,E}$ dominated the solution. The differences in slope of the experimental CGR curves were not always reflected in the FASTRAN predictions. This result could be due to deficiencies in the FASTRAN algorithm, FASTRAN input data, and/or the variation in the experimental CGRs.

Importantly, the promising trends observed for the F-111 cases were not reproduced for cases involving the P-3C spectrum. Here, total crack growth life predictions yielded poor correlation with experimental results. From Figure 13 it appears that the poor correlation may be due to the selection of inappropriate EIFS, but further examination of the numerical values show that this is not the case. Exponential back extrapolation of the crack growth data particularly for the RAAF spectrum produced unrealistic estimates of the initial flaw size. Thus, it is clear that the experimental data presented in Figure 3 must be preceded by a period of slower crack growth. The current implementation of the EBA is unable to deal with this situation, due to the non-log-linearity demonstrated by this early crack growth stage when the crack size is small. DCPD measurements were rejected in the early stages of crack growth based on the uncertainty in the DCPD readings. As a result, the EBA analysis was based on crack growth data that did not include this early stage of crack growth. Ignoring this early stage and only considering data in the later stages of crack growth compromises the EBA's capability to predict the total crack growth life, however including both stages would make it difficult to define valid EBA parameters. Despite difficulties in predicting total life, the calculation of fatigue crack growth beyond 1.27 mm did show a significantly better comparison.

It is worth noting that FASTRAN also had the previously identified difficulty in predicting the total crack growth life, based on the calibrated parameters and back-calculated equivalent flaw sizes. The calibration was made against FSFT coupon data, while the prediction was made for RAAF coupon data. The correct modelling of spectrum effect remains an unsolved technical problem.

6. Conclusion

In this study, the EBA developed in McDonald, Molent et al. (2006) was critically evaluated, using data obtained from different load spectra, different material and different crack configurations, to gauge its general applicability to other aircraft operated by the Royal Australian Air Force. The present investigation has shown that the effective block approach was able to model fatigue crack growth in 2024-T851 aluminium under F-111 flight spectra. It was not able to produce accurate predictions of total crack growth life for the P-3C spectrum, however predictions of fatigue crack growth in a chosen interval were reasonable.

Based on the analysis conducted in this report and within the following data source limitations:

- P-3C 7075-T6 Aluminium, $K_t = 4.0$, FSFT and RAAF spectra
- F-111 2024-T851 Aluminium, $K_t = 2.5$, selected small block spectra

the following conclusions may be drawn:

(1) The EBA was able to represent the F-111 crack growth rate adequately using a Paris-type equation;
(2) The loads used in the cold proof load test did not influence the effectiveness of the EBA;
(3) As demonstrated by the coefficients of determination in Appendix C the EBA produced improved fatigue life predictions over the results from (an un-calibrated) FASTRAN analysis in the case of the F-111 spectra from a process that relied on the relative severity predictions from FASTRAN;
(4) Based on the data presented in this report, a statistical analysis shows that the equivalent initial flaw size is not independent of spectra;
(5) The variable-m approach resulted in a minimal improvement over the fixed-m approach for both the P-3C and F-111;
(6) The EBA was unable to reliably model the fatigue crack growth of the P-3C coupon data in terms of the total crack growth life, due to its inability to represent the observed crack growth behaviour adequately. The large block size also contributed uncertainty to the calculation of the EBA crack growth parameters. However, it was able to produce satisfactory estimates for a chosen crack growth interval.
(7) Comparisons of the slope and the y-intercept of CGR data showed that under the FWELD spectrum at FASS 226 increasing or decreasing the scaling stress by 10% did not significantly alter the CGR parameters C and m.
(8) A study of F/A-18 low K_t coupon test data obtained under the APOL load spectra displayed similar trends. Increasing the scaling stress by 32% did not significantly alter the EBA crack growth parameters C and m and was within scatter bounds.

Importantly, the following <u>cannot</u> be concluded from the above work:

(1) That either FASTRAN or AFGROW or other predictive tools will always provide an accurate estimate of relative severity;

(2) That the EBA will allow predictions of crack growth under other spectra or stress levels not considered here;

(3) That the EBA will produce reasonable predictions of crack growth when the β factor changes between the tested data set and the area of interest;

(4) Stress variations beyond those studied will produce a similar stress invariance in relation to the calculated EBA crack growth parameters C and m.

(5) That the EBA can be applied to other materials and F-111 spectra not considered in this report.

(6) That the EBA will correctly predict relative crack growth between F-111 spectra for aircraft features different to the $K_t = 2.5$ coupon design.

7. References

Ball, D. L. and M. T. Doerfler (1996). Metallic Material Data for F-111 Durability and Damage Tolerance Analysis. FZS-12-626.

Budiansky, B. and J. W. Hutchinson (1978). "Analysis of Closure in Fatigue Crack Growth." Journal of Applied Mechanics **45**: 267-276.

Diab, H. and R. Goldsmith (2007). Fractography Results of F-111 Loads Interpretation and Truncation Validation (LITV) Coupon Test Program. DSTO-TR-2000.

Frost, N. E. and D. S. Dugdale (1958). "The Propagation of Fatigue Cracks in Sheet Specimens." Journal of the Mechanics and Physics of Solids **6**: 92-110.

Gallagher, J. P. (1976). "Estimating Fatigue-Crack Lives for Aircraft: Techniques." Experimental Mechanics **16**(11): 425-433.

Gallagher, J. P. and H. D. Stalnaker (1978). "Developing Normalized Crack Growth Curves for Tracking Damage in Aircraft." Journal of Aircraft **15**(2): 114-120.

Gravina, R. (2006). Beta Solution Determination Using FEA - Method Development. ER-P3-51-APM195.

Grummett, S. and N. Goldsmith (2003). Examination of Cracks from the Wings of a P-3 Full-Scale Fatigue Test. DSTO-DP-00824.

Harter, J. A. (2004). AFGROW User's Guide and Technical Manual. AFRL-VA-WP-TR-2004.

Hu, W. and K. F. Walker (2006). "Fatigue Crack Growth from a Notch under Severe Overload and Underload". The International Conference on Structural Integrity and Failure, Sydney, Australia.

Jackson, P. and R. Amaratunga (2007). "Application of the Effective Block Approach Process to P-3C Coupon Data". Internal DSTO Document, DSTO, 1 March.

McDonald, M. (2005). Fatigue Crack Growth Methodologies in Structural Life Assessment - F/A-18 Case Study. DSTO-DP-1045.

McDonald, M. (2006). Effective Block Approach to Crack Growth Analysis - PowerPoint Presentation.

McDonald, M. (2006). "Unpublished Work". Excel Spreadsheet, Defence Science and Technology Organisation.

McDonald, M. and L. Molent (2004). Fatigue Assessment of the F/A-18 Horizontal Stablator Spindle. DSTO-TR-1620.

McDonald, M., L. Molent and A. J. Green (2006). Assessment of Fatigue Crack Growth Prediction Models for F/A-18 Representative Spectra and Material. DSTO-RR-0312.

Molent, L. and Q. Sun (2006). Distribution of Equivalent Pre-Crack Size in 7050 Aluminium Alloy. DSTO-TR-1700.

Murtagh, B. J. (1998). Crack Growth Modelling of Aluminium 2024-T851 Multi Site Crack Initiation Specimens. ER-F111-51-014.

Newman, J. C., Jr. (1981). A Crack-Closure Model for Predicting Fatigue Crack Growth under Aircraft Spectrum Loading. Methods and Models for Predicting Fatigue Crack Growth under Random Loading, ASTM STP 748. J. B. Chang and C. M. Hudson, ASTM**:** 53-84.

Newman, J. C., Jr. (1992). FASTRAN II - a Fatigue Crack Growth Structural Analysis Program. NASA TM-104159.

Newman, J. C., E. P. Phillips and M. H. Swain (1997). Fatigue-Life Prediction Methodology Using Small-Crack Theory. NASA TM-110307.

Ord, D. (2004). F-111 Relative Spectra Severity Analysis - Coupon Test Program. Aerostructures ER-F111-51-APM172.

Paris, P. C. and F. Erdogan (1963). "A Critical Analysis of Crack Propagation Laws." Journal of Basic Engineering. Transactions of ASME **85**: 528-534.

Pell, R. A., P. J. Mazeika and L. Molent (2003). "The Comparison of Complex Load Sequences Tested a Several Stress Levels by Fractographic Examination". International Committee on Aeronautical Fatigue, Switzerland.

Pell, R. A., P. J. Mazeika and L. Molent (2005). "The Comparison of Complex Load Sequences Tested at Several Stress Levels by Fractographic Examination." Engineering Failure Analysis **12**(4): 586-603.

Potter, J. M. and B. G. W. Yee (1982). "The Use of Small Crack Growth Data to Bring About and Quantify Improvements to Aircraft Structural Integrity". AGARD specialist meeting on behaviour of short cracks in airframe structures, Toronto, Canada.

Stephens, R. I., A. Fatemi, R. R. Stephens, et al. (2001). Metal Fatigue in Engineering, John Wiley & Sons, Inc.

Teunisse, B., M. Phillips, P. Jackson, et al. (2006). Computer Programs and Methodology Used for DSTO P-3C SLAP Test Interpretation. DSTO-TR-1834.

Teunisse, B., M. Phillips, D. Mongru, et al. (2006). P-3C Service Life Assessment Program Australian Test Interpretation Report for the Usn Wing/Fuselage/Landing Gear Test Articles. DSTO-TR-1929.

Veul, R. P. G. and L. C. Ubels (2003). Results of the FMS Spectra Loading Coupon Tests Performed within the Framework of the P-3C Service Life Assessment Program. NLR-CR-2003-488.

Wallbrink, C. and W. Hu (2008). "An Evaluation of the Effective Block Approach for Predicting Crack Growth under an Untested Spectrum Using P-3C and F-111 Test Data." Advanced Materials Research **41-42**: 189-197.

Walpole, R., R. Myers and S. Myers (1998). Probability and Statistics for Engineers and Scientists. New Jersey, Prentice Hall International, inc.

Zhuang, W., R. Boykett, M. Phillips, et al. (2008). Effective Block Approach for Damage Tolerance Analysis of F-111 D/F Model Wing Structures. DSTO-TR-2124.

Zhuang, W. and L. Molent (2007). "EBA Discussion Group Meeting". PowerPoint Presentation, DSTO, 14th of March.

Appendix A: A statistical treatment of the F-111 LITV coupon test program

The following statistical analysis aims to answer the following question:

(1) Is a linear regression an adequate representation of the data

(2) Given a significance level α of 0.05, are the linear regressions statistically equivalent.

Section A.1 summarises the statistical formula used in this analysis. Further information can be found in Walpole, Myers et al. (1998).

A.1. The statistical treatment of linear regression lines

Given the equation

$$y = \kappa + \beta x \qquad (A1)$$

The confidence interval on β can be expressed as in Eqn. (A2) where b is an estimate of β.

$$b - \frac{t_{\alpha/2} s}{\sqrt{S_{xx}}} < \beta < b + \frac{t_{\alpha/2} s}{\sqrt{S_{xx}}} \qquad (A2)$$

where

$$s^2 = \frac{S_{yy} - bS_{xy}}{n-2} \qquad (A3)$$

$$S_{xx} = \sum_{i=1}^{n} (x_i - \bar{x})^2 \qquad (A4)$$

$$S_{yy} = \sum_{i=1}^{n} (y_i - \bar{y})^2 \qquad (A5)$$

$$S_{xy} = \sum_{i=1}^{n} (x_i - \bar{x})(y_i - \bar{y}) \qquad (A6)$$

$$\bar{x} = \frac{1}{n} \sum_{i=1}^{n} x_i \qquad (19)$$

$$\bar{y} = \frac{1}{n}\sum_{i=1}^{n} y_i \tag{A7}$$

and $t_{\alpha/2}$ is the t-distribution evaluated at a confidence of $(100-\alpha)\%$.

The confidence interval on κ can be expressed by the following where k is an estimate of κ.

$$k - \frac{t_{\alpha/2} s \sqrt{\sum_{i=1}^{n} x_i^2}}{\sqrt{nS_{xx}}} < \kappa < k + \frac{t_{\alpha/2} s \sqrt{\sum_{i=1}^{n} x_i^2}}{\sqrt{nS_{xx}}} \tag{A8}$$

These equations can be used to evaluate the confidence intervals associated with the parameters predicted from a simple regression analysis. Another useful interval is the prediction interval and it can be expressed as

$$\hat{y}_0 - t_{\alpha/2} s \sqrt{1 + \frac{1}{n} + \frac{(x_0 - \bar{x})^2}{S_{xx}}} < y_0 < \hat{y}_0 + t_{\alpha/2} s \sqrt{1 + \frac{1}{n} + \frac{(x_0 - \bar{x})^2}{S_{xx}}} \tag{A9}$$

This interval has a probability of (1-α) of containing a new measurement y_0 based on the regression predicted $\hat{y}_0$.

To assess the agreement between the fitted slopes of the regression lines, a two sample t test was used. In using this approach the variance between samples are assumed to be equal.

The pooled estimate s_P^2 of the theoretical variance σ^2 can be calculated from the two sample variances s_1^2 and s_2^2.

$$s_P^2 = \frac{(n_1 - 2)s_1^2 + (n_2 - 2)s_1^2}{n_1 + n_2 - 4} \tag{A10}$$

If the hypothesis that the slopes of the regression lines are equal, *i.e.* $\beta_1 = \beta_2$ then the variance of $\beta_1 - \beta_2$ is

$$\sigma_{\beta_1 - \beta_2}^2 = \sigma^2 \left(\frac{1}{S_{xx1}} + \frac{1}{S_{xx2}} \right) \tag{A11}$$

Then the t distribution to compare two slopes obtained from regression analysis can be written as:

$$t = \frac{b_1 - b_2}{\sqrt{s_P^2\left(\frac{1}{S_{xx1}} + \frac{1}{S_{xx2}}\right)}} \tag{A12}$$

If the hypothesis that the y-intercepts of the regression lines are equal i.e. $\kappa_1 = \kappa_2$ then the variance of $\kappa_1 - \kappa_2$ is

$$\sigma^2_{\kappa_1=\kappa_2} = \sigma^2\left(\frac{\sum_{i=1}^{n_1} x_{1i}}{n_1 S_{xx1}} + \frac{\sum_{i=1}^{n_2} x_{2i}}{n_2 S_{xx2}}\right) \tag{A13}$$

Then the statistic t to compare two y-intercepts obtained from regression analysis can be written as:

$$t = \frac{k_1 - k_2}{\sqrt{s_P^2\left(\frac{\sum_{i=1}^{n_1} x_{1i}}{n_1 S_{xx1}} + \frac{\sum_{i=1}^{n_2} x_{2i}}{n_2 S_{xx2}}\right)}} \tag{A14}$$

A.2. Analysis of the F-WELD spectra at FASS 226

There were a total of 9 sets of fatigue crack growth data from coupons tested under the F-WELD FASS 226 spectrum, with three stress levels. The raw crack growth data are plotted in Figure 24. The CGRs for the 9 data sets were evaluated using the method described in section 2.1.2, and they were plotted in Figure 25 against the reference stress intensity factor.

The fatigue CGR data plotted in Figure 25 appear to indicate invariance to the applied reference stress, but to make a quantitative assessment of invariance of slope of the regression lines, a statistical analysis needs to be carried out. For this purpose, the equations in Section A.1 have been used to evaluate confidence levels associated with the fatigue CGR parameters evaluated from a linear regression of the fatigue CGR data set. In the following analysis a significance level of 0.05 has been used.

In the following, we examine whether the m and C values obtained from linear regression analysis of the data from different spectra are statistically different. In other words, we check using statistics whether the assumption $m_1 = m_2$ (and $C_1 = C_2$) could be rejected with confidence.

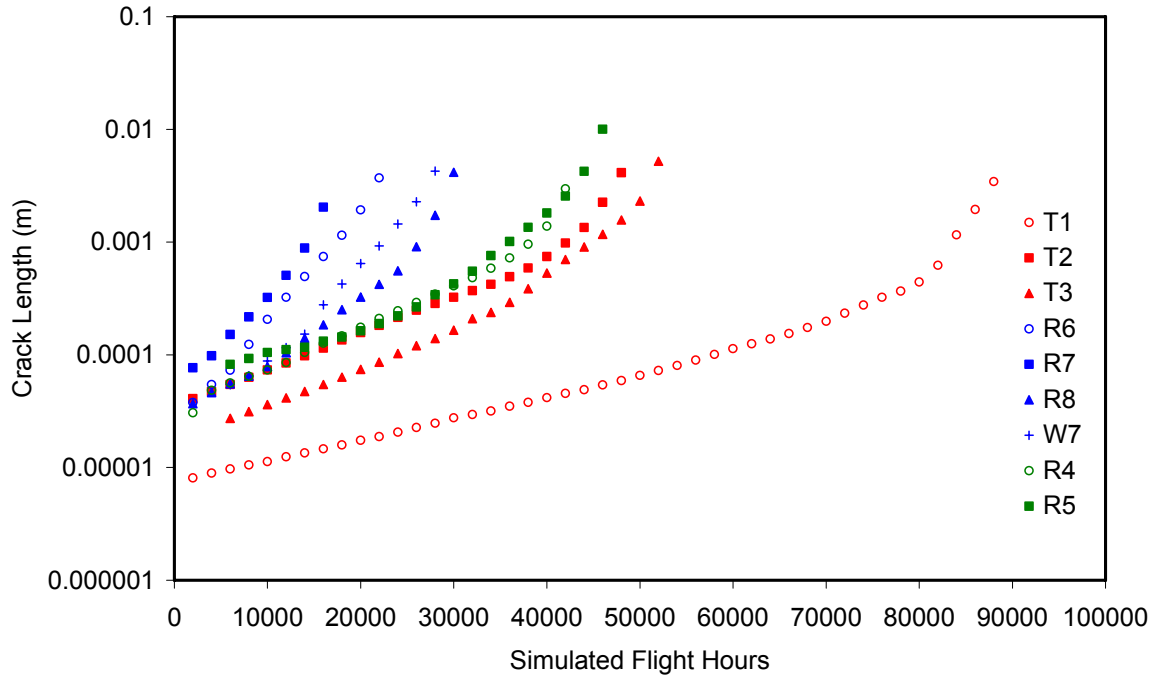

Figure 24: Raw fatigue crack growth data acquired under the old test controllers for load spectra FL3, FL4 and FL5

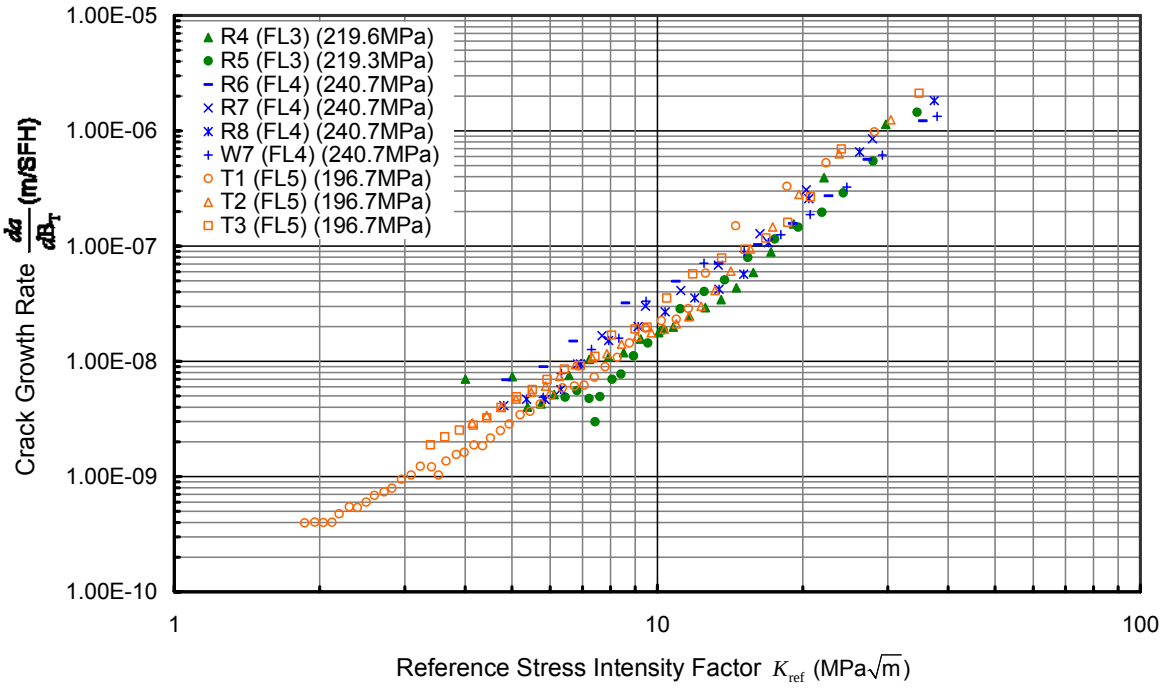

Figure 25: The crack growth rate curves for load spectra FL3, FL4 and FL5

Plotted in Figures 26 to 28 are the CGRs versus K_{ref} for the F-WELD spectra at FASS 226. A least squares linear regression was performed on data obtained from each load spectrum. The results have been plotted in Figures 26 to 28 along with their associated prediction intervals.

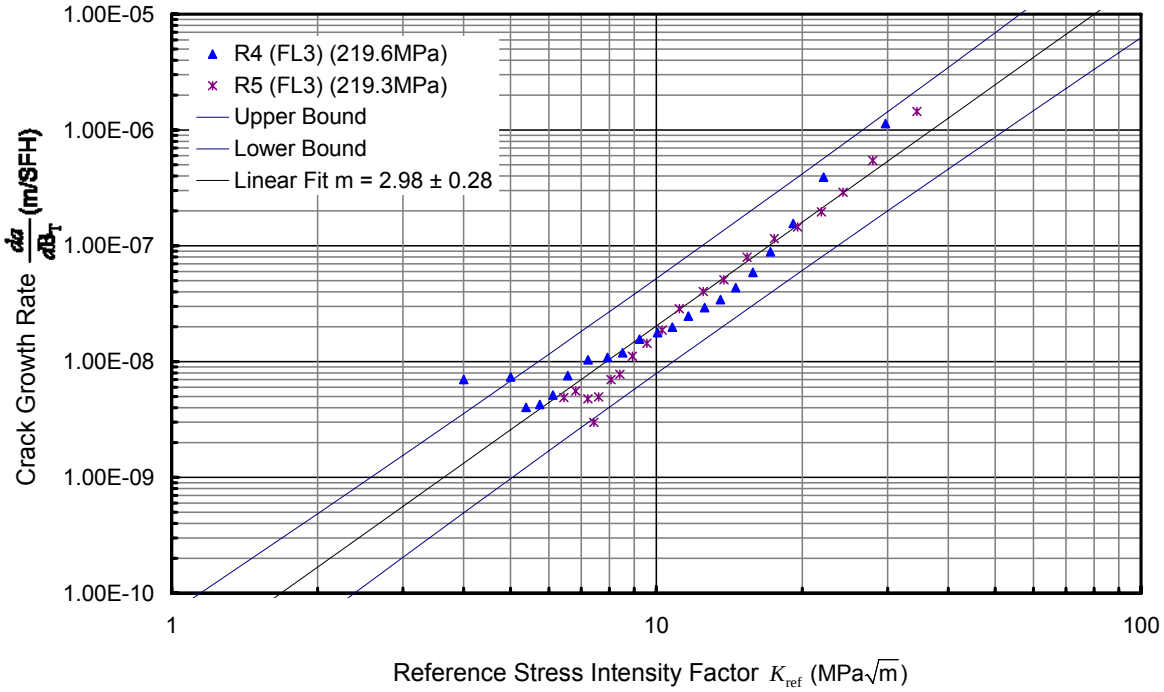

Figure 26: Crack growth rate data obtained from QF coupons subjected to the FL3 spectrum

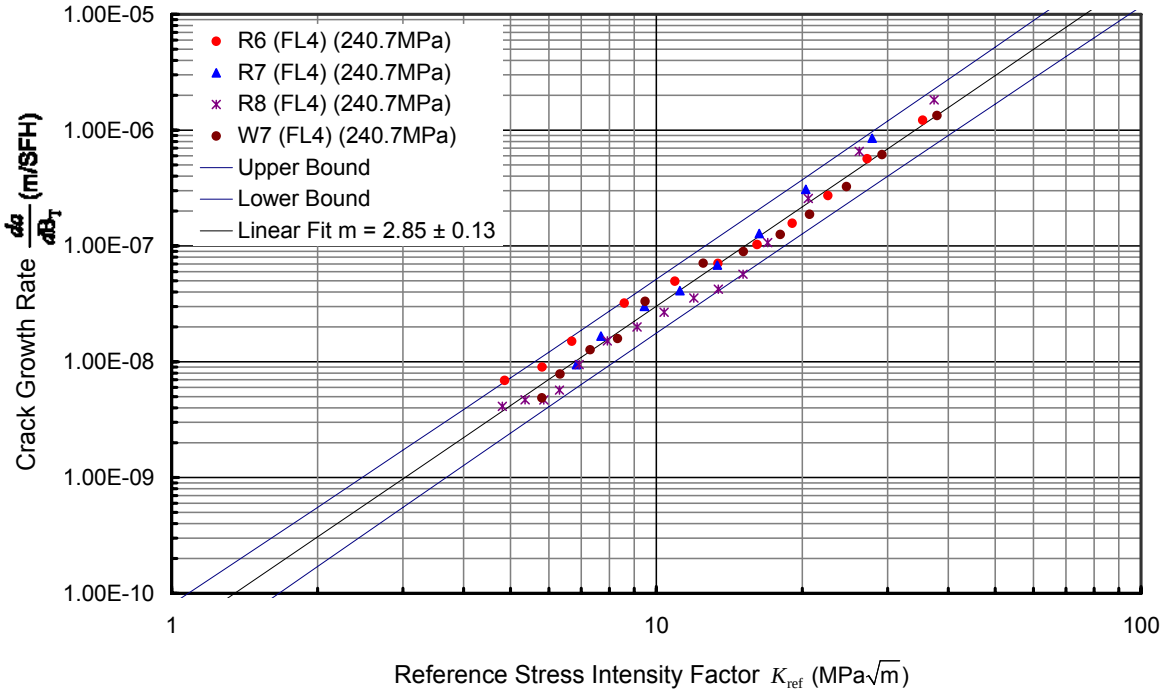

Figure 27: Crack growth rate data obtained from QF coupons subjected to the FL4 spectra

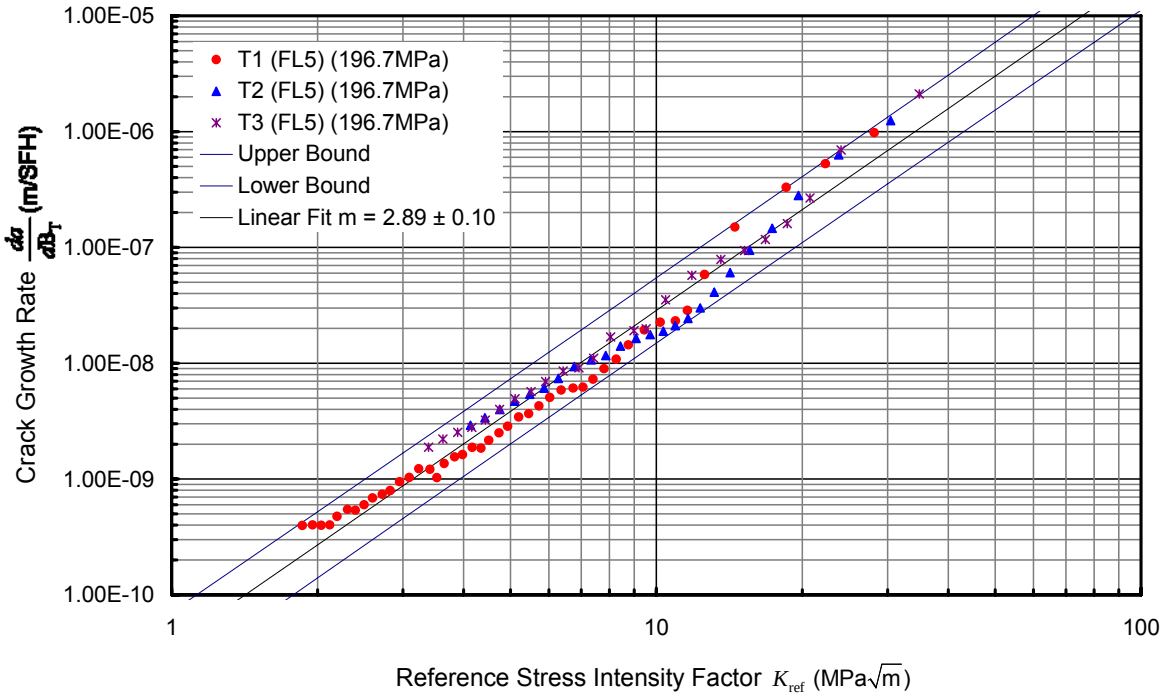

Figure 28: Crack growth rate data obtained from QF coupons subjected to the FL5 spectra

The CGR parameters C and m have been obtained from the least-square linear regression and presented in Tables 14. Confidence intervals of 95% were used to ascertain the level of uncertainty associated with the predicted crack growth parameters.

Table 14. The Uncertainties and Correlation associated with the Crack Growth Constants for the F-WELD test spectra

Spectra	***m***	***Uncertainty in m***	***ln(C)***	***Uncertainty in ln(C)***	***C***	***R^2***	***No. of Coupons***
FL3	2.98	0.28	-24.57	0.69	2.13×10^{-11}	0.9602	2
FL4	2.85	0.13	-23.88	0.34	4.27×10^{-11}	0.9884	4
FL5	2.89	0.10	-24.04	0.20	3.64×10^{-11}	0.9887	3

A two sample t-test was used to evaluate the significance of the predicted slopes. The results are presented in Table 15. p values below 0.05 are deemed to be significant and thus in these instances we reject the hypothesis that $\beta_1 = \beta_2$ and say that it is probable that the slopes are not the same. The three comparisons in Table 15 do not reject the hypothesis that $\beta_1 = \beta_2$, indicating that the slopes of the regressions for the spectra considered are statistically identical.

Table 15. Comparing regression slopes for the F-WELD test spectra using a t-test

Comparison	*t-value*	p value	*Reject* $\beta_1 = \beta_2$
FL3 with FL4	0.894	0.374	No
FL3 with FL5	0.678	0.499	No
FL4 with FL5	-0.505	0.614	No

The above analysis indicates that the slopes are homogeneous and thus the exponent m is not significantly affected by increasing or decreasing the maximum peak stress of the spectrum by 10%. To demonstrate complete homogeneity of the regression curves a comparison of the y-intercepts should also be conducted, which can only be done after the homogeneity of the exponent m is established. Comparisons when the slopes are not equivalent would not make sense. Table 16 lists the results of a two-sample t-test performed on the y-intercept of the regression curves.

From Table 16, we can see that within the accepted significance level the *y*-intercepts agree. In two cases the *p* value is close to the significance level of 0.05 indicating that further testing may improve confidence in the results, if the assumption that the regression curves are homogeneous.

Table 16. Comparing y-intercept for the F-WELD test spectra using a t-test

Comparison	*t-value*	p value	*Reject* $\kappa_1 = \kappa_2$
FL3 with FL4	-1.909	0.060	No
FL3 with FL5	-1.802	0.074	No
FL4 with FL5	0.728	0.468	No

In comparing the y-intercept we see that within the accepted significance level the y-intercepts agree. In two cases the p value is close to the significance level of 0.05 indicating that further testing may improve confidence in the results, if the assumption that the regression curves are homogeneous.

A.3. Analysis of the discriminated F-WELD spectra at FASS 226

As part of the LITV coupon test program a discriminated F-WELD spectrum at FASS 226 was also investigated. As with the data obtained under the F-WELD test spectra, crack growth data were obtained at the nominal stress level, and $\pm 10\%$ stress levels.

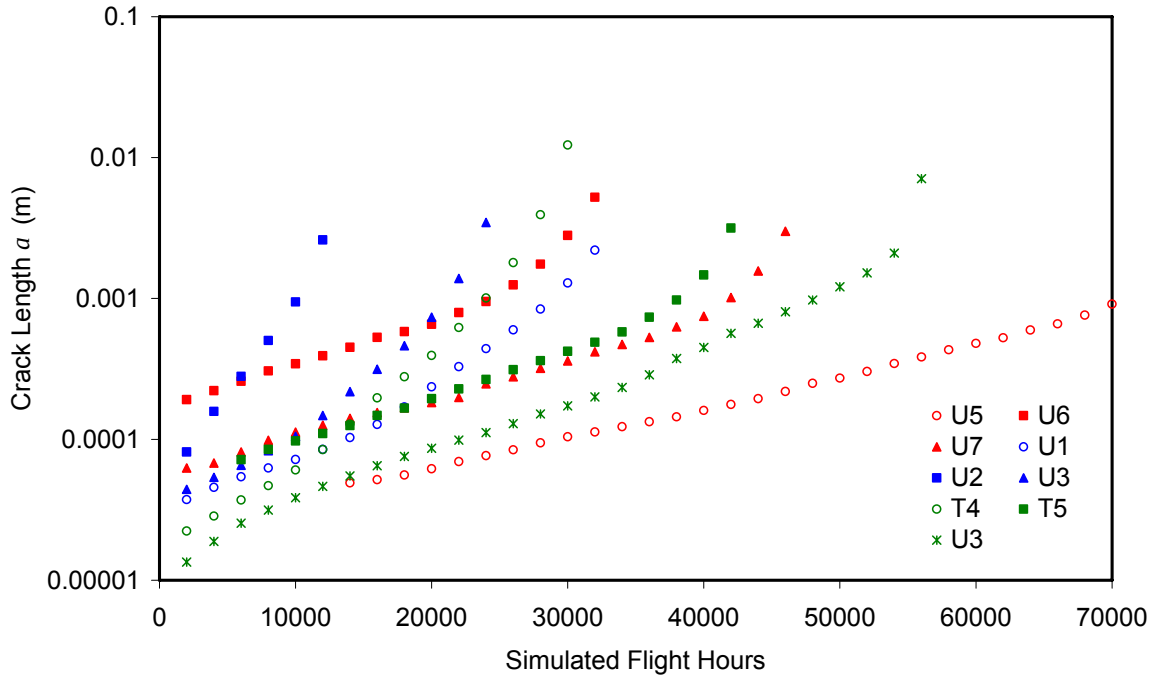

Figure 29: Raw fatigue crack growth data acquired under the old test controllers for load spectra FL6, FL7 and FL8

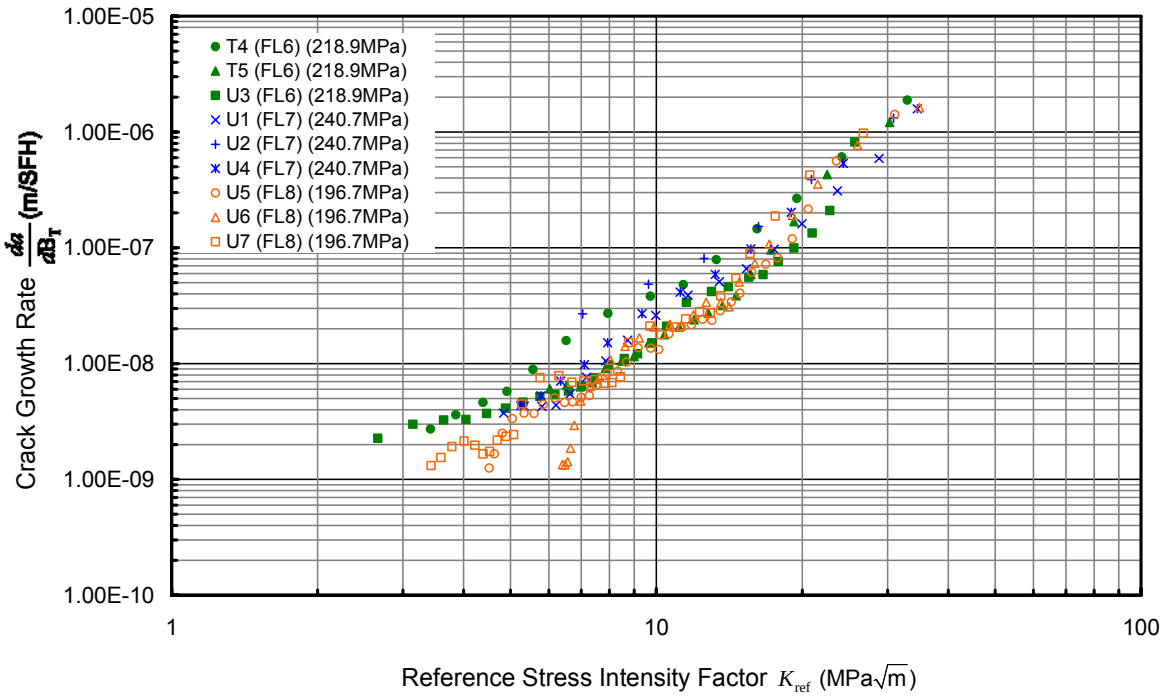

Figure 30: The crack growth rate curves for load spectra FL6, FL7 and FL8

Plotted in Figures 31 to 33 are the CGRs versus K_{ref} for the discriminated F-WELD spectra at FASS 226. A least-square linear regression was conducted on data obtained from each load spectrum. The results are also plotted in Figures 31 to 33 together with the associated prediction interval.

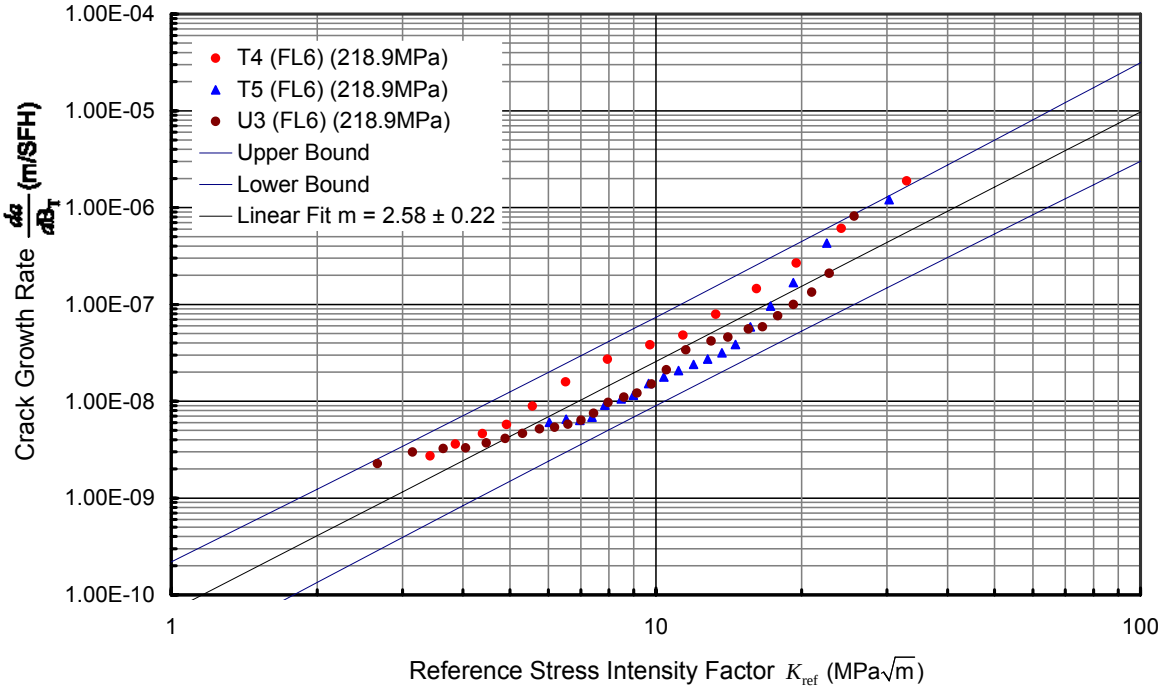

Figure 31: Crack growth rate data obtained from QF coupons subjected to the FL6 spectrum.

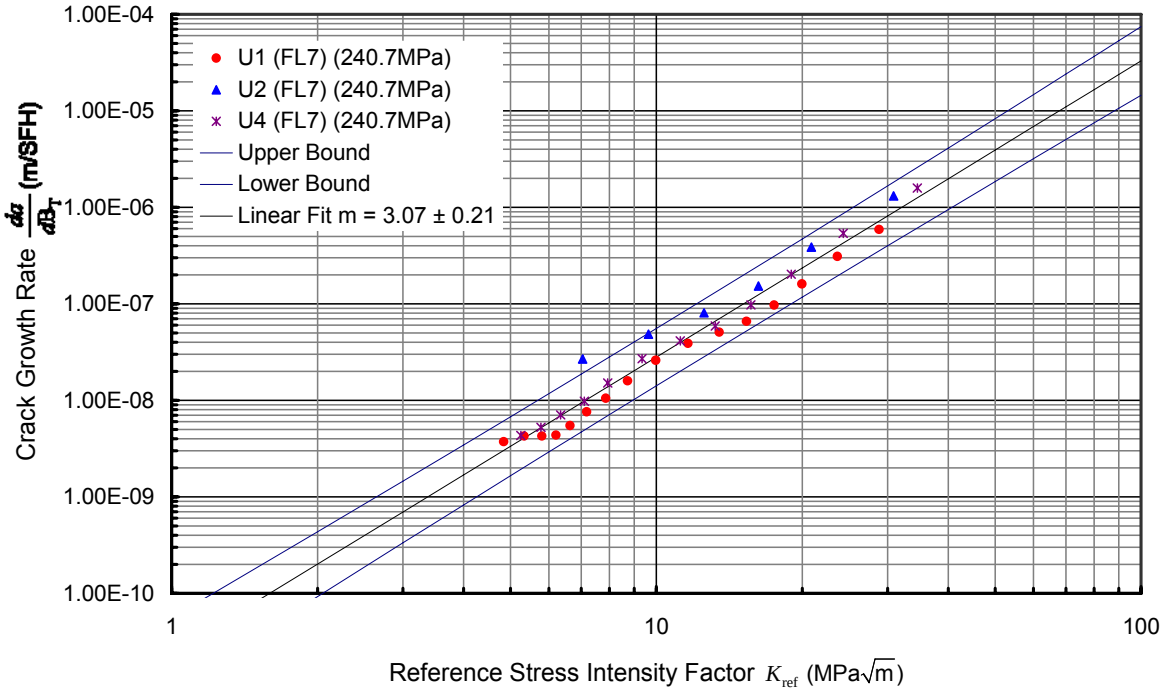

Figure 32: Crack growth rate data obtained from QF coupons subjected to the FL7 spectrum

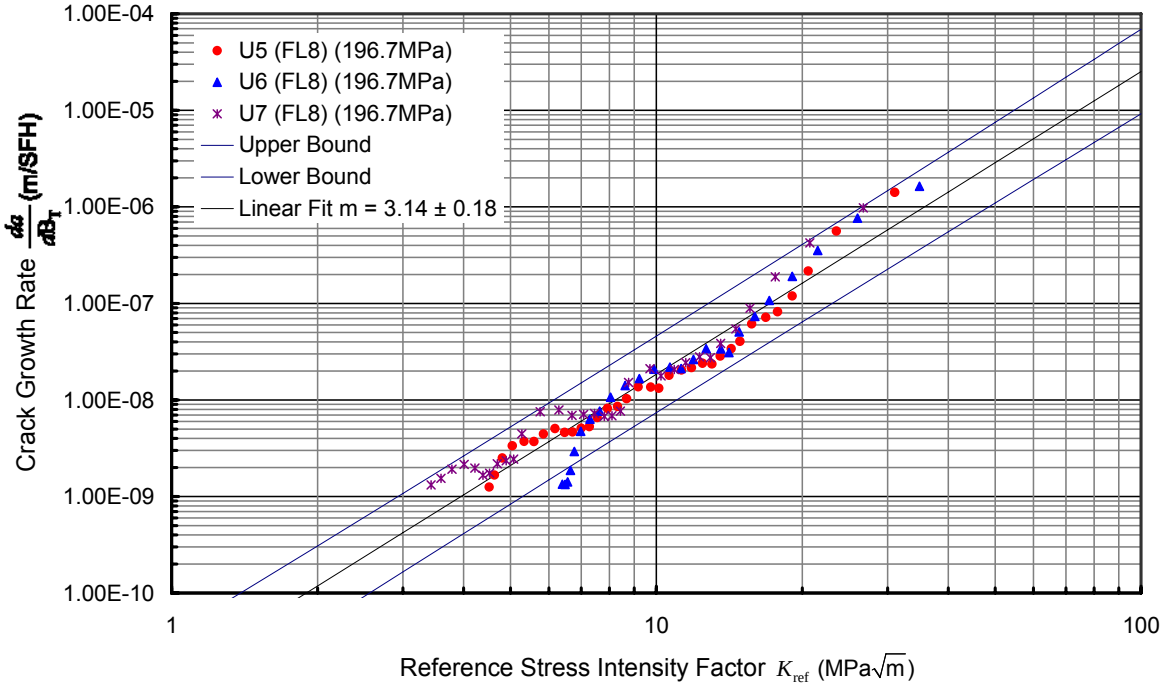

Figure 33: Crack growth rate data obtained from QF coupons subjected to the FL8 spectrum

Regression analysis has been performed for each of the spectra FL6, FL7 and FL8 and the regression coefficients are presented in Table 17 along with their associated uncertainties. 95% confidence intervals were used to ascertain the level of uncertainty associated with the predicted crack growth parameters.

Table 17. The Uncertainties and Correlation associated with the Crack Growth Constants for the discriminated F-WELD test spectra

Spectra	*m*	*Uncertainty in m*	*ln(C)*	*Uncertainty in ln(C)*	*C*	R^2	*No. of Coupons*
FL6	2.58	0.22	-23.41	0.53	6.82×10^{-11}	0.9494	3
FL7	3.07	0.21	-24.45	0.51	2.40×10^{-11}	0.9829	3
FL8	3.14	0.18	-25.03	0.42	1.35×10^{-11}	0.9645	3

Table 18. Crack Growth Constants for the discriminated F-WELD test spectra

Spectra	*m*	*C*
FL6	2.58	6.82×10^{-11}
FL7	3.07	2.40×10^{-11}
FL8	3.14	1.35×10^{-11}

A two sample t-test was used to evaluate the significance of the predicted slopes. The results are presented in Table 19. p values below 0.05 are deemed to be significant and thus in these instances we reject the hypothesis that $\beta_1 = \beta_2$ and say that it is probable that the slopes are not the same.

Table 19. Comparing regression slopes for the discriminated F-WELD test spectra using a t-tests

Comparison	*t-value*	p **value**	*Reject* $\beta_1 = \beta_2$
FL6 with FL7	-2.839	0.006	Yes
FL6 with FL8	-3.949	0.00012	Yes
FL7 with FL8	-0.428	0.670	No

As can be seen in Table 19, homogeneity between regression slopes was only achieved for crack growth data obtained under the FL7 and FL8 load spectra. Since we hope that the slopes should be equal but the hypothesis test indicates that they are not, we now consider the possibility of type I error. In other words we could be rejecting the hypothesis that the slopes are equal when in fact they are equal. This result suggests that more than three coupons should be tested.

Appendix B: Criterion for determining Small Scale Yielding (SSY)

To apply linear elastic facture mechanics to a problem it should not violate the small scale yield criterion. In order to comply with small scale yield conditions the plastic zone size should be much smaller than the size of the crack and the stress intensity factor at the crack tip should not exceed the plain strain fracture toughness. Further information can be found in Stephens, Fatemi et al. (2001).

The Irwin plane stress plastic zone size is defined as

$$\rho = \frac{1}{\pi}\left(\frac{K_I}{\sigma_{ys}}\right)^2 \tag{B1}$$

where ρ is the plastic zone size, K_I is the mode I stress intensity factor and σ_{ys} is the yield strength.

In the small scale yielding model the stresses in an annulus $r>\rho$ and where the plastic zone size $\rho \ll a$, can be well represented by $\sigma = \frac{K_I}{\sqrt{2\pi r}} f(\theta)$. According to (Stephens, Fatemi et al. 2001) pp. 135 an approximate suggested restriction for the use of K under monotonic loading without significant violation of LEFM principles is:

$$\rho \le \frac{a}{4} \tag{B2}$$

This restriction can often be relaxed to the criterion specified in Eqn. (B3) in conditions where the cyclic plastic zone is smaller than the monotonic plastic zone.

$$\rho \le \frac{a}{2} \tag{B3}$$

The plane stress cyclic plastic zone size can be approximated by (Stephens, Fatemi et al. 2001) pp. 160:

$$\rho^* = \frac{1}{4\pi}\left(\frac{\Delta K_I}{\sigma_{ys}}\right)^2 \tag{B4}$$

where the cyclic plastic zone ρ^* is evaluated in terms of the stress intensity range ΔK_I.

In the present analysis of the F-111 the stress intensity range ΔK_I is replaced by the reference stress intensity factor K_{ref}. Therefore, comparing Eqn. (B1) and Eqn. (B4) we see that the cyclic

plastic zone size is always less than the monotonic plastic zone size, since the factor $1/4\pi$ is less than $1/\pi$. As a result we can use Eqn. (B3) as a criterion for SSY in the analysis of the F-111 data.

The plane strain plastic zone size can be approximated with the following equation:

$$\rho = \frac{1}{3\pi}\left(\frac{K_I}{\sigma_{ys}}\right)^2 \tag{B5}$$

Appendix C: Comparison of crack growth rate parameters evaluated using the EBA

C.1. FASTRAN analysis

In this section the CGR is defined as crack growth per spectrum block, da/dB. As mentioned in section 2.2 the predictive methodology proposed in McDonald (2005) requires crack growth analysis for the two spectra. This technique assumes that the predictive tool does not accurately model the crack growth in absolute terms, but assumes that it can predict the relative severity correctly. In other words, the errors in the predictive tools are systematic. The objective of taking the ratio of the CGRs is to minimise this systematic error and provide an improved EBA prediction for an unknown spectrum. In other words the ratio of the predicted CGRs for spectra 1 and 2 is used to modify the experimentally evaluated fatigue crack growth parameters for spectrum 1. The result is a prediction of *C* and *m* for spectrum 2.

In the present analysis FASTRAN (Newman 1992) has been used to make fatigue crack growth predictions under the various spectra considered here. Specifically the analysis used CGAP (Hu and Walker 2006) version 1.6c to run FASTRAN 3.8. The spectrum files were created using the input spectrum files used in the LITV coupon test program. The following material properties were used in the analysis. The material data was originally used in the present analysis was sourced from (Ball and Doerfler 1996).

Table 20: Material properties used in the FASTRAN analysis

Material	2024-T851
Yield Strength	400 MPa (58 ksi)
Ultimate tensile strength	462 MPa (67 ksi)
Elastic Modulus	73774 MPa (10700 ksi)
Poisson's ratio	0.3
Width	0.0288 m (1.134 inches)
Thickness	0.00891 m (0.351 inches)
a_i	3.048×10^{-5} m (0.0012 inches)

The following ΔK_{eff} data in Table 21 was originally sourced from (Murtagh 1998) and is used in the present analysis. The ΔK_{eff} data in Murtagh (1998) was originally sourced from (Newman, Phillips et al. 1997). The data in Newman, Phillips et al. (1997) is related to 2024-T3 material data and not 2024-T851 material data. (Murtagh 1998) makes an argument by comparing 2024-T851 material data to the 2024-T3 ΔK_{eff} curve and concludes that the 2024-T3 ΔK_{eff} curve is a reasonable estimate of the 2024-T851 ΔK_{eff} curve.

Table 21: ΔK_{eff} versus crack growth rate data for 2024-T851

ΔK_{eff} ($MPa\sqrt{m}$)	*da/dN*
0.8	1.00E-11
1.05	1.00E-10
2.05	2.00E-09
4	8.00E-09
7.7	1.00E-07
13.5	1.00E-06
23	1.00E-04
36	1.00E-03
85	1.00E-02

The α constraint factor used in the FASTRAN analysis is presented in Table 22. The constraint factor here differs from that used in Newman, Phillips et al. (1997). Through a trial and error approach it was found that the constraint factors used in Table 22 provided a more consistent interpretation for small ΔK_{eff} data (Murtagh 1998). However it is suggested that further research be conducted to establish constraint factors consistent with the method recommended in Newman (1992).

Table 22: FASTRAN constraint factor for 2024-T851

da/dN	α
0.00000254	1.73
0.00000508	1

Information with regard to the coupon geometry can be found in the Aerostructures report ER-F111-51-APM202.

FASTRAN predictions were produced for all the cases considered in Table 10 and are presented in the following section.

C.2. EBA crack growth rate predictions

Figure 34 shows FASTRAN predictions for both the D20 and A15-5 spectra at FASS 226. The FASTRAN predictions did not include the effects of fatigue crack threshold or the fracture toughness of the material. The results were generated to produce results in the Paris region. A least squares linear regression was performed to evaluate the CGR parameters for each of the spectra. Also plotted in Figure 34 is the QF data from the LITV coupon test program for both spectra. Least squares linear regressions were evaluated for these two sets of coupon data and the associated fatigue CGR parameters were evaluated.

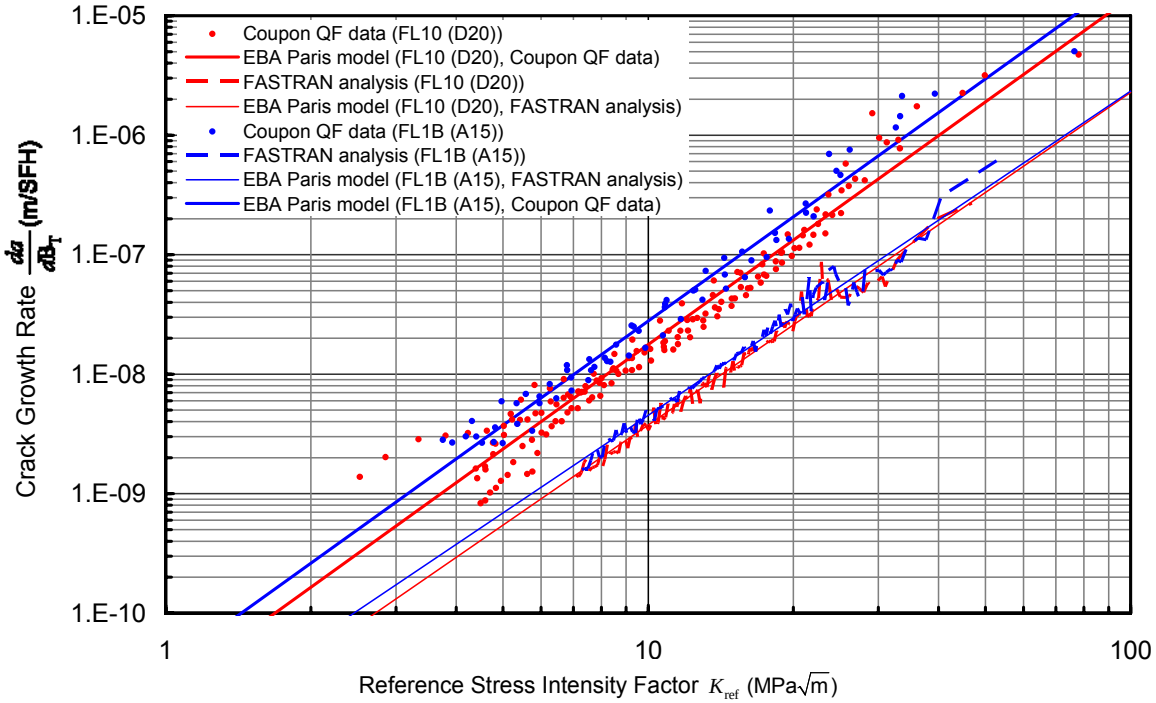

Figure 34: Crack growth rate data for the A15-5 at FASS 226 and D20 at FASS 226 spectra plotted along with FASTRAN predictions

The CGR parameters evaluated from the linear regressions above of both the FASTRAN predictions and the LITV QF coupon data are used to make two separate predictions. The first predicts the CGR parameters for the FL1B spectrum from the FL10 spectrum and the second predicts the CGR parameters for the FL10 spectrum from the FL1B spectrum. Figure 35 shows three predictions of the CGRs under the FL1B load spectrum. The three predicted lines were created with the CGR parameters using the three methods described in section 2.2. Also presented in Figure 35 is the QF data for the FL1B spectrum along with a least squares linear regression line. This data is used to evaluate the three predictions of the FL1B load spectrum associated CGRs in 2024-T851 aluminium.

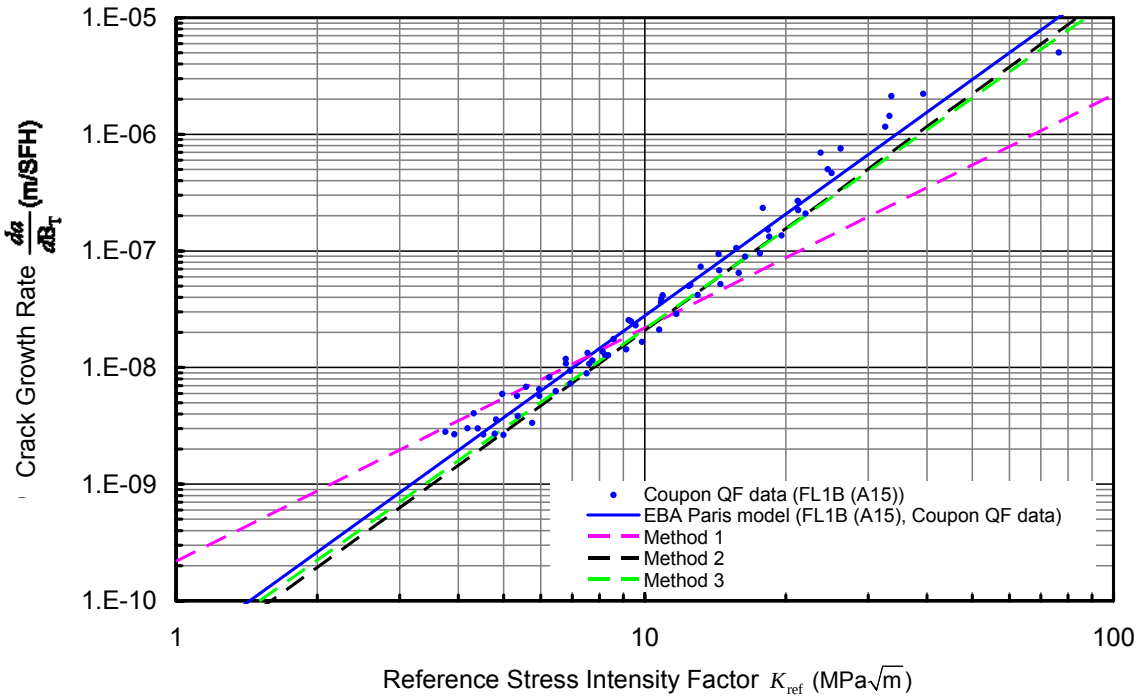

Figure 35: EBA prediction of FL1B from FL10 Coupon data

Presented in Table 23 are the CGR parameters evaluated using the three methods discussed in section 2.2. The CGR parameters evaluated from a least squares linear regression of the QF data we are attempting to predict is also presented for comparison. Coefficients of determination (R^2) are also presented in Table 23 to assess the goodness of fit for each of the predictions. In comparing the predictions it is clear that both the variable-m and $m_{2,E} = m_{1,E}$ approaches provide a good estimate of the true CGRs. The $m = 2$ approach produced the worst result in this case.

Table 23: EBA prediction of FL1B from FL10 Coupon data

Method	***m***	***C***	**R^2**
Least Squares fit	*2.898*	*3.509×10^{-11}*	*0.9719*
Method 3: Variable-m	2.835	3.114×10^{-11}	0.9517
Method 2: $m_{2,E} = m_{1,E}$	2.906	2.569×10^{-11}	0.9507
Method 1: $m = 2$	2.000	2.180×10^{-10}	0.7703

Figure 36 presents the opposite prediction to that above. Here we present three predictions for the CGRs for the FL10 spectrum from the FL1B spectrum. Also presented is the QF data associated with the FL10 load spectrum.

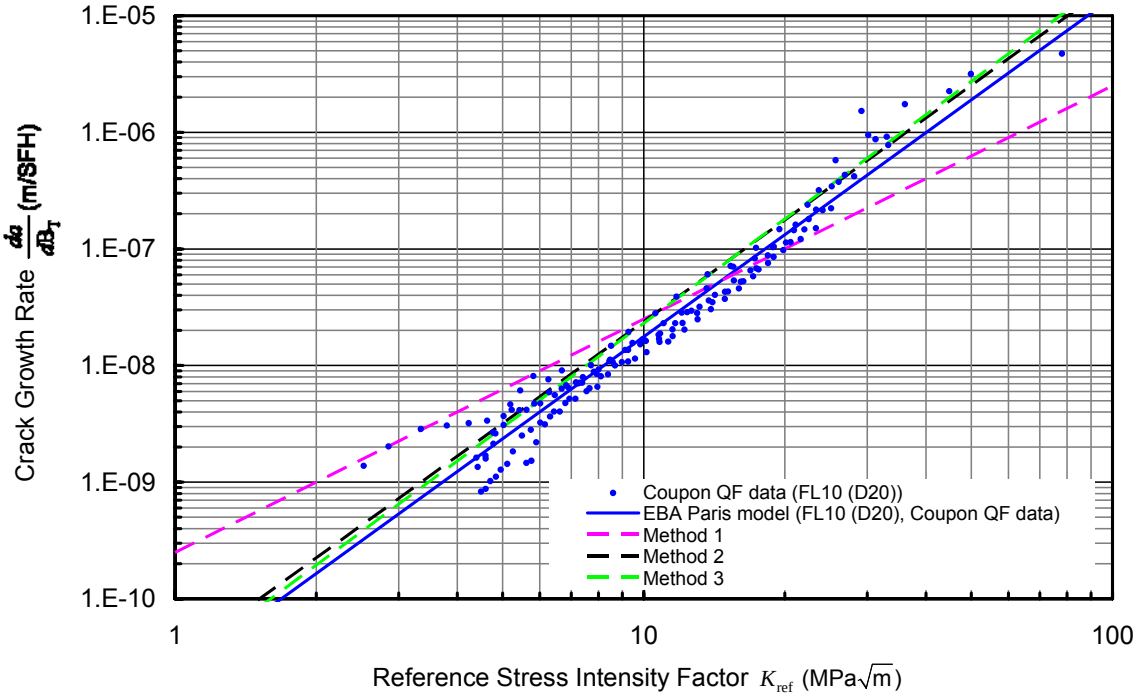

Figure 36: Prediction EBA prediction of FL10 from FL1B Coupon data

As before, the variable-m and $m_{2,E} = m_{1,E}$ approaches provide the best correlations. Setting m to 2 produced the poorest correlation in this comparison.

Table 24: EBA prediction of FL10 from FL1B Coupon data

Method	***m***	**C**	**R^2**
Least Squares fit	*2.906*	*2.195×10^{-11}*	*0.9540*
Method 3: Variable-m	2.969	2.473×10^{-11}	0.9392
Method 2: $m_{2,E} = m_{1,E}$	2.898	2.998×10^{-11}	0.9334
Method 1: $m = 2$	2.000	2.499×10^{-10}	0.7460

Data for cases 3 and 4 are presented in Figure 37. In a similar way as before, FASTRAN predictions of the CGRs associated with the FL11 and FL2B spectra are presented. QF data for both the FL11 and FL2B spectra are also presented.

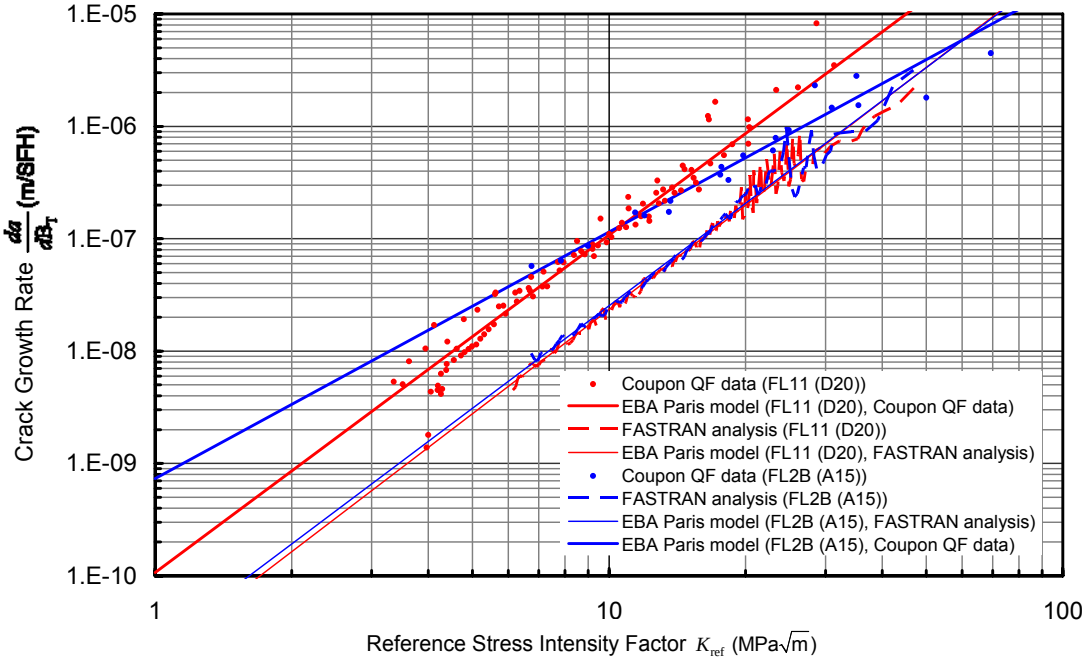

Figure 37: Prediction Crack growth rate data for the FL2B and FL11 spectra plotted along with FASTRAN predictions

Presented in Figure 38 are predictions for the CGRs evaluated for the FL2B load spectrum from the FL11 load spectrum. As before a comparison is made with the QF data and linear regressions for the FL2B load spectrum.

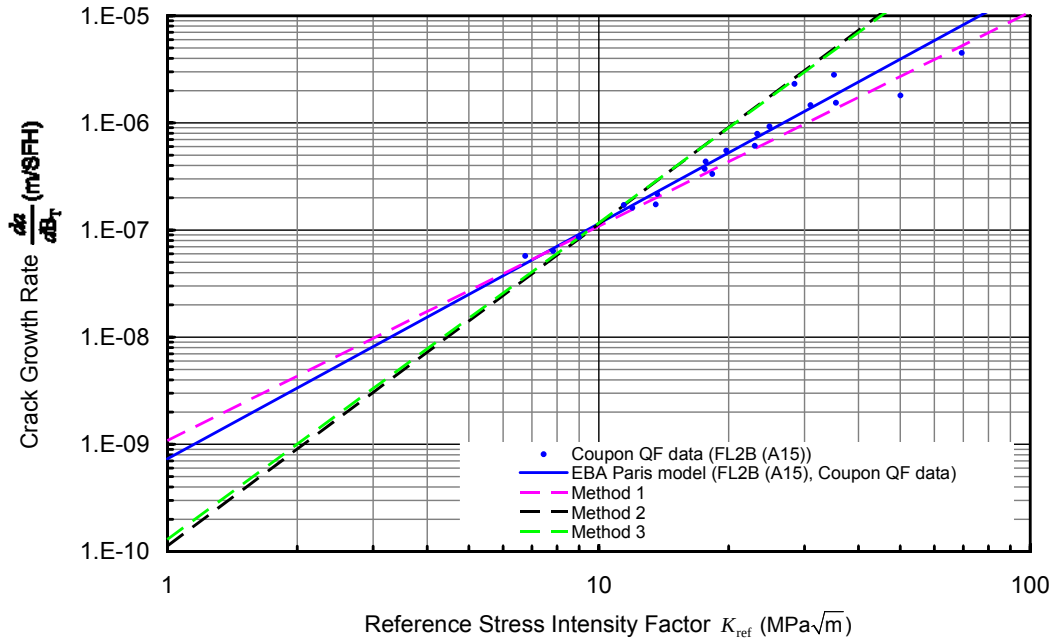

Figure 38: EBA prediction of FL2B from FL11 Coupon data

Examining the coefficients of determination in this case shows that the setting m equal to 2 provides the best correlation followed closely by the variable-m and $m_{2,E} = m_{1,E}$ approaches which give similar coefficients of determination.

Table 25: EBA prediction of FL2B from FL11 Coupon data

Method	m	C	R^2
Least Squares fit	*2.194*	*7.351×10^{-10}*	*0.9565*
Method 1: $m = 2$	2.000	1.083×10^{-9}	0.9204
Method 3: Variable-m	2.954	1.292×10^{-10}	0.8569
Method 2: $m_{2,E} = m_{1,E}$	3.004	1.126×10^{-10}	0.8517

As before Figure 39 presents crack growth predictions for the opposite case to that above. Presented in Figure 39 are predictions for CGRs under the FL11 spectrum evaluated from the FL2B load spectrum.

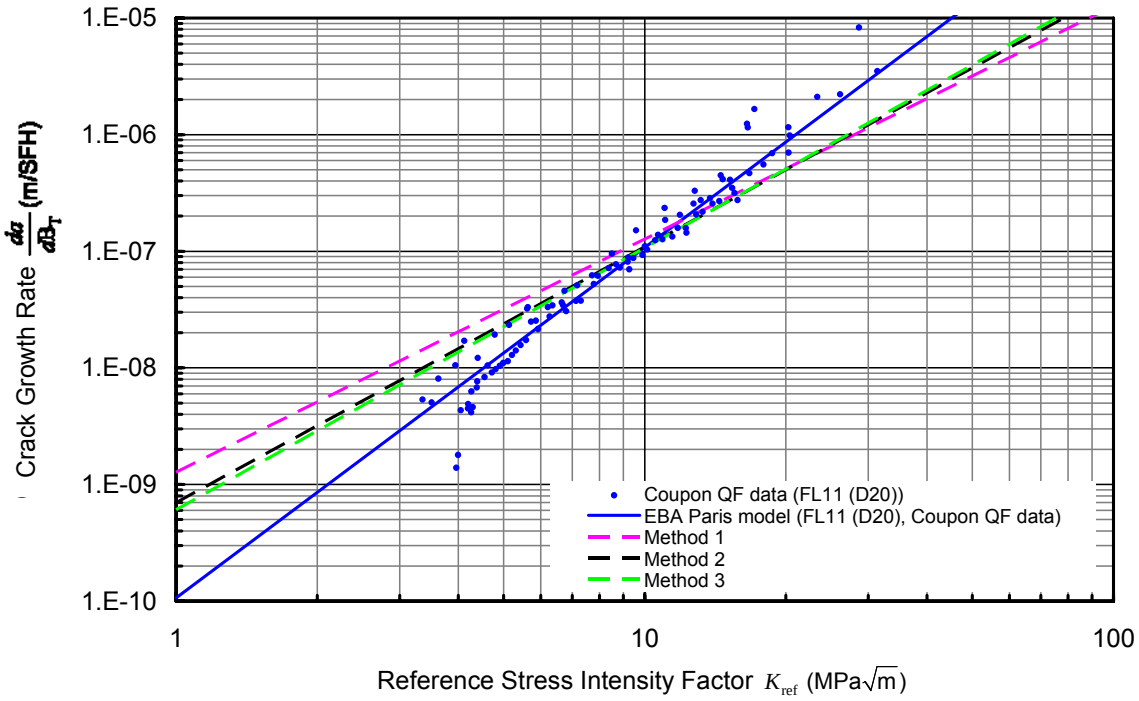

Figure 39: EBA prediction of FL11 from FL2B Coupon data

In this particular case setting m equal to 2 gives the poorest correlation. The variable-m and $m_{2,E} = m_{1,E}$ approaches provide the best correlations.

Table 26: EBA prediction of FL11 from FL2B Coupon data

Method	m	C	R^2
Least Squares fit	*3.004*	*1.069×10^{-10}*	*0.9628*
Method 3: Variable-m	2.245	6.085×10^{-10}	0.8447
Method 2: $m_{2,E} = m_{1,E}$	2.194	6.980×10^{-10}	0.8269
Method 1: $m = 2$	2.000	1.275×10^{-9}	0.7391

Figure 40 presents data used in the evaluation of cases 5 and 6. Presented in Figure 40 are FASTRAN predictions of CGRs for the FL10 and FL3 load spectra. Also presented is the QF crack growth data for the FL10 and FL3 load spectra.

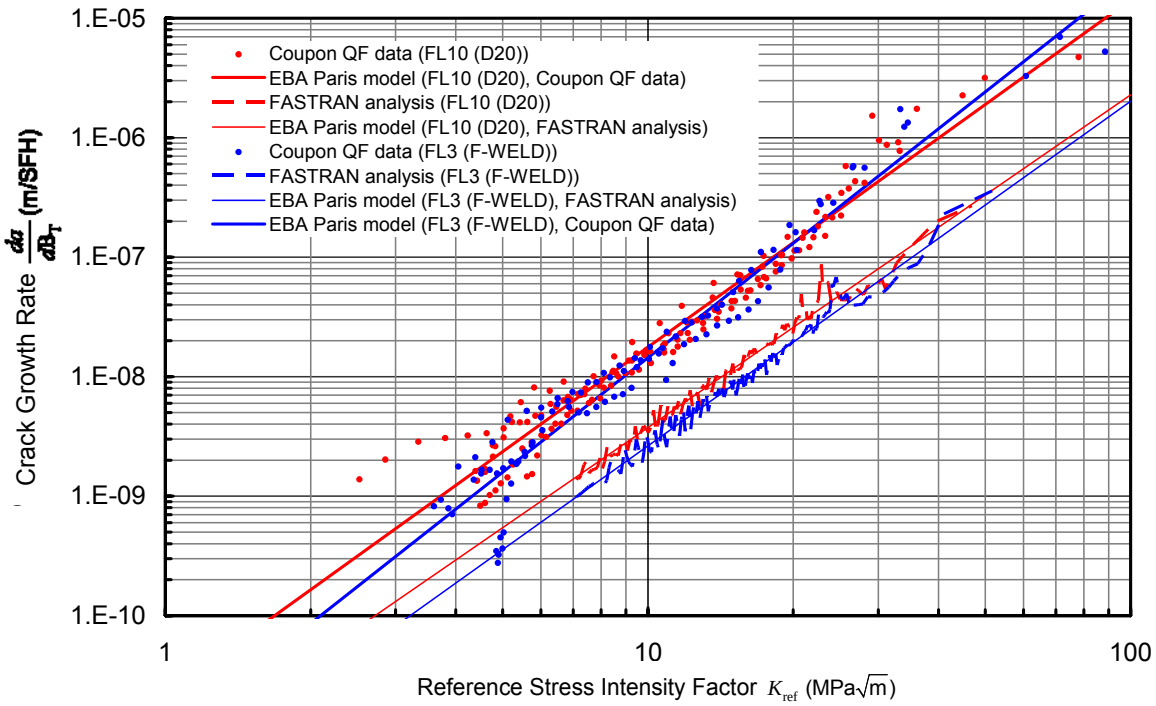

Figure 40: Crack growth rate data for the FL3 and FL10 spectra plotted along with FASTRAN predictions

Presented in Figure 41 are predictions of the CGRs under the FL3 load spectrum predicted from QF data from coupon test conducted under the FL10 load spectrum. QF data for the FL3 load spectrum is also presented.

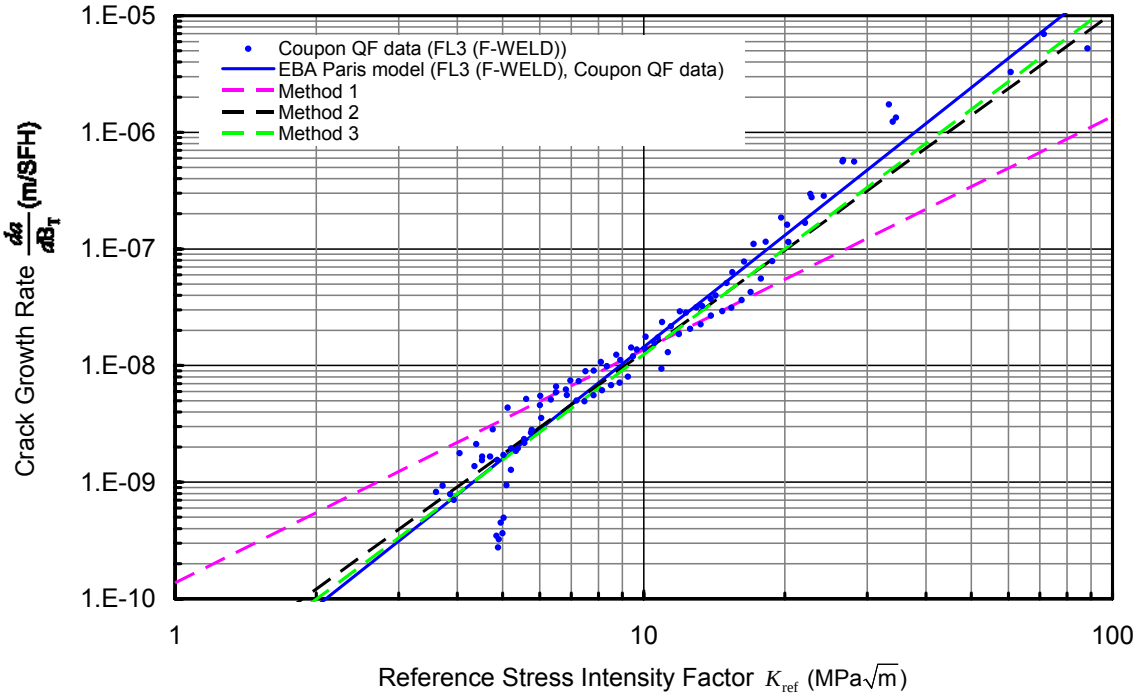

Figure 41: EBA prediction of FL3 from FL10 Coupon data

The coefficients of determination presented in Table 27 indicate that both the variable-m and $m_{2,E} = m_{1,E}$ approaches provide the best predictions. In this case setting m equal to 2 did not produce a good correlation.

Table 27: EBA prediction of FL3 from FL10 Coupon data

Method	***m***	***C***	**R^2**
Least Squares fit	*3.182*	*9.476×10^{-12}*	*0.9454*
Method 3: Variable-m	3.005	1.229×10^{-11}	0.9322
Method 2: $m_{2,E} = m_{1,E}$	2.906	1.611×10^{-11}	0.9253
Method 1: $m = 2$	2.000	1.367×10^{-10}	0.6687

Presented in Figure 42 are predictions for the CGRs under the FL10 load spectrum predicted from the FL3 load spectrum. Also presented is the QF data for the FL10 load spectrum.

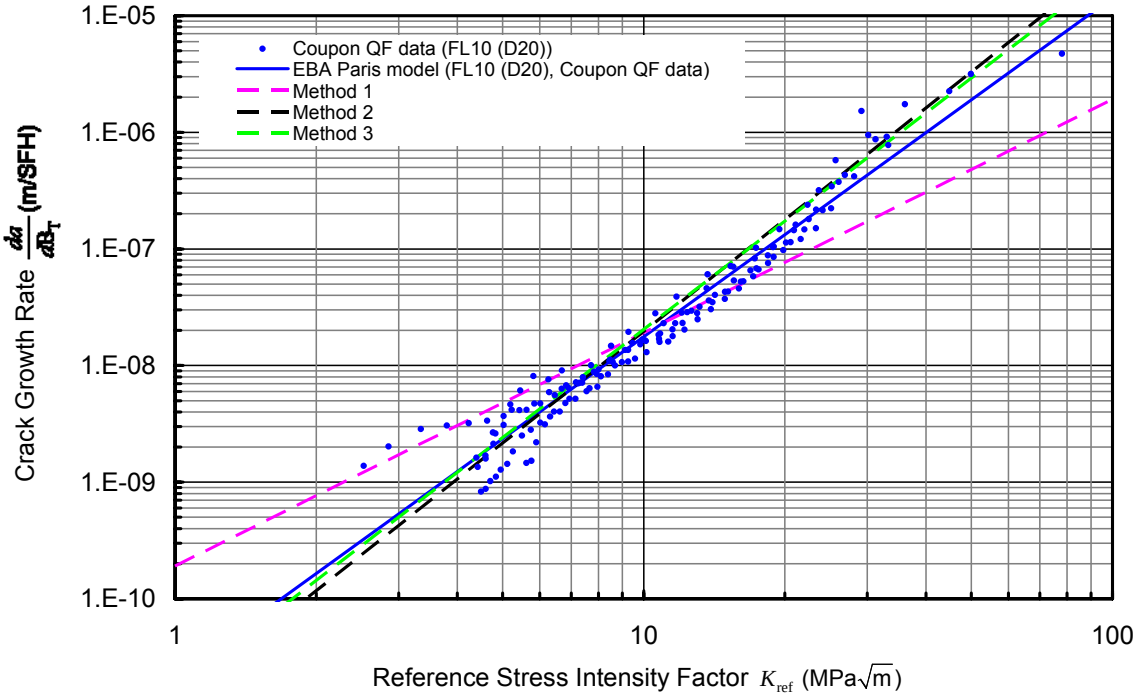

Figure 42: EBA prediction of FL10 from FL3 Coupon data

Again the $m_{2,E} = m_{1,E}$ and variable-m approaches provide the best correlations followed by setting m equal to 2.

Table 28: EBA prediction of FL10 from FL3 Coupon data

Method	***m***	***C***	**R^2**
Least Squares fit	*2.906*	*2.195×10^{-11}*	*0.9540*
Method 2: $m_{2,E} = m_{1,E}$	3.182	1.291×10^{-11}	0.9514
Method 3: Variable-m	3.082	1.693×10^{-11}	0.9506
Method 1: $m = 2$	2.000	1.912×10^{-10}	0.7651

Presented in Figure 43 is the data used in the predictions for cases 7 and 8. Shown in Figure 43 are FASTRAN predictions of the fatigue CGR for the FL15 and FL14 load spectra. Also presented is the QF data for coupons tested under the FL15 and FL14 load spectra.

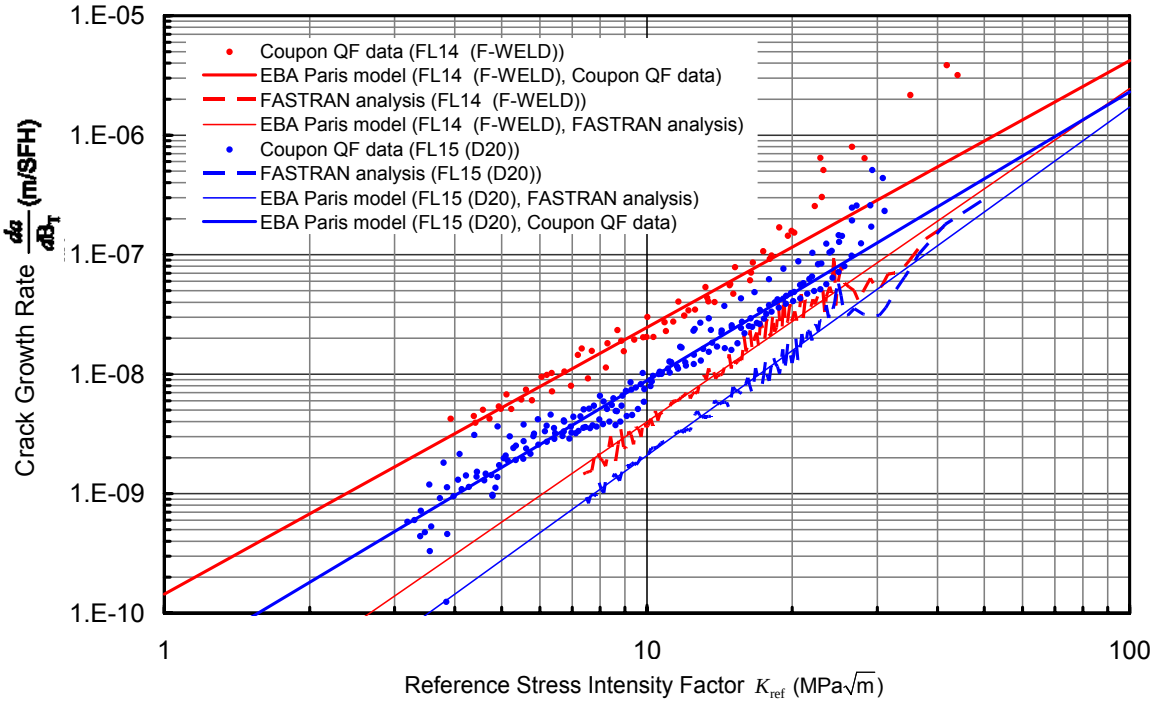

Figure 43: Crack growth rate data for the FL14 and FL15 spectra plotted along with FASTRAN predictions

Presented in Figure 44 are the three predictions of fatigue CGR under the FL14 load spectrum. Also presented is the QF CGR data obtained under the FL14 load spectrum. CGRs above 20 MPa√m appear to depart from a linear approximation and were ignored in the following analysis.

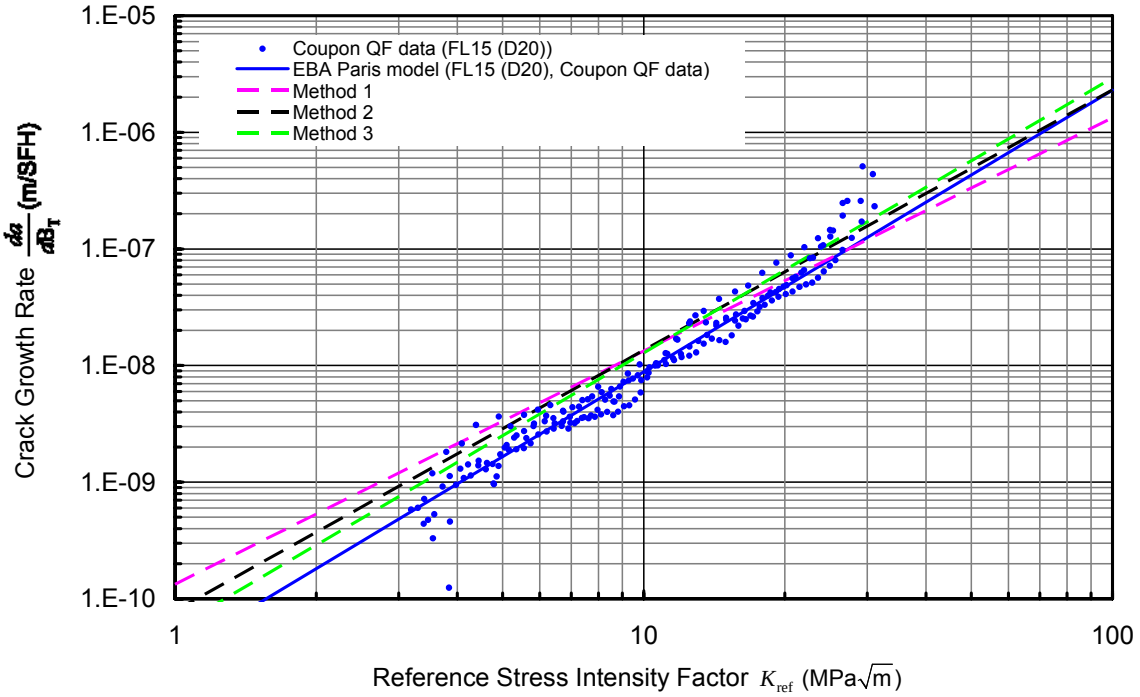

Figure 44: EBA prediction of FL15 from FL14 Coupon data

The coefficients of determination presented in Table 29 indicate that the variable-m and $m_{2,E} = m_{1,E}$ approaches provide the best correlation. In this case setting m equal to 2 only marginally reduces the coefficient of determination with respect to the other two prediction techniques.

Table 29: EBA prediction of FL15 from FL14 Coupon data

Method	***m***	***C***	**R^2**
Least Squares fit	*2.415*	*3.403×10^{-11}*	*0.9349*
Method 3: Variable-m	2.359	5.625×10^{-11}	0.8614
Method 2: $m_{2,E} = m_{1,E}$	2.233	7.928×10^{-11}	0.8208
Method 1: $m = 2$	2.000	1.331×10^{-10}	0.7666

Presented in Figure 45 are three predictions of CGR under the FL15 load spectrum. Also presented in Figure 45 is the QF data for the FL15 load spectrum.

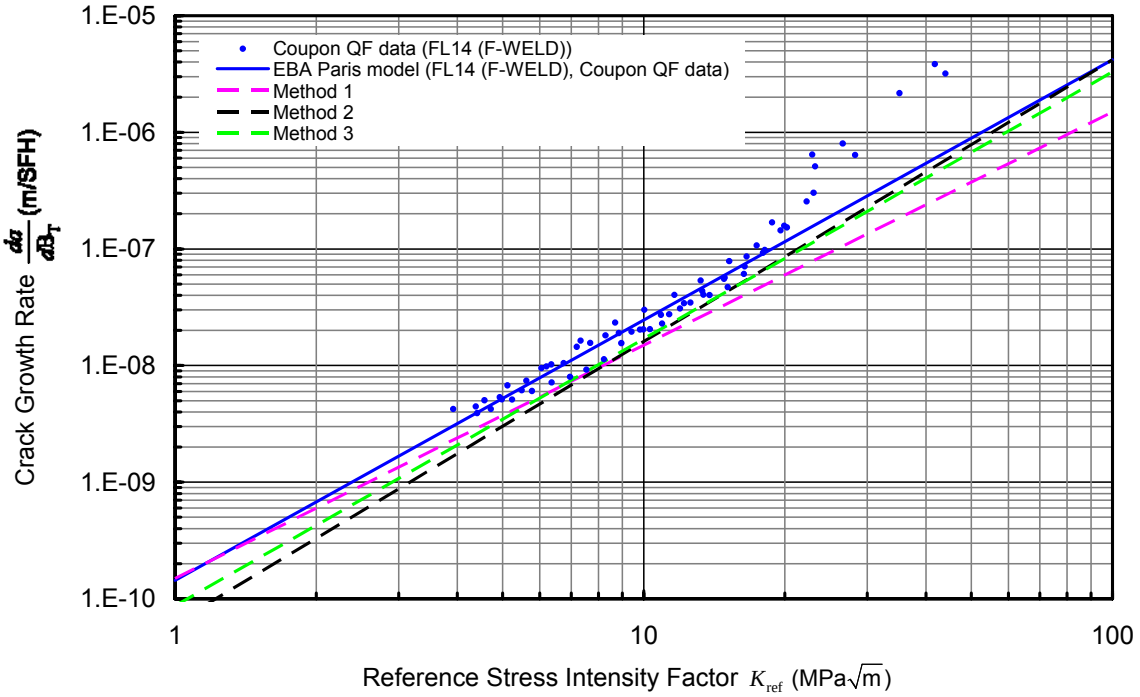

Figure 45: EBA prediction of FL14 from FL15 Coupon data

Again with reference to Table 30, the variable-m and $m_{2,E} = m_{1,E}$ approaches provide the best correlation followed by setting m equal to 2.

Table 30: EBA prediction of FL14 from FL15 Coupon data

Method	***m***	***C***	**R^2**
Least Squares fit	*2.233*	*1.440×10^{-10}*	*0.9649*
Method 3: Variable-m	2.289	8.715×10^{-11}	0.8715
Method 2: $m_{2,E} = m_{1,E}$	2.415	6.184×10^{-11}	0.8575
Method 1: $m = 2$	2.000	1.495×10^{-10}	0.7933

Appendix D: F-111 crack growth predictions using the EBA and FASTRAN

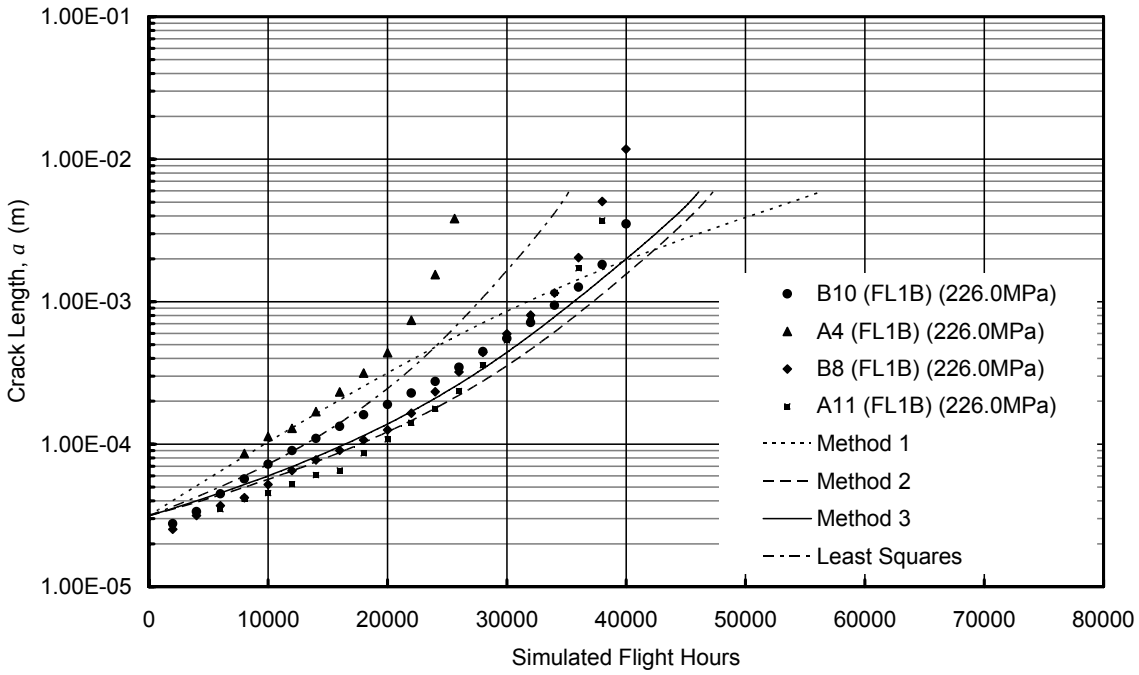

Figure 46: EBA crack growth curves created with FL10 QF data to predict crack growth under FL1B and compared to experimental QF data obtained under FL1B

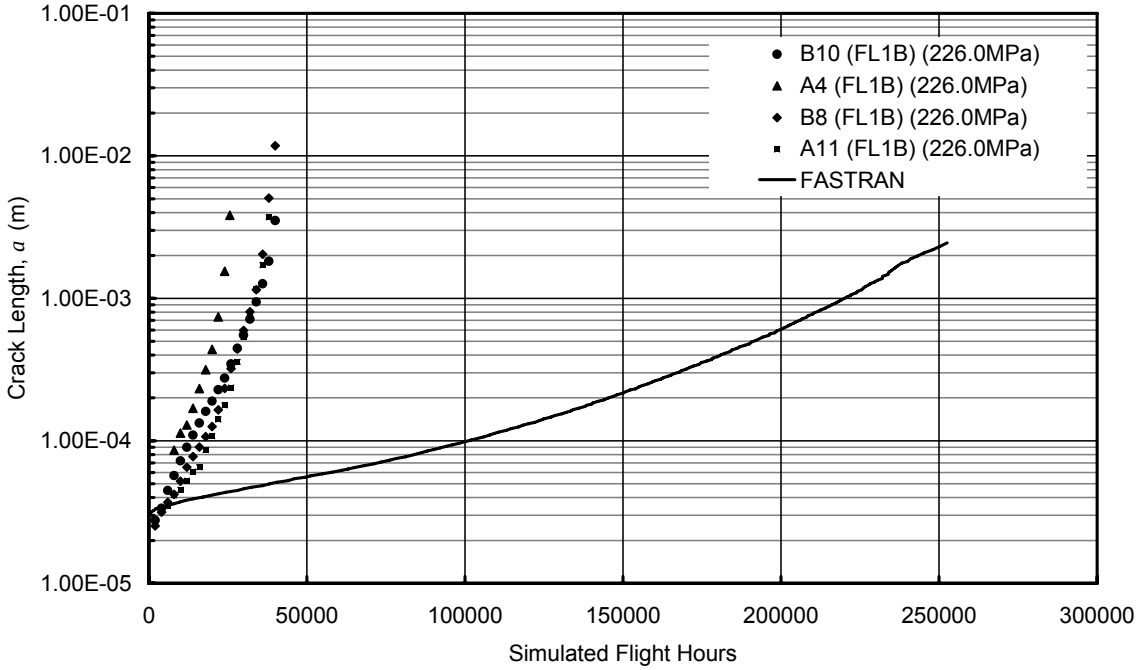

Figure 47: FASTRAN crack growth prediction under FL1B and compared to QF data obtained under FL1B

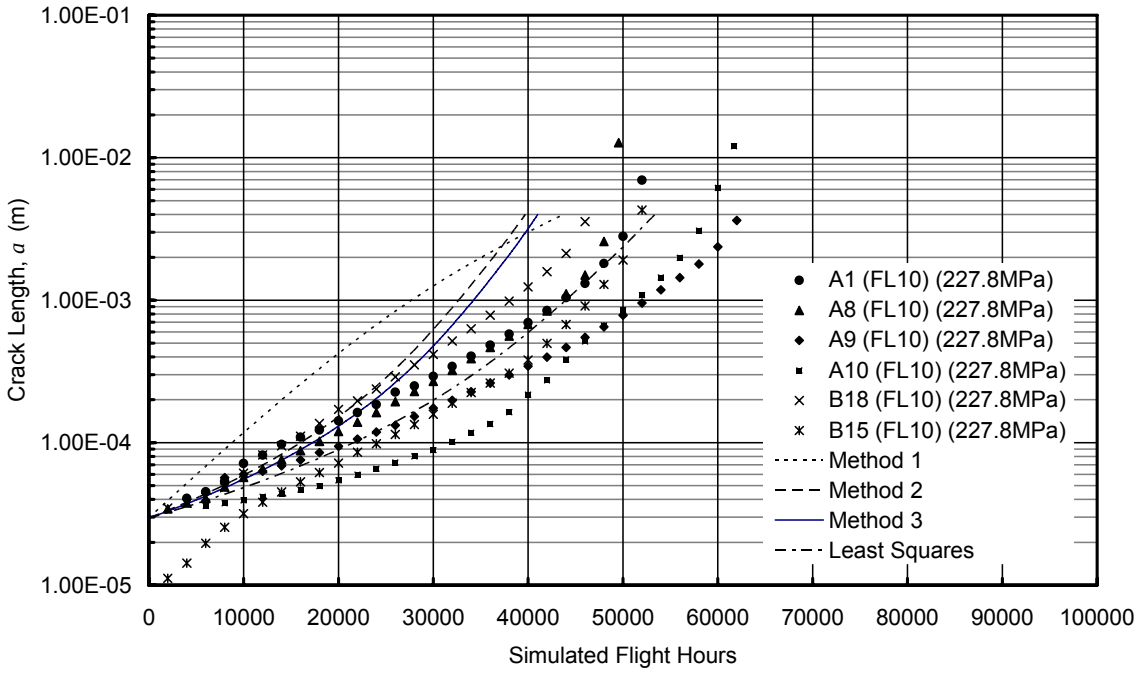

Figure 48: Crack growth curves created with FL1B QF data to predict crack growth under FL10 and compared to QF data obtained under FL10

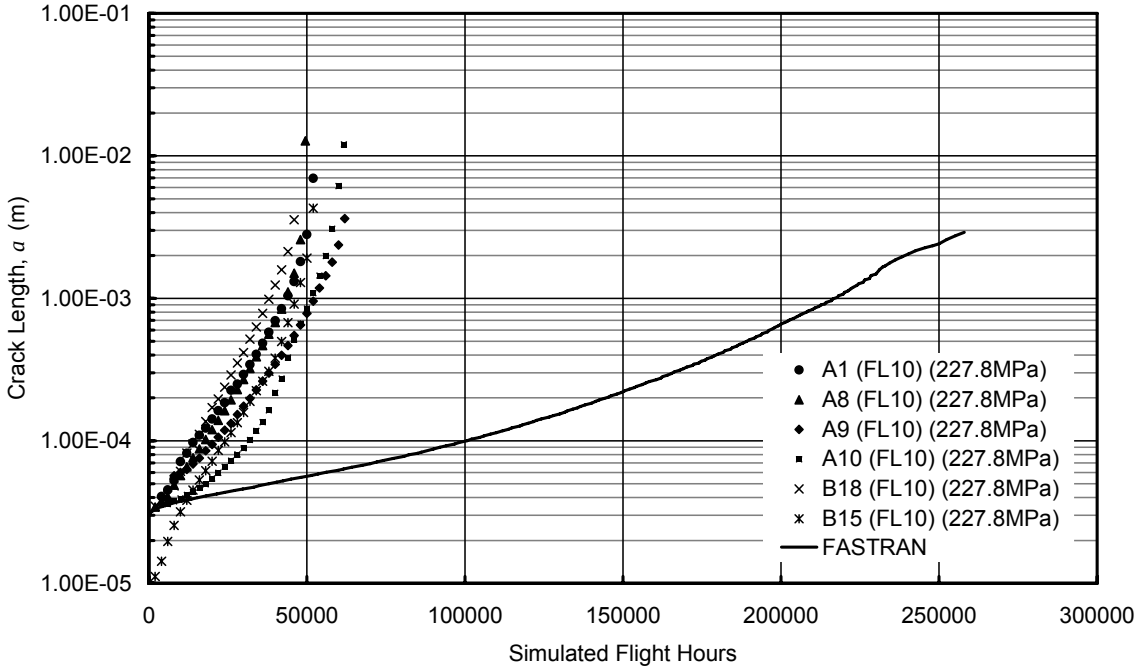

Figure 49: FASTRAN crack growth prediction under FL10 and compared to QF data obtained under FL10

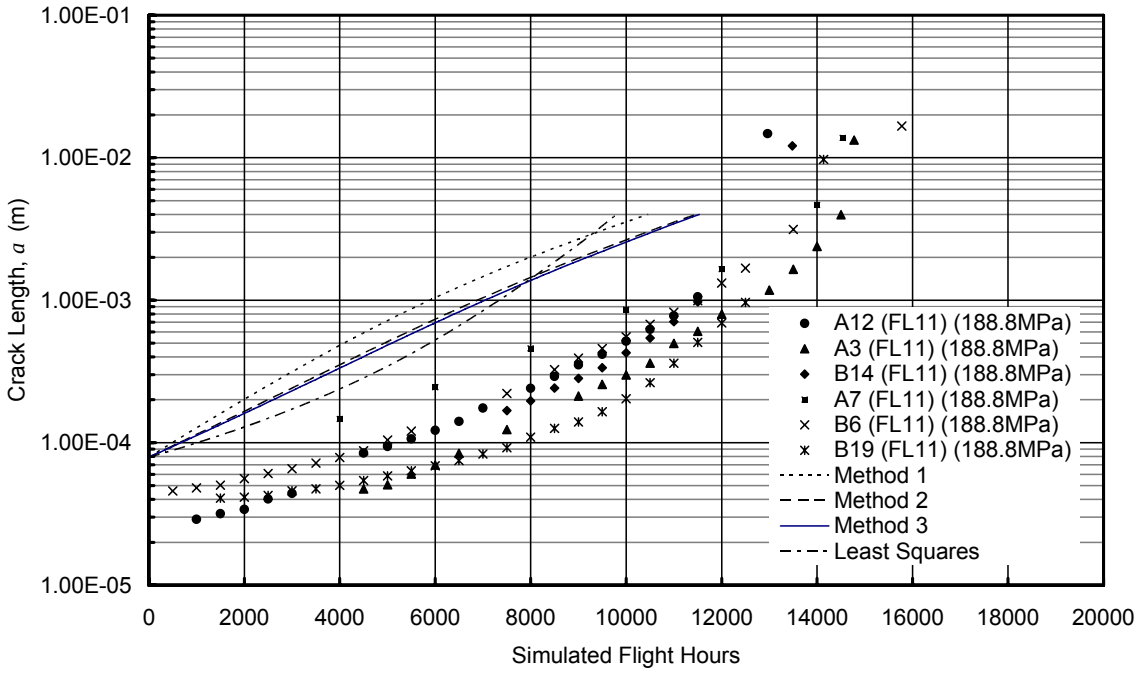

Figure 50: Crack growth curves created with FL2B QF data to predict crack growth under FL11 and compared to QF data obtained under FL11

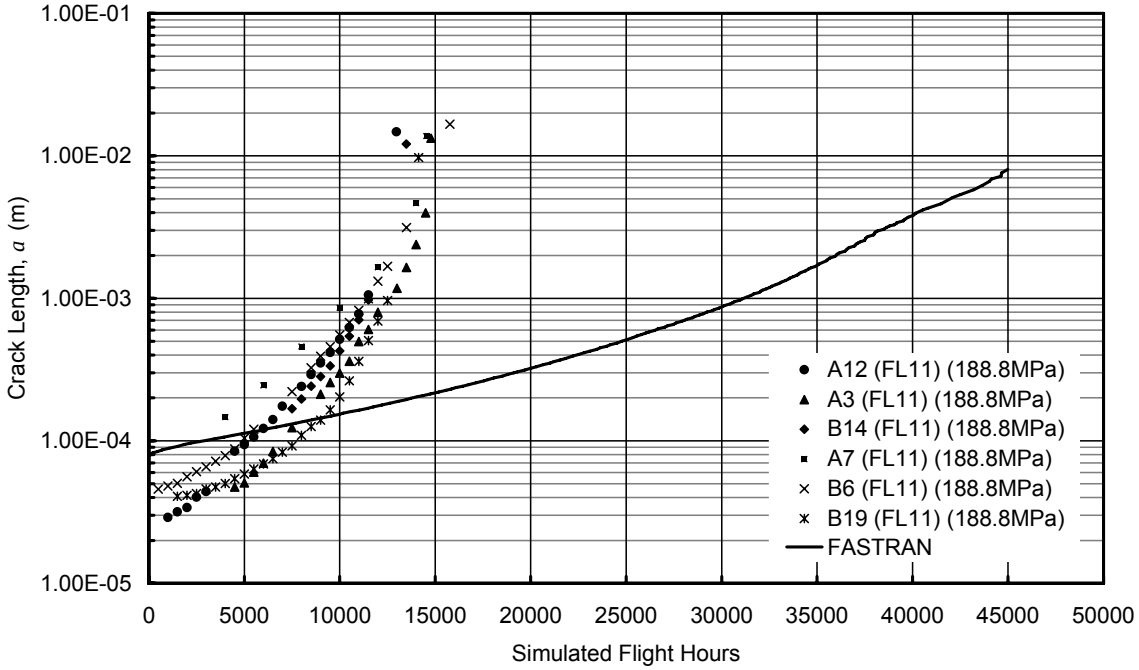

Figure 51: FASTRAN crack growth prediction under FL11 and compared to QF data obtained under FL11

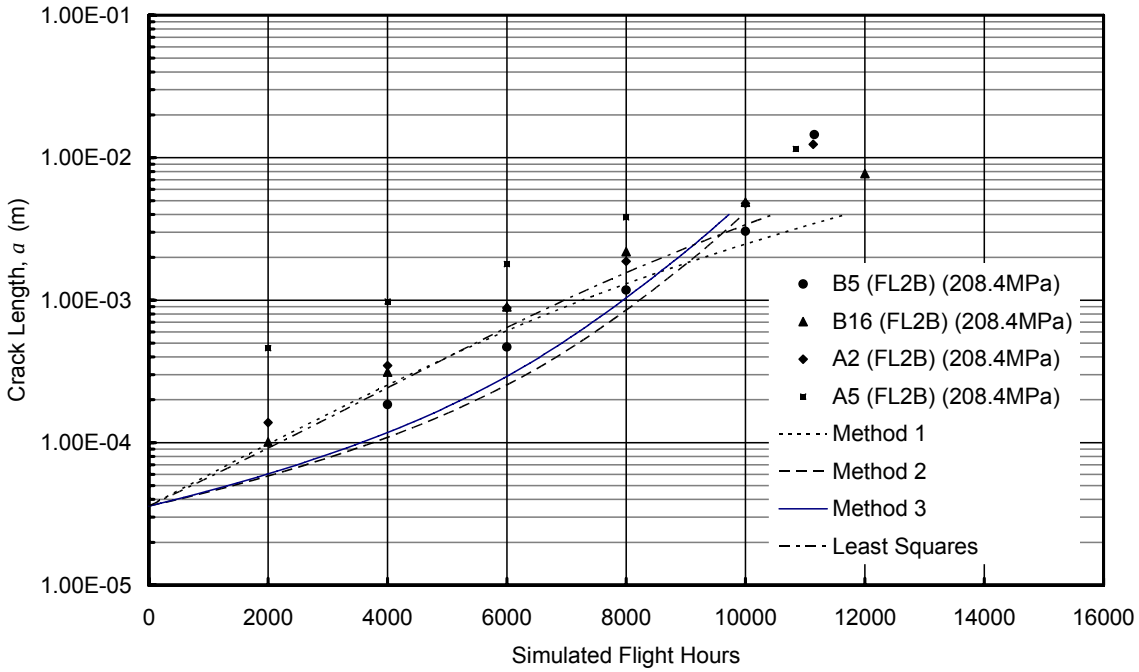

Figure 52: Crack growth curves created with FL11 QF data to predict crack growth under FL2B and compared to QF data obtained under FL2B

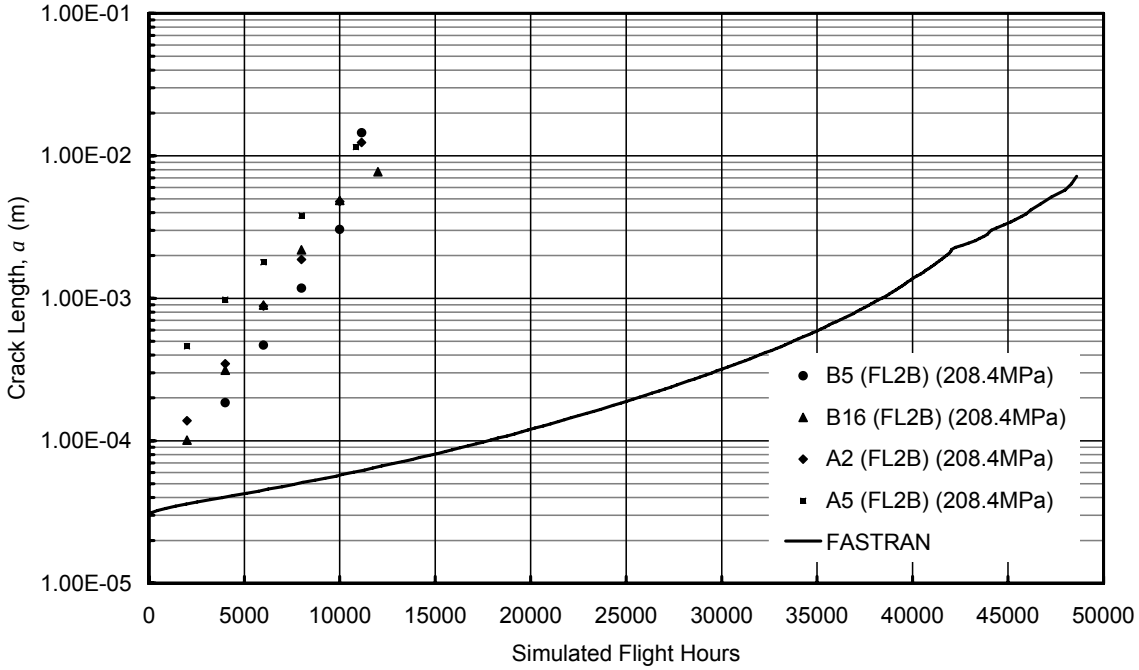

Figure 53: FASTRAN crack growth prediction under FL2B and compared to QF data obtained under FL2B

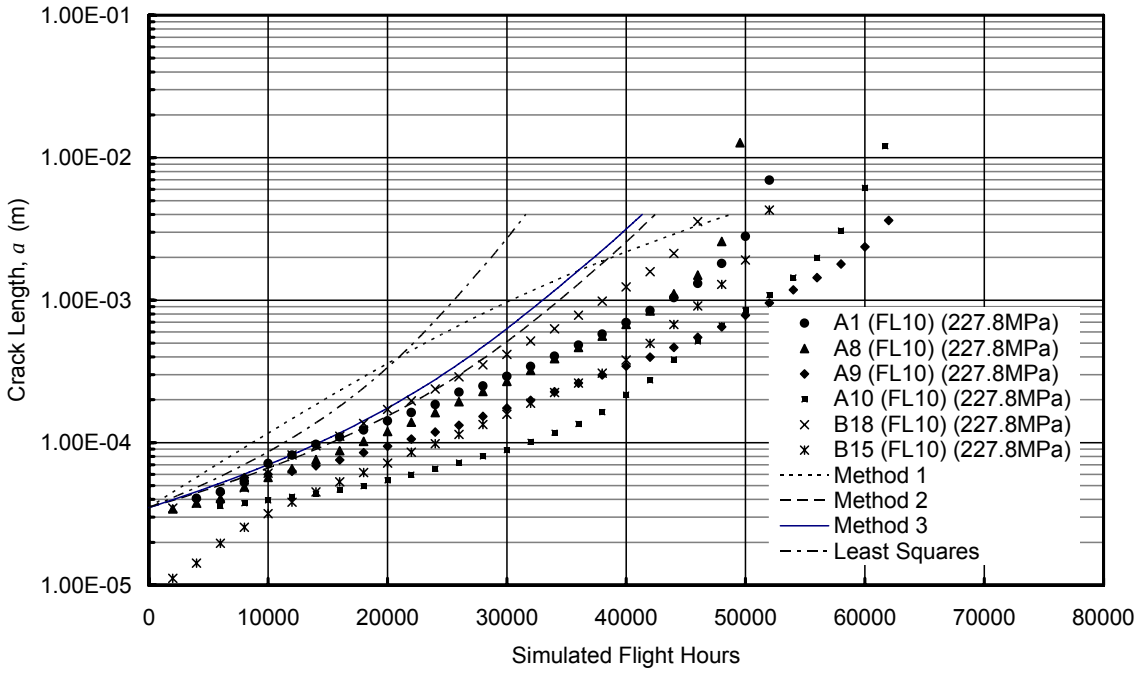

Figure 54: Crack growth curves created with FL3 QF data to predict crack growth under FL10 and compared to QF data obtained under FL10

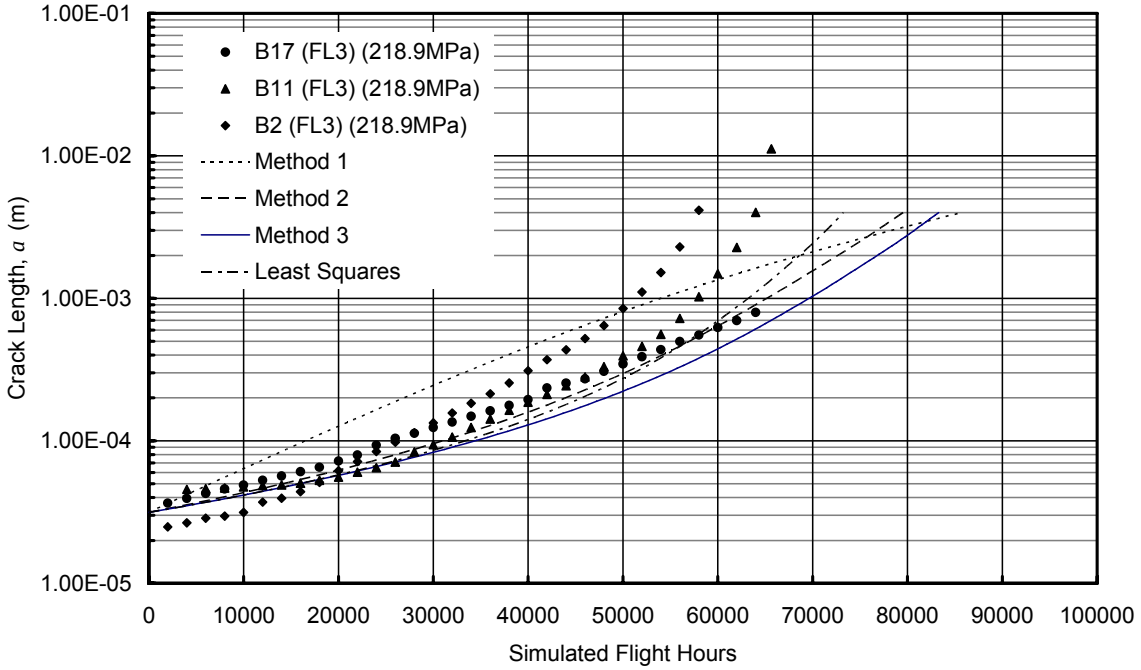

Figure 55: Crack growth curves created with FL10 QF data to predict crack growth under FL3 and compared to QF data obtained under FL3

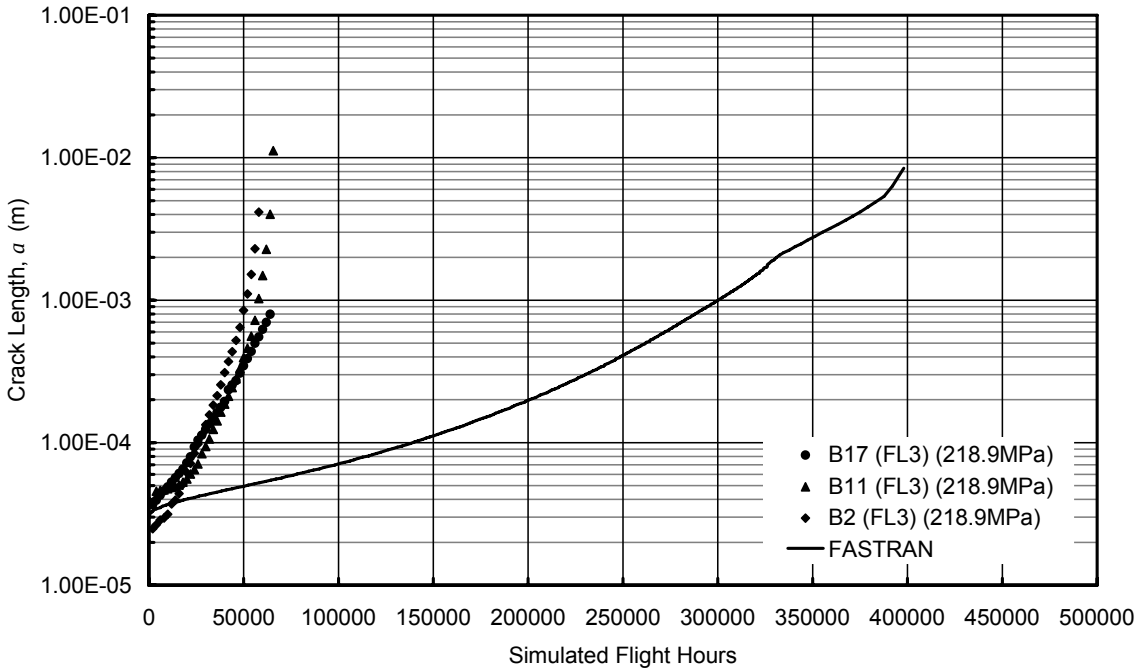

Figure 56: FASTRAN crack growth prediction under FL3 and compared to QF data obtained under FL3

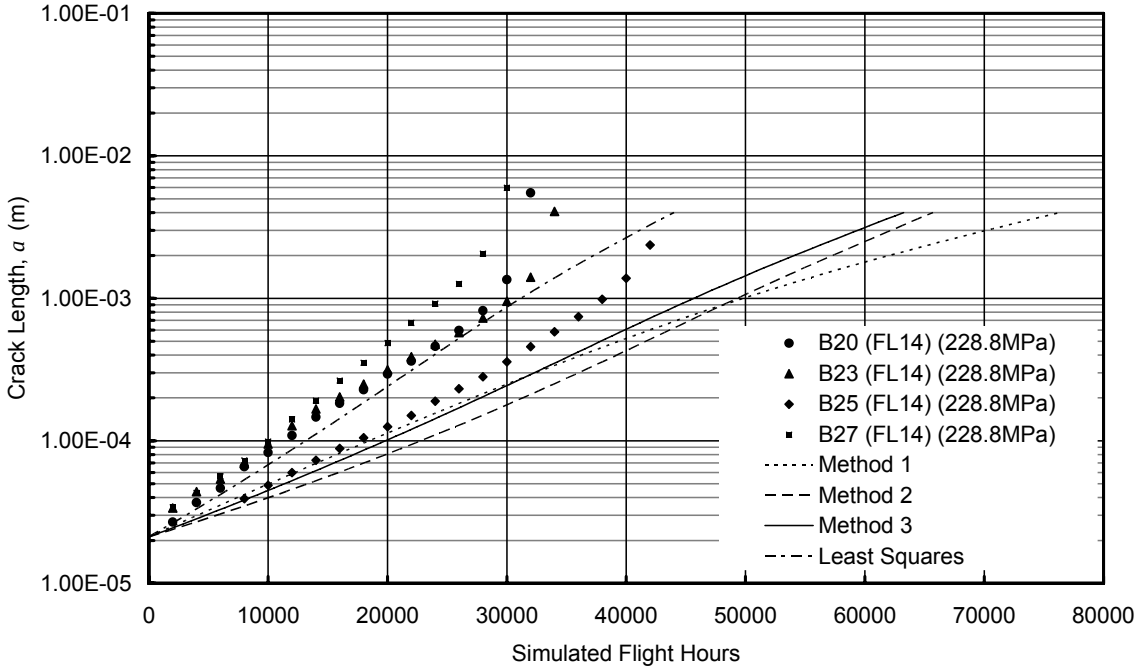

Figure 57: Crack growth curves created with FL15 QF data to predict crack growth under FL14 and compared to QF data obtained under FL14

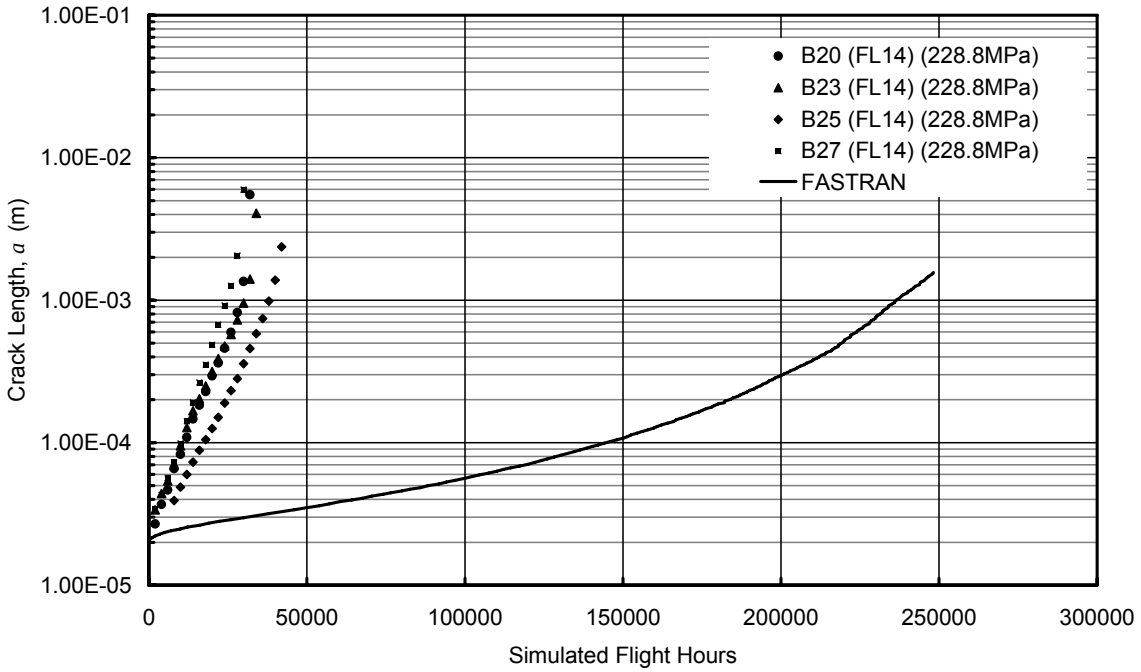

Figure 58: FASTRAN crack growth prediction under FL14 and compared to QF data obtained under FL14

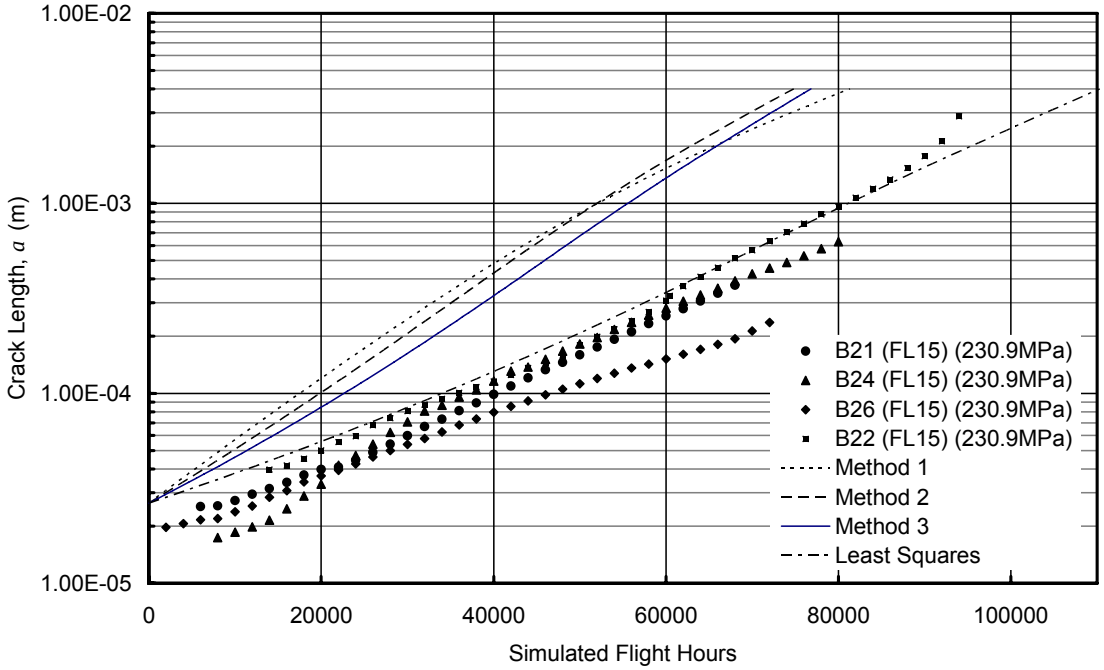

Figure 59: Crack growth curves created with FL14 QF data to predict crack growth under FL15 and compared to QF data obtained under FL15

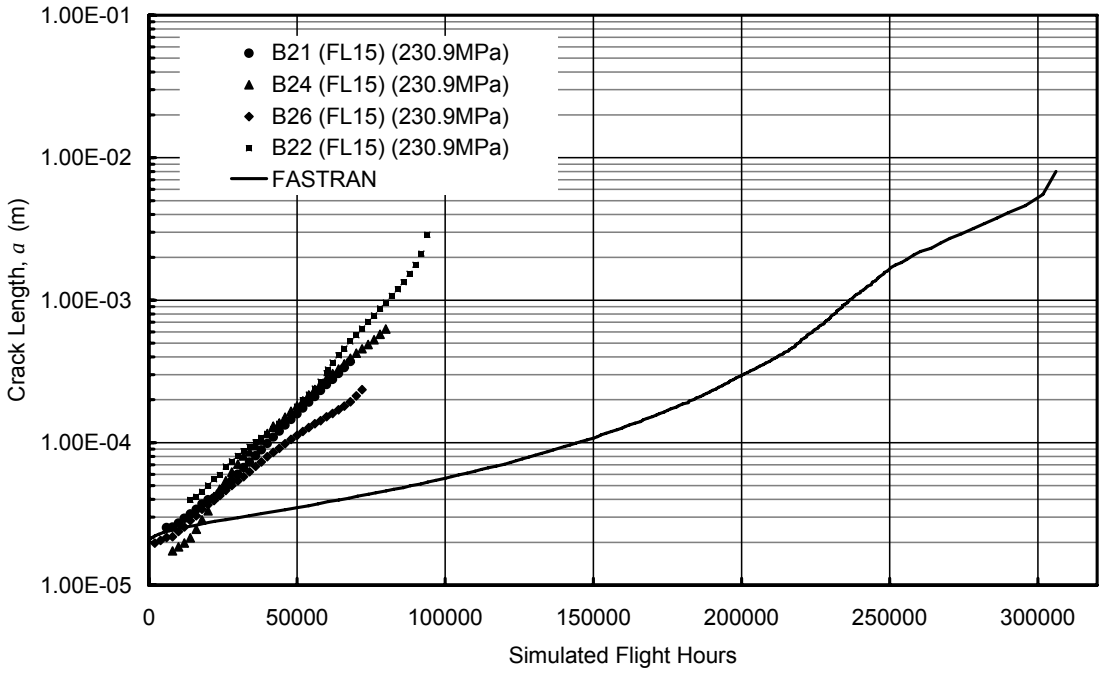

Figure 60: FASTRAN crack growth prediction under FL15 and compared to QF data obtained under FL15

Appendix E: Statistical Analysis of the F/A-18 APOL Coupon Test Data

A coupon test program completed by the DSTO examined the fatigue performance of F/A-18 aircraft materials under a variety of aircraft operational flight profiles (Pell, Mazeika et al. 2003; Pell, Mazeika et al. 2005) including the APOL spectrum. The APOL spectrum is the Australian post-LEX fence usage spectrum. These results are presented here to compare the observed trends in the F-111 coupon test data with those of the F/A-18 coupon test program (Pell, Mazeika et al. 2003; Pell, Mazeika et al. 2005). The F/A-18 coupon test program examined fatigue crack growth under four stress scaling levels using the APOL spectra. The coupons were designed to duplicate a detail on the mould line flange on the FS488 wing carry through bulkhead using a "dog bone" type geometry. The coupons were manufactured from 7050 T7451 Aluminium with the appropriate surface treatment to best represent the detail. β factors for a corner crack were assumed as per (McDonald 2005). Further details in regard to loading, coupon geometry and testing can be found in Pell, Mazeika et al. 2003; Pell, Mazeika et al. (2005). The spectrum identification codes are presented in Table 31.

Table 31: Spectrum ID and scaling stress

Spectrum ID	*Scaling Stress (MPa)*	*No. Coupons*	*No. of data points*
Phase I	324.1	6	223
Phase II	358.5	4	122
Phase III	396.5	7	196
Phase IV	428.9	5	117

Presented in Figure 61 is the fatigue CGRs evaluated for the QF data obtained at each scaling stress level subjected to the APOL spectrum. The linear regression for each scaling stress level has also been presented along with the 95% prediction intervals. (McDonald 2005) examined this data with respect to using a Paris based model and the Frost and Dugdale model (Frost and Dugdale 1958). It was argued that the observed scatter in the F/A-18 QF data was too large to detect an effect due to the scaling stress level. The two sample t-test, as previously used, was employed to assess the similarity of the slopes and y-intercepts of the linear regressions. The QF data for coupon KS1G41 displayed crack growth inconsistent from the rest of the QF data used in the present investigation. The validity of this data could not be confirmed and thus was eliminated from this investigation. The F/A-18 coupon test data contains more data than that of the F-111 coupon test data used earlier in this investigation which helps to better interpret the scatter in the data.

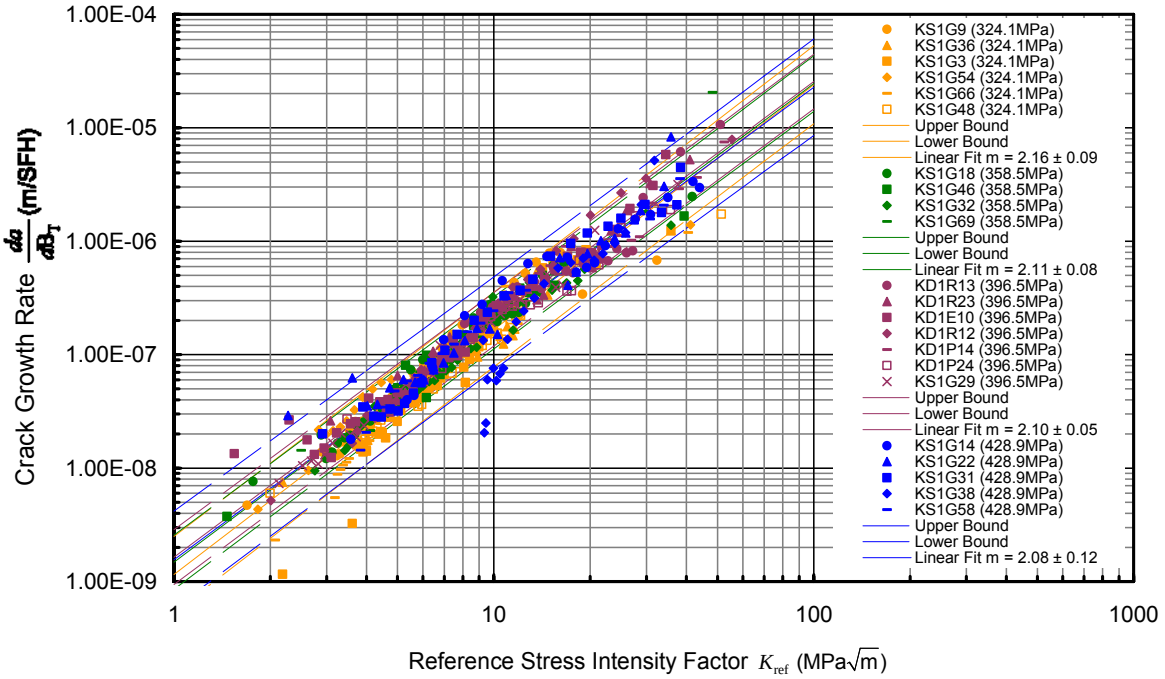

Figure 61: QF data from coupons subjected to the F/A-18 APOL spectrum at different stress scale levels. 95% prediction intervals are plotted along with linear regressions of the data at each stress scale level.

The results of the two sample t-test in Table 32 show that the slopes of the four linear regressions are homogeneous within the associated scatter. In other words, within the scatter the slopes of the linear regressions can be considered the same.

Table 32. Comparing regression slopes for the F/A-18 APOL test spectra using a t-tests

Comparison	*t-value*	*p value*	*Reject $\beta_1 = \beta_2$*
Phase I with Phase II	-0.199	0.842	No
Phase I with Phase III	-0.611	0.541	No
Phase I with Phase IV	0.203	0.839	No
Phase II with Phase III	-0.384	0.701	No
Phase II with Phase IV	0.357	0.722	No
Phase III with Phase IV	0.767	0.444	No

After establishing the homogeneity of the regression slopes a further two sample t-test was conducted to examine the y-intercept. The results presented in Table 33 indicate that the y-intercepts agree within experimental uncertainty.

Table 33. Comparing the y-intercept for the F/A-18 APOL test spectra using a t -tests

Comparison	*t-value*	*Pr(>|t|)*	*Reject* $\kappa_1 = \kappa_2$
Phase I with Phase II	-0.883	0.378	No
Phase I with Phase III	-1.201	0.230	No
Phase I with Phase IV	-0.999	0.318	No
Phase II with Phase III	-0.165	0.869	No
Phase II with Phase IV	-0.294	0.769	No
Phase III with Phase IV	-0.232	0.816	No

The stress scaling level was raised from 324.1 MPa to a maximum stress scaling level of 428.9 MPa, a 32% increase. The statistical analysis of the F/A-18 coupon data tested under the APOL spectrum indicates that there is no discernable effect associated with the stress scaling level on the EBA constants evaluated with a Paris based model. If a stress scaling effect is present, a 32% increase in stress scaling is insufficient to create a discernable change in the EBA CGR constants. In comparison with the previous analysis of the F-111 coupon test data the F/A-18 results appear to support the previous observations.

If the CGR constants are independent of the stress scaling level, this would indicate that sequence effects must be a function of the relative magnitude of the spectrum peaks and their order and not a function of the stress scaling level.

DEFENCE SCIENCE AND TECHNOLOGY ORGANISATION
DOCUMENT CONTROL DATA

1. PRIVACY MARKING/CAVEAT (OF DOCUMENT)

2. TITLE

An Evaluation of the Effective Block Approach Using P-3C and F-111 Crack Growth Data

3. SECURITY CLASSIFICATION (FOR UNCLASSIFIED REPORTS THAT ARE LIMITED RELEASE USE (L) NEXT TO DOCUMENT CLASSIFICATION)

Document	(U)
Title	(U)
Abstract	(U)

4. AUTHOR(S)

C. Wallbrink, R. Amaratunga, W. Hu, P. Jackson and D. Mongru

5. CORPORATE AUTHOR

DSTO Defence Science and Technology Organisation
506 Lorimer St
Fishermans Bend Victoria 3207 Australia

6a. DSTO NUMBER	6b. AR NUMBER	6c. TYPE OF REPORT	7. DOCUMENT DATE
DSTO-TR-2195	AR-013-294	Technical Report	September 2008

8. FILE NUMBER	9. TASK NUMBER	10. TASK SPONSOR	11. NO. OF PAGES	12. NO. OF REFERENCES
2007/1084753	AIR 07/051	DGTA-ASI	84	33

13. URL on the World Wide Web

http://www.dsto.defence.gov.au/corporate/reports/DSTO-TR-2195.pdf

14. RELEASE AUTHORITY

Chief, Air Vehicles Division

15. SECONDARY RELEASE STATEMENT OF THIS DOCUMENT

Approved for public release

OVERSEAS ENQUIRIES OUTSIDE STATED LIMITATIONS SHOULD BE REFERRED THROUGH DOCUMENT EXCHANGE, PO BOX 1500, EDINBURGH, SA 5111

16. DELIBERATE ANNOUNCEMENT

No Limitations

17. CITATION IN OTHER DOCUMENTS Yes

18. DSTO RESEARCH LIBRARY THESAURUS http://web-vic.dsto.defence.gov.au/workareas/library/resources/dsto_thesaurus.shtml

Effective Block Approach, fatigue life, crack growth, P-3C, F-111

19. ABSTRACT

Recently an effective block approach has been proposed to address the experimentally observed growth rates of fatigue cracks at critical locations on F/A-18 airframes. In this approach, each program of spectrum load is treated as an equivalent constant amplitude cycle, and the baseline crack growth rate data are obtained using a similar spectrum load of interest. A procedure was devised to allow the use of the model parameters obtained under one load spectrum to predict the crack growth under a different load spectrum. In this study, we critically evaluate the capability of the effective block approach, using data obtained for the F-111 and P-3C coupon test programs, to gauge its general applicability to other aircraft operated by the Royal Australian Air Force. The data used in the evaluation encompasses different load spectra, different materials and different crack configurations. This investigation has found that the effective block approach was able to model fatigue crack growth in 2024-T851 aluminium under the F-111 flight spectra examined, but it could not produce an acceptable estimation of the total crack growth life for the P-3C spectra studied. It was, however, able to produce reasonable predictions of fatigue crack growth in a chosen interval of crack length. This report provides an independent evaluation and guidance for the application of the effective block approach.